University of Alberta

Experimental and Computational Investigation of Sewer Flow at Combining Junctions

by

Can-Hua Zhao 

A thesis submitted to the Faculty of Graduate Studies and Research
in partial fulfillment of the requirements for the degree of
Doctor of Philosophy

in

Water Resources Engineering
Department of Civil and Environmental Engineering

Edmonton, Alberta

Fall 2006

Your file Votre référence
ISBN: 978-0-494-23137-1
Our file Notre référence
ISBN: 978-0-494-23137-1

ABSTRACT

Sewer flow at combining junctions with two inflows and one outflow is investigated experimentally and numerically. The thesis is written in paper format and includes four contributions.

The first contribution is a physical model study of the 25.8° Edworthy junction. The junction was designed to retrofit the Edworthy trunk sewer in Calgary, Alberta. This case study investigated hydraulic performance of the design and revealed features of sewer junction flow with a small merging angle. Transition of flow regimes in the chamber was observed and three flow regimes were identified as Regime I: open-channel flow through the junction chamber; Regime II: partially surcharged flow featured by orifice flow into the outlet pipe; and Regime III: fully surcharged flow with all connecting pipes running full.

The second contribution presented further discussions and analysis on surcharged flow in combining sewer junctions. With more experimental observations in the Edworthy model junction and a 90° junction, it was found that the transition from Regime II to III may be related to the inlet waves at the entrance of the outlet pipe. Criteria for the transition are presented. A theoretical model was derived to predict water depth and energy loss in the junction chamber. Flow structure of surcharged flow in the Edworthy junction was presented and analyzed.

The third contribution investigated the feasibility of applying computational fluid dynamics simulation to the study of sewer junctions. Fully surcharged flow at a 90° combining sewer junction was simulated with a commercial code, Ansys CFX 10.0. A

homogeneous and an inhomogeneous free-surface flow models were validated and evaluated by comparisons with detailed experimental measurements. Details of the flow were presented and discussed, including flow structure, energy dissipation and air entrainment.

The fourth contribution is a general discussion on combining flow at sewer junctions. Results of laboratory experiments and numerical simulations were generalized and presented with the assistance of theoretical analysis. The generalized results, including criteria for regime transitions, water depth and submergence factor in junction chambers, and energy coefficients, provide a basis for improving current municipal servicing guidelines and for optimizing design and construction.

ACKNOWLEDGEMENTS

I would like to sincerely thank Dr. D. Z. Zhu and Dr. N. Rajaratnam for their support and guidance through the course of this study. They have provided excellent supervision for this work. Their encouragement and enthusiasm provided a constant source of inspiration.

Gratitude is extended to Mr. Perry Fedun and Mr. Sheldon Lovell for building and helping with the experimental arrangements. Thanks to Dr. P. Steffler for his helpful suggestions on this study.

Funding from the NSERC, the City of Calgary, and the City of Edmonton is gratefully acknowledged. I also deeply appreciate the financial support for myself given from the University of Alberta Dissertation Fellowship, the Province of Alberta Fellowship, and the Bruce F Willson Graduate Scholarship.

I owe the greatest debt of gratitude to my wife, Zhaohui Li, for her understanding, her encouragement and her love.

Finally, I would like to express my great appreciation to my parents and my parents-in-law for their continued support.

To My Wife and My Parents

TABLE OF CONTENTS

LIST OF TABLES

LIST OF FIGURES

NOTATIONS

A = pipe area or flow area;

$A_{\alpha\beta}$ = interfacial area density;

$b_{0.5}$ = half width of a jet;

C_c = contraction coefficient;

C_d = discharge coefficient;

C_D = drag coefficient;

D = pipe diameter;

D_M = size of junction chamber;

f = frequency;

F_r = Froude number

g = the gravitational acceleration;

G = power spectrum;

H = total energy head;

H_L = total head loss per-unit-weight across a junction

h_m = mean water depth in a junction chamber;

h_{mc} = critical mean water depth in a junction chamber;

h_s = level of the swell in a junction chamber;

h^* = water depth scaled by D;

k = turbulent kinetic energy;

K_{13} = energy loss coefficient for the stream from inlet 1 to the outlet;

K_{23} = energy loss coefficient for stream from inlet 2 to the outlet;

K = energy loss coefficient for the junction;

L = chamber length;

M = interfacial force term;

$\boldsymbol{M}^D$ = drag force per unit volume (vector);

n = roughness (Manning's n)

p = pressure;

P = pressure force;

Q = flow rate;

Q^* = non-dimensional discharge;

Q_{3c} = choking flow rate;

r = volume fraction;

R_h = hydraulic radius;

S = water surface slope;

S_c = critical slope;

S_0 = pipe slope;

t = time;

T = top width of open-channel flow in a pipe;

$\mathbf{u}$ = velocity vector;

u, v, w = instantaneous velocities;

U, V, W = mean velocities;

U^*, V^*, W^* = normalized mean velocity;

u', v', w' = fluctuation components of velocities;

$\mathbf{U}_x$ = x component of the mean velocity vector;

$\mathbf{U}_y$ = y component of the mean velocity vector;

V = average velocity in a pipe (always has subscripts);

$\mathbf{V}$ = mean velocity vector in the central plane;

V_m = maximum value of the mean velocity vector;

x, y, z = coordinates;

y' = local transverse coordinate;

δ = the average entry angle of the lateral flow;

ε = turbulent energy dissipation rate;

η = efficiency of energy dissipation;

θ = junction angle;

μ = viscosity;

ρ = density;

σ = correction factor;

ψ = submergence factor.

Subscripts

a = air;

f = free-flow capacity;

i and j = 1, 2, and 3;

m = mixture of multiphase fluids;

w = water;

rms = root-mean square;

α and β = phase indicators;

1 = the straight inlet pipe or the direction of x;

2 = the lateral inlet pipe or the direction of y;

3 = the outlet pipe or the direction of z.

Chapter 1

General Introduction

Drainage systems are vital components of urban infrastructures. In many large municipalities, it represents an asset of multi-billion dollars of investment. The recent urban development and economic growth, together with issues related to ageing facilities and possible climate change, have induced urgent need to upgrade existing drainage systems and to improve current municipal servicing guidelines. To achieve effective and sustainable urban drainage solutions, it is essential to improve knowledge of sewer systems at various aspects, from fundamental to practical levels, including sewer design, construction, operation and maintenance.

Sewer networks consist of sewer pipes/conduits and various auxiliary hydraulic structures, such as junctions, weirs, drop shafts, siphons, and pumps. Junctions are one of the most important components in sewer networks. A sewer junction has two or more sewer conduits joined to it, typically in the form of a chamber with/without a manhole. The junction provides access for sewer inspection and maintenance, and/or serves as a transition structure where flow merges or divides, or where sewer conduits change in size, slope, alignment, or cross-sectional shape. Performance of the drainage systems, in many cases, is restricted by the improper design of junctions.

Sewer systems are designed to carry free-surface flow in normal operation. Sewer pipes are usually sized and sloped according to free surface flow conditions. While the hydraulics of flow in a single pipe is reasonably well understood, knowledge about flow phenomena associated with sewer junctions is still limited. Yet this information is

important as the hydraulic performance of sewer junctions can directly affect the free-flow capacity of the system. Improper design of junctions can make them be the bottleneck of the system. When the flow rate exceeds the free-flow capacity of a system, pipe-full flow (or pressurized flow) will form in sewers, which is referred to as surcharged flow. While weakly surcharged flows are allowed in sewer design, strongly surcharged flows produce serious problems, such as blown-off manhole covers, sewer pipe rupture, fountaining, flooding, soil erosion, etc. Such hydraulic failures related to surcharged flow in existing sewer systems are frequently encountered today. Guo and Song (1991) reported manhole cover blowout and fountaining at two drop manholes in Minnesota. Zhou et al. (2002) reported severe infrastructure damage due to surcharged flow at the Gallagher Hill Park manhole in Edmonton, Alberta, during a storm event of 1995. During an extreme storm event of 2004 in Edmonton, a number of manholes had problems of overflow and flooding and one manhole cover at the Whitemud Creek was washed out. Zhao et al. (2004) reported that a combining junction manhole at the Edworthy storm trunk in Calgary, Alberta, was blown off in 1998 resulting in a large fountain of several meters high. These failures can be related to various complicated mechanisms, while some of them may be primarily attributed to hydraulic performance of sewer junctions. Therefore, there is an urgent need to study the hydraulics of different types of sewer junctions to improve current municipal servicing guidelines.

1.1 Background

Sewer junctions can be basically classified according to the arrangement of connecting pipes:

1. Straight-through junction: inflow and outflow pipes are in a straight line in the horizontal alignment.
2. Bend junction: inflow and outflow pipes join the junction at an angle.
3. Combining junction: one outflow pipe and multiple inflow pipes join the junction.
4. Dividing junction: one inflow pipe and multiple outflows join the junction.

Sewers may join a junction at different elevations. If the elevation difference is significant (e.g. larger than 1 m in the City of Edmonton), the type of such a junction may be referred to as drop shafts or drop manholes. Other methods of the classification of sewer junctions were summarized by Yen (1986).

The base shape (the horizontal cross-section) of a sewer junction chamber is typically circular or square, but rectangular, trapezoidal or polygonal junction chambers are not uncommon for large sewer trunks. The diameter or size of a junction is usually not smaller than 1 m in order to allow operator room. Marsalek (1985) reported that the size of most frequent use for combining sewer junctions ranges from 2.3 to 4.6 times the joining pipe diameter.

In sewer design and sewer network modelling, the energy concept is generally applied to sewer junctions. Therefore, energy losses at sewer junctions have been of interest to researchers and engineers. Sewer junction flow can be subcritical flow, supercritical flow, or surcharged flow. Subcritical flow at sewer junctions has relatively small energy losses and they may be described as open-channel junction flow. Previous studies emphasized energy losses in surcharged flows.

One of the earliest studies of energy losses at sewer junctions was a field investigation conducted by Ackers (1959). The investigation included two straight-through manholes and two bend manholes of 45° and 52° with supercritical flow and surcharged flow. Most other studies were conducted in laboratories using model junctions and flows were subcritical or surcharged. Marsalek (1984) conducted a series of experiments to test straight-through junctions with square and circular chambers. Focus was given to effects of benching designs on reducing energy losses in the flow. Other studies of surcharged flows at straight-through sewer junctions include: Howarth and Saul (1984) who studied head losses in unsteady junction flow; Johnston et al. (1990) who observed less energy losses in deeply submerged flow; and Sakakibari et al. (1997) who tested rectangular junction manholes. An elegant theoretical tool was derived for surcharged straight-through junction flow by Pedersen and Mark (1990) based on the jet theory, which explained the effect of the chamber length on energy losses. At bend junctions, sewer flows are deflected and energy losses are expected to be larger than that at straight-through junctions. Archer et al. (1978) conducted laboratory experiments in model junctions of 30° and 60° bends to investigate head losses in surcharged flows. Hare (1983) reported an experimental study of bend junctions with various angles from 0°~90°. 90° bend junctions were studied by Marsalek and Greck (1988) and several types of benching designs were compared.

Combining junctions are widely used in sewer networks as sewers are connected from one level to the other with larger trunks and eventually transported into treatment plants or receiving water such as rivers or lakes. The most common type of combining junctions would be the three-way junction with two inflows and one outflow. This

junction may be regarded as a combination of a straight-through junction with a bend one, and the basic model of other combining junctions.

Flow at combining junctions is complicated. While involving interactions of multiple incoming streams, regions of mixing, separation, turbulence and transition of free-surface flow and surcharged flow exist. The flow changes rapidly at the junction and junctions usually have very limited transition room for it. Also, combining junctions can have significant impact on the carrying capacity of the sewer system and special considerations are required in design. However, only few studies of combining sewer junctions can be found in the literature. Marsalek (1985) conducted laboratory experiments of head losses in subcritical and surcharged flows at 90° combining junction manholes, and guidance for benching design was proposed. A recent study of three-way and four-way right angle junctions was presented by Wang et al. (1998).

Supercritical flow is considerably different from subcritical flow. In supercritical junction flows, shock waves are generated due to changes in flow conditions at the junction. Wave patterns at the junction are the most important feature of the flow. Under such conditions, the traditional sewer design concept of uniform flow may not be applicable because shock waves can choke the sewer before the uniform flow depth reaches its limit. Supercritical sewer junction flows have received attention in the recent past. Experimental studies were conducted at a straight-through junction by Gargano and Hager (2002), a bend junction by Del Giudice et al. (2000), a 45° combining junction by Del Giudice and Hager (2001), and a 90° combining junction by Gisonni and Hager (2002). These studies were confined to observations of wave configurations and measurements of water surface profiles in sewer junctions.

In previous sewer junction studies, methodologies used were primarily traditional hydraulic experimentations without looking into details of the fluid mechanics. With recent advances in computational power and advanced numerical solution algorithms, three-dimensional (3-D) computational fluid dynamics (CFD) simulations are now more and more widely used in hydraulic studies as an alternative and/or a complement to lab experiments. An example is the 3-D simulation study by Huang et al. (2002) for flows in open-channel junctions. Through the CFD simulation, detailed information about flows can be obtained. However, the author did not find applications of CFD on sewer junction flows in the literature.

Overall, flows at sewer junctions are complicated, while knowledge of their hydraulic characteristics is very limited. A general hydraulic description is yet to be derived. Current practices of sewer junction designs mostly rely on empirical relations from a limited number of experimental studies and on the knowledge of channel junctions or pipe junctions. Insufficient attention has been paid to optimize the flow in junctions other than standard benchings. Such situations can be hazardous to sewer design and management practices. Further study to advance the knowledge of sewer junction hydraulics is necessary and valuable, especially when existing drainage systems are challenged today by a combination of urban growth, ageing of sewers and climate change.

1.2 Scope and Approaches of the Study

The present research focuses on the hydraulics of sewer flows at three-way combining junctions. The objectives of this study are to

- Examine flow patterns and flow regimes in combining junctions with 25.8°, 45°, and 90° lateral inflows and two opposite lateral inflows for different combinations of incoming flows in the laboratory and by computer simulation.
- Evaluate the application of CFD modelling for simulating sewer junction flows.
- Provide information and knowledge for improving current municipal servicing guidelines and for optimizing sewer junction design and construction.
- Provide a basis of generalizing hydraulic descriptions for combining sewer junctions.

The research started with a case study of the Edworthy storm trunk junction in Calgary, Alberta. As presented in Chapter 2 of this thesis, the junction has two inflows merging at 25.8°. The junction was designed to retrofit the problematic junction at the Edworthy trunk. A physical model was constructed to test the performance of the design. Observations and theoretical analyses were carried out for water depth variation and energy losses in the junction chamber. Three flow regimes were identified in this study as supercritical flow across the junction, partly surcharged flow, and fully surcharged flow. The effectiveness of the retrofitting design was validated in this experimental study and information and recommendations were provided for design improvement.

In Chapter 3, surcharged flows at the Edworthy model junction were further investigated. Velocity measurements were taken using a micro acoustic Doppler velocimeter (MicroADV) and mean velocity distributions in the flows were presented. The velocity measurements revealed the flow structures in the junction. Then, efforts were made in experiments of a 90° model junction with more general geometry to seek

causes and criteria for the flow regime transitions, and to generalize the study. The downstream pipe of the junction was laid at various slopes. In the experiments, the general existence of the three flow regimes was confirmed. It was found that the transition from the partly surcharged flow regime to the fully surcharged flow regime may be related to the inlet waves in the outlet pipe. A theoretical tool based on one-dimensional momentum equation was established for the surcharged flows. Generalized results of water depth variations and energy coefficients in the flows were presented.

Chapter 4 presents a computational study of the fully surcharged flow at the 90° model junction. CFD simulations were carried out using a commercial code, Ansys CFX 10.0. Two types of multiphase flow models were employed and evaluated. At the same time, velocities of the flow were measured using a MicroADV and water surface profiles in the junction chamber were recorded. These measurements provided strong validation for the numerical models. Details of the flow were obtained and discussed, including flow structure, energy dissipation and air entrainment. Then the validated numerical model was applied to test effects of the junction chamber size on energy losses. The feasibility of using CFD to study sewer junction flows was confirmed through this study.

In Chapter 5, an attempt is made to develop a comprehensive picture of sewer flow at three-way combining junctions. Experiments of colliding inflows at a model junction with two opposite lateral inflows were carried out. Meanwhile, the validated numerical model was used to simulate the fully surcharged flow at a 45° junction. All the results along with those obtained in previous chapters were compiled, analyzed and presented in a generalized form useful for practical design.

Chapter 6 concludes this study and provides some suggestions for further study.

References

Archer, B., Bettess, F. and Colyer, P. J. (1978). "Head losses and air entrainment at surcharged manholes." *Report No. IT 185*, Hydraulics Research Station, Wallingford.

Ackers, P. (1959). "An investigation of head losses at sewer manholes." *Civil Engineering and Public Works Review*, 54(637): 882-884 and 1033-1036.

Del Giudice, G., Gisonni, C. and Hager, W. H. (2000). "Supercritical flow in bend manhole."

Del Giudice, G. and Hager, W. H. (2001). "Supercritical flow in 45 degree junction manhole." *Journal of Irrigation and Drainage Engineering*, ASCE, 127(2): 100-108.

Gargano, R. and Hager, W. H. (2002). "Supercritical flow across sewer manholes." *Journal of Hydraulic Engineering*, ASCE, 128(11): 1014-1017.

Gisonni, C. and Hager, W. H. (2002). "Supercritical flow in the 90° junction." *Urban Water*, 4(4): 363-372. *Journal of Irrigation and Drainage Engineering*, ASCE, 126(1): 48-56.

Guo, Q. and Song, C.S. (1991). "Dropshaft hydrodynamics under transient conditions. *Journal of Hydraulic Engineering*, ASCE, 117(8): 1042-1055.

Hare, C. M. (1983). "Magnitude of hydraulic losses at junctions in piped drainage systems." *Civil Engineering Transactions, the Institution of Engineers, Australia*, CE 25 (1): 71-76.

Howarth, D.A. and Saul, A.J. (1984). "Energy loss coefficients at manholes." *Proceedings of the Third International Conference on Urban Storm Drainage*, Vol.(1): 127-136, Chalmers University of Technology, Gothenburg, Sweden.

Huang, J., Weber, L. J., and Lai, Y. G. (2002). "Three-dimensional numerical study of flows in open-channel junctions." *Journal of Hydraulic Engineering*, ASCE, 128(3): 268-280.

Johnston, A.J., Volker, R.E. and Saul, A.J. (1990). "Head losses at a two-pipe junction box." *Transactions of the Institution of Engineers, Australia: Civil Engineering*, CE 31(4): 169-175.

Marsalek, J. (1984). "Head losses at sewer junction manholes." *Journal of Hydraulic Engineering*, ASCE, 110(8): 1150-1154.

Marsalek, J. (1985). *Head Losses at Selected Sewer Manholes*. National Water Research Institute, Canada Centre for Inland Waters, Burlington, Ontario.

Marsalek, J. and Greck, B. J. (1988). "Head losses at manholes at 90° bend." *Canadian Journal of Civil Engineering* 15: 851-858.

Pedersen, F.B. and Mark, O. (1990). "Head losses in storm sewer manholes: submerged jet theory." *Journal of Hydraulic Engineering*, ASCE, 116(11): 1317-1328.

Sakakibari, T., Tanaka, S. and Imaida, T. (1997). "Energy loss at surcharged manholes – model experiment." Water Science and Technology, 36(8-9): 65-70.

Wang, K.H., Cleveland, T.G., Towsley, C. and Umrigar, D. (1998). "Head loss at manholes in surcharged sewer systems." *Journal of the American Water Resources Association*, 34(6): 1391-1400.

Jia, Y., Scott, S., Xu, Y., Huang, S. and Wang, S. S. (2005). "Three-dimensional numerical simulation and analysis of flows around a submerged weir in a channel bendway." *Journal of Hydraulic Engineering*, ASCE, 131(8):682-693.

Yen, B.C. (1986). "Hydraulics of sewers." *Advances in Hydroscience*. Edited by B. C. Yen, Academic Press, New York. Vol.14: 1-122.

Zhao, C.H., Zhu, D.Z. and N.Rajaratnam (2004). "Supercritical sewer flows at a combining junction: a case study of Edworthy Trunk Junction, Calgary, Alberta." *Journal of Environmental Engineering and Science,* NRC, 3(5): 343-353.

Zhou, F., Hicks, F. E. and Steffler, P. M. (2002). "Transient flow in a rapidly filling horizontal pipe containing trapped air." *Journal of Hydraulic Engineering*, ASCE, 128(6): 625-634.

Chapter 2

Supercritical Sewer Flows at a Combining Junction: A Model Study of the Edworthy Trunk Junction, Calgary, Alberta*

2.1 Introduction

As urban areas continue to develop, existing storm sewer systems are frequently overloaded hydraulically as evidenced by surcharged manholes and flooded inlets. Surcharged manholes could result in serious problems such as the blowout of manhole covers, occurrence of fountains and flooding (Guo and Song 1991; Zhou et al. 2002). In the City of Calgary, Alberta, a manhole cover on Edworthy Road was blown off and a fountain was formed during the storm on 18 June, 1998 (Figure 2.1). Denoted as MH525 in Figure 2.2, the problematic manhole has a 90° T junction consisting of two inflow conduits: a circular pipe with an inner diameter of D = 1.372 m and a box with a width of W = 1.067 m and a height of Y = 1.219 m. The outlet conduit is also a box duct having the same dimensions as the inflow box. The circular pipe carries the main flow from an upstream subdivision with a design discharge of 10 m^3/s, while the rectangular duct carries a smaller controlled flow from a storm pond with a design discharge of 2.26 m^3/s. The free-flow capacity of the inflow pipe (i.e. the discharge of uniform flow in a closed conduit that is just full but pressure free) is 12 m^3/s based on a slope of 0.05 and the outflow duct has a capacity of 14 m^3/s at a slope of 0.07. Therefore, the sewer conduits are believed to have enough carrying capacity. Given that the capacity of the outflow

* *A version of this chapter has been published. Zhao, C.H., Zhu, D.Z. and N. Rajaratnam (2004). Journal of Environmental Engineering and Science, National Research Council, 3(3): 343-353.*

duct increases downstream, the junction could be the bottleneck of the sewer trunk. As the main inflow is routed to turn 90°, the manhole is prone to surcharge and fountains as the hydraulic grade line (HGL) rises above the ground level.

A retrofitting scheme was proposed by Stantec Consulting and the City of Calgary to make the two inflows merge more smoothly in a new junction chamber, shown as MH525A in Figure 2.2, which has a smaller junction angle of 25.8°. The scheme is expected to reduce the energy loss and retain kinetic energy of the flow to avoid the excessive submergence in the manhole. The main inflow will be delivered to the junction using a new diversion pipe consisting of three 38° bends while manhole MH524 will be plugged. In addition, the duct downstream of MH525A (FH) will be replaced with a circular pipe. The proposed new junction, MH525A, is shown in Figure 2.3.

Given that the sewer conduits have steep slopes and the flows can be supercritical, the hydraulic performance of such a junction chamber as MH525A is of crucial concern to designers. Supercritical flow behaves quite differently from subcritical flow. One distinctive characteristic of supercritical flow is that, any disturbance on highly energetic supercritical flow could produce violent waves. The shock wave may result in a breakdown of supercritical sewer flow in the form of choking or surcharge of the sewer. Thus, behavior of supercritical sewer flow needs to be carefully studied.

Both pipe flow and open-channel flow in combining junctions have been investigated recently (Ramamurthy et al. 1988; Ramamurthy & Zhu 1997; Hsu et al. 1998). Most studies about open-channel junctions have primarily focused on subcritical flow and a forthright application in manhole flows is difficult given that (1) significant changes in both boundary geometry and hydraulic conditions exist in manholes and (2)

transition from open-channel to pressurized flow could occur. Supercritical flow in a junction manhole is even more complicated.

Lindvall (1984) measured energy losses at a surcharged 90° model junction manhole. In his experiment, the outlet pipe was controlled to flow full. Del Giudice & Hager (2001) and Gisonni & Hager (2002) investigated wave configurations of open-channel flow in supercritical junction manholes. In practice, surcharge of manholes is permitted as long as the water level in the manhole is not overtopping and it is important to understand the transition of possible flow regimes in manholes and how the surcharged flow develops. So far, however, not much is known about flow developing and regime transition in a junction manhole.

In the present study, supercritical flows at a combining junction manhole were investigated using a physical model of the retrofit design for Edworthy Trunk. Various combinations of inflow rates were tested. The study focuses on the behavior of the combining flows and the water level in the chamber. The change of flow regime in the chamber was investigated and its relation to the incoming and outgoing flow regimes was explored. A theoretical approach was also developed to predict the water depth in the surcharged chamber. The energy loss of flow through the junction was measured and observations of supercritical flow in the bend diversion pipe were also made. This study aims not only to test the performance of the retrofit design, but also to further our knowledge of supercritical junction flow to aid in the design and retrofitting of these junctions.

2.2 Experimental Design

The supercritical junction flow at MH525A of the Edworthy trunk was modeled in the Hydraulics Laboratory in the Department of Civil and Environmental Engineering at the University of Alberta. The model was designed based on the Froudian similitude, i.e. $(F_r)_m = (F_r)_p$, where Froude number $F_r = V/\sqrt{gA/T}$; V is mean velocity, A is flow area and T is top width of the flow; g is the gravitational acceleration; and the subscripts m and p refer to the model and prototype respectively.

For the purpose of visual observation of flow, the model was built with Plexiglas™. Based on the available size of commercial acrylic pipes, a length scale of 1:9.00 was adopted, i.e. L_r = 9. This scale ratio results in a diameter of 152.4 mm (6 inches) for the circular pipe in the model. The range of the modeled sewer was determined to start at point A for the inflow pipe, M for the lateral box conduit, and end at point G (Figure 2.2). Dimensions of the model are summarized in Table 2-1. In Table 2-1, the free-flow capacity of each conduit, Q_f, is based on Manning's equation for uniform flow, i.e. $Q = AR_h^{2/3} S_0^{1/2} / n$, where R_h is the hydraulic radius and S_0 is the bottom slope. Obviously, all conduits will not flow full at the design discharges if the uniform flow is established.

In the experiment, two inflows were supplied with a constant head tank, and the inflow rates were measured with two in-line magnetic flow meters. The outlet of the downstream pipe, FG, was uncontrolled and the water was discharged freely to the underground reservoir through a large plastic pipe.

Experiments were mainly carried out for the model junction with a half benching (Figure 2.4a) and a square-edged entrance of the outlet pipe. In a supplementary test, a

rounded entrance (Figure 2.4b) was installed on the outlet pipe. Flow in the junction without benching (Figure 2.4c) was also investigated. As listed in Table 2-2, 168 combinations of inflows were tested, where Q_1 is the main flow from the inlet pipe and Q_2 is the lateral flow from the duct. The range of tested inflow rates covered the design discharges of 40.5 L/s for Q_1 and 9.3 L/s for Q_2.

2.3 Experimental Results

2.3.1 Flows in the Approaching Conduits

Most of the tested flows were supercritical in the sewer conduits with the Froude number F_r = 2~3, while at some large discharges the inlet pipe flowed full. When the supercritical flow Q_1 reached the first bend at B (Figure 2.2), the abrupt deflection caused a portion of the water to rotate along the outside wall of the bend. Thus, a part of the flow ran in a spiral longitudinally and the rest followed the bend with a separation zone at the inside of the bend (Figure 2.5). Actually all three bends (i.e. B, C and D in Figure 2.2) tended to make the supercritical flow rotate and become pressurized, but for a wide range of discharges, open-channel flow could be maintained due to the significant slope of 0.1737 of the diversion pipe (pipe BE, see Table 2-1).

For a relatively large discharge (about $0.5Q_{f1}$ where Q_{f1} is the free-flow capacity of the pipe AB as shown in Table 2-1), the pipe was choked at B and a hydraulic jump formed. Further increase in Q_1 resulted in pressurized flow in the diversion pipe BE and then in pipe AB. It was believed that the pipe-full flow in AB was mainly due to the limitation of the pipe length with which uniform open-channel flow cannot be developed, regarding that: (1) pipe AB started to be full from its inlet when open-channel flow was still maintained in the downstream part of the pipe at smaller discharges; (2) the tested

discharges were smaller than the free-flow capacity of pipe AB; and (3) at the maximum tested flow, the pressure in pipe AB was not very high (close to zero in fact) as was indicated by the observation that water did not continuously jet out from the air holes drilled at the crest of the pipe. Therefore, in the prototype the corresponding flow may be open-channel flow, but the discrepancy could be acceptable because the major concern of this study is the junction chamber and the deflection of the bends pressurized the flow in the diversion pipe BE first.

For the tested discharges, the lateral flow in the duct MN (Figure 2.2) was open-channel flow. A hydraulic jump occurred in the conduit when the chamber was surcharged. The location of the jump was mainly dependent on the lateral flow rate. Increase of Q_2 made the jump move upstream. The hydraulic jump did not reach the inlet of MN for the tested discharges. The slope of the duct was thus justified to be steep enough as it is expected that the choking of downstream will not affect the upstream condition of the approaching flow.

2.3.2 Flow in the Junction Chamber

In the experiment, observation was made on flow in the junction chamber with the variation of Q_1 for each fixed Q_2 listed in Table 2-2. At a small Q_1, supercritical flow could run through the junction and shock waves were formed due to the changes in geometry and hydraulic conditions. Two types of waves were observed (Figure 2.6a), so-called wave C and a swell (Del Giudice and Hager 2001): wave C is caused by the twin deflection of the two inflows, and the swell is due to the impingement of the surface flow portion on the end wall of the manhole. As discussed by Del Giudice and Hager (2001), the swell is predominant in determining the maximum wave height in the junction.

With increasing Q_1 wave C and the swell developed and finally made the manhole surcharged. Both the inlets and the outlet were submerged (Figure 2.6b). Near the entrances to the chamber, the two inflows transformed to pressurized flow with the occurrence of hydraulic jumps, but the outlet pipe was still partially full and the outflow performed as an orifice flow. The water level in the chamber rose relatively fast with the increase in Q_1.

When Q_1 was increased further, sudden priming in the outlet pipe and a significant drop of the water level in the junction chamber were observed. The outlet pipe became pressurized and the water level in the chamber was much smaller (Figure 2.6c). With increasing Q_1, the water level rose but more slowly.

Based on these observations, three flow regimes are distinguished and sketched in Figure 2.6:

(1) Regime I — In Regime I, supercritical open-channel flow can go through the chamber. Shock waves in the manhole are the dominant feature of the flow.

(2) Regime II — Regime II starts when the manhole is surcharged and it can be distinguished by the orifice flow at the exit of the chamber and open-channel flow in the outlet pipe. The inlet conduits are full near the entrance. The water level in the chamber increases quickly with increasing discharge.

(3) Regime III — Regime III starts with sudden priming in the outlet pipe and a considerable drop of water level in the junction chamber when the discharge reaches a certain level. This regime is primarily characterized by the pipe-full flow in the outlet pipe.

The variation of the water level in the surcharged chamber with Q_1 was measured for each Q_2. In Figure 2.6, h_m is defined as the vertical distance from the mean water surface to the invert of the outlet pipe and h_s similarly denotes the level of the swell. The measurements for Q_2/Q_{f3} = 0.10 and Q_2/Q_{f3} = 0.17 are shown in Figure 2.7 as h^* vs. Q_1/Q_{f3}, where the normalized depths, $h_s^* = h_s/D$ *and* $h_m^* = h_m/D$ respectively; Q_{f3} is the free-flow capacity of the outlet pipe FG shown in Table 2-1, Q_{f3} = 58.3 L/s. In Regime II, the water level increases relatively fast and reaches the maximum. (When Q_2 is relatively large, it even approaches the ground that is located at the corresponding level of $h^* = 3.14$) In Regime III, both the water level in the chamber and its rate of increase ($\partial h^*/\partial Q_1$) are smaller. At the transition from Regime II to III, the drop of water level is noticeable. Therefore, if Regime II flow can be developed in a surcharged manhole, Regime II will be the design flow condition in the sewer design as its water level is more critical than that of Regime III. It was also observed that the maximum water level in the chamber was dependent on the lateral discharge Q_2. As shown in Figure 2.8, the maximum mean depth in the chamber, $(h_m^*)_{max}$, increases with an increase in Q_2/Q_{f3}.

In Regime III the chamber flow was more violent, which is evidenced by the larger difference between h_s and h_m. To quantify the difference, the mean water surface slope S is defined as

$$S = (h_s - h_m)/L \tag{2.1}$$

where L is the length of the model chamber and L = 0.44 m. Variation of S with Q_2/Q_{f3} is presented in Figure 2.9. As shown in Figure 2.9, S was found to have little dependence on Q_1 (when Q_1 varied from 23 to 40.5 L/s the change in S was less than 0.05 in Regime III flow). Also, S appears to be independent of Q_2 in Regime II; but in Regime III, it

decreases from about 0.2 to 0.07 as Q_2 increases from 4 to 10 L/s. At a larger Q_2, S in Regime III approaches the value in Regime II. Given that the swell was caused by the combined flow impinging on the end of the chamber with a transformation of kinetic to potential hydraulic energy, Figure 2.9 may indicate that kinetic energy of the main flow is diffused in Regime II much more than in Regime III and, as a result, Regime II flow is less violent. Also most likely, S decreases and flow tends to be calm in Regime III as larger Q_2 leads more kinetic energy of the main flow to be dissipated and to transform to potential energy.

In Figure 2.10, the three flow regimes are classified as functions of Q_1/Q_{f3} and Q_2/Q_{f3}, where the solid lines were obtained in the procedure of increasing Q_1 for each fixed Q_2 and the broken lines were obtained in the reverse procedure of decreasing Q_1. It can be seen that the potential range of Regime II becomes wider for a larger Q_2. In addition, when the lateral flow was small ($Q_2/Q_{f3} < 0.04$), no stable Regime II could be formed in the procedure of increasing Q_1, where Regime I flow directly transformed to Regime III as evidenced by pressurized flow in the downstream pipe and the abrupt decrease in the swell height in the chamber.

It is worth pointing out that the transition from Regime II to Regime III does not appear to be caused by the total discharge ($Q_3 = Q_1+Q_2$, i.e. the discharge in the outlet pipe) exceeding the free-flow capacity of the outlet pipe. The transition happened at Q_3 around only 65% of Q_{f3}. Regarding the fact that the larger lateral flow helps diffuse more kinetic energy and results in a wider potential range of Regime II (Figure 2.10), the transition between Regime II and III is expected to be dependent on the mixing extent of

the two inflows, as well as the entrance condition of the outlet pipe, and not just the carrying capacity of the outlet pipe.

Figure 2.10 also shows that in the reverse test procedure of decreasing Q_1, both boundaries of the regimes move backwards to a smaller Q_1. This hysteretic phenomenon suggests that, once a regime is set up, it is stable and some kind of excitation may be needed for the regress of the regime. Besides, within the overlapped region of Regime II and III in Figure 2.10 (between the two boundaries of the transitions from Regime II to III and from III to II), stable Regime III flow could be set up. In other words, it may be possible to avoid the high water level occurring in Regime II flow by inducing the formation of Regime III flow in that region.

2.3.3 Energy Losses

Significant energy losses are expected due to the bends of the diversion pipe, the hydraulic jump in the box conduit and the mixing in the chamber. Total energy losses are defined as

$$\Delta H = [(Q_1 H_1 + Q_2 H_2) - Q_3 H_3] / Q_3 \tag{2.2}$$

and the total head H is defined as

$$H = z + y + \frac{V^2}{2g} \tag{2.3}$$

where z is the invert elevation of conduits at the point where the water depth was measured; y is water depth and V is the mean velocity that could be calculated based on y and Q.

The efficiency of energy dissipation η is defined

$$\eta = \Delta H Q_3 / (Q_1 H_1 + Q_2 H_2) \tag{2.4}$$

Here H_1 was measured at the first bend of the approaching pipe (B in Figure 2.2); H_2 was measured in the inflow box near the entrance of the chamber and upstream of the jump (if it occurs) and H_3 was measured in the outlet pipe at 1 m from the chamber where the flow tended to be established. Based on the measurements, the efficiency of energy dissipation for Regime I and II flow was calculated and the results are shown in Figure 2.11. It can be seen that the magnitude of efficiency for Regime I was close to that for Regime II with η ranging from 0.35 to 0.55. In Regime I flow, η appears well correlated with Q_1/Q_3 but not in Regime II flow.

Previous studies on surcharged manholes suggested that submergence in a surcharged manhole could have significant effects on the energy loss coefficient (Lindvall 1984). In Figure 2.11(c), η is plotted against the water depth, h_m^*. It is shown that when h_m^* increases with increasing Q_1, η decreases. It may be speculated that, when the loss in the chamber becomes smaller, more kinetic energy in the flow could be maintained and finally Regime III would occur.

One should notice that, in Regime II, a hydraulic jump occurred in the approaching box, which is a source of energy dissipation that did not occur in Regime I. At this stage, investigations on the energy dissipation are quite preliminary and data for Regime III were not obtained.

2.4 Theoretical Analysis on Regime II Flow

In previous studies on manhole junctions, surcharged flow was usually controlled to be Regime III by forcing the pipe-full flow in the outlet pipe. Thus Regime II was not observed. As Regime II flow could be the most critical condition in the consideration of water level in a surcharged manhole, it would be useful to predict the water level for

Regime II flow under given flow conditions. Here a theoretical analysis was conducted based on the momentum equation.

As is shown in Figure 2.9, the mean water surface slope in the chamber is about 0.05 for Regime II flow. Accordingly the difference between h_s and h_m can be neglected in this analysis. A simplified junction is shown in Figure 2.12. With the assumptions of hydrostatic pressure distribution and negligible friction forces, the momentum equation can be applied over the control volume defined in Figure 2.12. In the direction of the main flow Q_1,

$$\rho\left(\frac{Q_3^{\,2}}{C_c A_3} - \frac{Q_1^{\,2}}{A_1} - \frac{Q_2^{\,2}}{A_2}\cos\theta\right) = P_{ux} - P_{dx} - P_{ws}\sin\theta \tag{2.5}$$

where A_i is cross-sectional area of sewer conduits; in the present study $A_1 = A_3 = \pi D^2/4$ and $A_2 = WY$; θ is the junction angle; P_{ux} and P_{dx} are upstream (subscript u) and downstream (subscript d) net pressure forces in the longitudinal direction respectively and P_{ws} is sidewall pressure force; C_c is contraction coefficient. At section 3, water depth in the outlet pipe is C_cD. In a circular pipe (with diameter D and the cross-sectional area $A = \pi D^2/4$) with a water depth of y, the flow area can be approximated by $(y/D)A$ with an error of less than 5% if $y/D > 0.4$. Therefore, to avoid complications with the geometry of a partially filled pipe, the flow area at section 3 is approximated by C_cA_3 in Eq (2.5).

The pressure forces,

$$P_{ux} = \tfrac{1}{2}\rho g h_m^{\,2} B_u \tag{2.6}$$

$$P_{dx} = \tfrac{1}{2}\rho g h_m^{\,2} B_d - \rho g A_3 (h_m - D/2) + P_3 \tag{2.7}$$

where, B_u and B_d are the upstream width and downstream width of the chamber respectively; P_3 is the pressure force at section 3.

For partially-full flow in a circular pipe, similar with the approximation for flow area, the hydrostatic pressure force on a cross-section can be approximated by $P = \frac{1}{2}\rho g A D(y/D)^{2.2}$ with an error of less than 3% when the filling ratio $y/D > 0.5$. Accordingly,

$$P_3 = \tfrac{1}{2}\rho g A_3 D C_c^{2.2} \tag{2.8}$$

The x component of sidewall pressure force is

$$P_{ws}\sin\theta = \tfrac{1}{2}\rho g h_m^{2}\cdot(B_u - B_d) \tag{2.9}$$

Substituting Eqs.(2.6~2.9) into the right hand section of Eq. (2.5), the net pressure force can be obtained by

$$R.H.S. = \sum P = \rho g A_3 h_m - \tfrac{1}{2}\rho g A_3 D(1 + C_c^{2.2}) \tag{2.10}$$

Accordingly, with $Q_3 = Q_1 + Q_2$, some algebraic manipulations on Eq. (2.5) with Eq. (2.10) gives

$$h_m^{*} = \frac{h_m}{D} = \frac{1}{C_c}Q_3^{*2} - \frac{A_1}{A_3}Q_1^{*2} - \frac{A_2}{A_3}Q_2^{*2}\cos\theta + \tfrac{1}{2}(C_c^{2.2} + 1) \tag{2.11}$$

where $Q_i^{*} = Q_i/(gD_3A_i^2)^{1/2}$ and $i = 1$, 2, and 3. Thus, once the contraction coefficient C_c is determined, water depth in the chamber in Regime II can be predicted with Eq. (2.11) for any given Q_1 and Q_2.

The outflow in the Regime II behaves like an orifice flow. For flow under a sluice gate, a contraction coefficient of 0.61 is commonly recommended (Henderson, 1966). For a circular pipe, a different value of the contraction coefficient is expected. Smith (1995) suggested a contraction coefficient of 0.7 for orifice flow in circular-pipe culverts with a square-edged entrance. Based on observation in the present experiment, C_c varies around 0.7~0.8 for the square-edged entrance of the outlet pipe. Hence, a value of 0.75 was used

for the contraction coefficient for the square-edged entrance. The predicted water depth using Eq. (2.11) is compared with measurements in Figure 2.13 and satisfactory agreement is seen.

One should notice that the contraction coefficient C_c is affected by various parameters including inlet/chamber geometry, discharge, water depth in the chamber, etc. In the present flow, C_c appeared to be mainly dependent on Q_1 probably because the approaching velocity of the main flow was dominant, which could distinguish the flow from culvert flow or gate flow where effects of approaching velocity are usually neglected. For more accurate prediction, variation of C_c needs to be calibrated. However, based on Eq. (2.11), an uncertainty analysis showed that using a constant C_c of 0.75 for the present flow (with an uncertainty of ±0.05) resulted in the uncertainty in predicted h_m^* of less than 15%, which would be acceptable in practice.

The effect of C_c on the submergence level can be estimated using Eq. (2.11) for Regime II flow. Based on Eq. (2.11), $\partial h_m^*/\partial C_c < 0$ for $Q_3^* > 0.7$, which means that underestimating C_c will result in a larger prediction of h_m^* (more conservative). In other words, a modified entrance to the downstream pipe with a larger C_c could mitigate the submergence in the chamber. This is similar with orifice flow in other systems like culverts, but the effect would be smaller since in comparison, one can find a quite smaller slope (the magnitude of $\partial h_m^*/\partial C_c$) from Eq. (2.11) and physically the approaching velocity head in the present flow is not negligible.

Once the water depth is predicted, energy losses in Regime II flow can be evaluated. Over the control volume in Figure 2.12, the energy head of each section (subscripts 1, 2, and 3) can be written as

$$H_1 = h_m + \frac{Q_1^2}{2gA_1^2}; H_2 = h_m + \frac{Q_2^2}{2gA_2^2}; \; H_3 = C_c D + \frac{Q_3^2}{2g(C_c A_3)^2} \tag{2.12}$$

Energy loss coefficient is defined as

$$K = \Delta H \Big/ (\frac{V_3^2}{2g}) \tag{2.13}$$

where $V_3 = Q_3/A_3$. As h_m can be computed from Eq. (2.11), the coefficient K could be determined. A sample computation is carried out for junctions of 25.8° (this study), 60° and 90°. Assuming a C_c value of 0.75, variations of K with Q_1/Q_2 are shown in Figure 2.14 for $Q_2^* = 0.4$. It is clear that when the two inflows are equivalent, a larger junction angle will give rise to a much larger K. But when the main flow becomes more dominant (Q_1), K is less sensitive to the angle. Notice that this energy loss analysis is limited to the junction chamber with Regime II flow.

2.5 Effect of Rounded Entrance and Benching

The maximum depth in the junction chamber occurred in Regime II. Based on the theoretical analysis, the water level in the surcharged chamber with Regime II flow is dependent on the contraction coefficient C_c at the exit of the chamber and increase of C_c is expected to suppress the submergence. One approach was tested in the experiment by using a partially rounded entrance to replace the square-edged entrance to the outlet pipe (Figure 2.4b). Besides, in order to evaluate the effect of the benching on the flow behavior in the junction, the model junction without benching (Figure 2.4c) was tested for comparison.

2.5.1 Performance of the Rounded Entrance

A rounded entrance was produced for the outlet pipe (Figure 2.4b). With this modification, the three flow regimes were still observed as in the original chamber with the square-edged exit. A positive result is that, for the same combination of Q_1 and Q_2, the water level was smaller. In Figure 2.15 measurements of h_m in Regime II flow with and without the rounded entrance are compared. For the rounded entrance, the contraction factor of about 0.8~0.85 was observed in the experiment. It is believed that the increase in C_c is the main reason for the smaller water level. Nevertheless, there was a transition zone in which the flow oscillated between Regime II and Regime III. In other words, the outflow oscillated between pipe-full and open-channel flow. The water level in the chamber dropped and rose periodically but the entrance of the outlet pipe remained submerged all the time. This oscillation became more frequent with an increase in Q_1, but eventually a stable Regime III was set up. As such oscillations are usually undesirable in hydraulic structures, the modification of the entrance should be carefully designed and further investigation is required.

In Figure 2.16 the measured water depth in the chamber with the rounded outlet pipe is compared with Eq. (2.11) based on the assumption of $C_c = 0.85$. The comparison again verifies the validity of the prediction for Regime II flow.

2.5.2 Effect of Benching

In this test, the benching in the chamber was removed with a small drop left (Figure 2.4c). The small drop in the chamber formed a pool; therefore, the free flow in the manhole was different from Regime I flow in the benched manhole as the shock waves were not distinct. After the manhole was surcharged, Regime II and III were

observed. At a transition region, oscillation between Regime II and III occurred as observed in the chamber with the rounded exit. The reason for the oscillation is not clear.

The water depth measured in the no-benching chamber was compared with that obtained in the original benched chamber in Figure 2.17. In Regime II, the results are slightly smaller than that in the benched manhole. The difference, though, is very small. In Figure 2.13, the measurement is also compared with predictions of Eq. (2.11) based on the assumption C_c=0.75 (shown as the solid squares). Obviously, Eq. (2.11) works well for the case without benching. Therefore, the conclusion may be drawn that benchings have very little influence on the water depth for Regime II flow in the junction.

However, in Regime III, the water depth is quite larger in the non-benched chamber (Figure 2.17). This may suggest that the water depth in Regime III flow be dependent on mixing losses in the junction flow since the loss in a benched manhole might be less than in a non-benched one. It should also be noted that, in the non-benched chamber, Regime III occurred at much smaller Q_1 than in the half-benched one. So, the water level in the chamber did not reach as high as in the benched manhole in the full range of tested flow rates. This fact suggests the possibility to enforce the occurrence of Regime III flow to avoid excessive submergence.

2.6 Summary and Conclusions

An experimental study on a supercritical junction manhole was conducted using a model of the retrofit design for the Edworthy trunk. The junction manhole with a small combining angle can merge inflows smoothly and help to retain kinetic energy of the flow, increase the discharge capacity of the sewer and prevent the occurrence of fountains.

In the junction chamber, three flow regimes were observed. Regime I is featured by open-channel flow with a shock wave and a swell in the chamber; Regime II is characterized with surcharge flow in the chamber and orifice flow to the outlet pipe; Regime III occurs accompanied with priming and pipe-full flow in the outlet pipe. For a fixed lateral discharge Q_2, the submergence in the chamber initially increases with Q_1 when the flow evolves from Regime I to Regime II. However, further increase in Q_1 leads to Regime III flow where the water level actually drops significantly. For the consideration of water level in a surcharged manhole, Regime II could be the design condition as the highest water level was observed in this regime.

A theoretical prediction for water depth in junction manholes in Regime II was developed. The prediction compared well with measurements. The analysis showed that the entrance to the outlet pipe with a larger contraction coefficient is potentially able to mitigate the submergence in Regime II flow. This was verified by a test on the rounded entrance, but an oscillation between Regime II and Regime III flow was observed in the chamber. Therefore, a proper design and investigation for the application of this technique are necessary since such oscillation needs to be avoided in hydraulic structures.

The effect of benching in the junction chamber was also studied. It was found that benching does not have significant effect on the water level in the chamber in Regime II flow. However, in Regime III, benching helps in suppressing the water depth in the chamber.

Significant energy losses were observed in the flow through the studied design. Experimental results showed an energy loss of about 35~55% that included head losses

due to friction, deflection of the bend pipe, hydraulic jump in the upstream conduits, flow mixing in the chamber, and local losses at the entrance and exit of the chamber.

Table 2-1 Model Dimensions

Segment	Size (D or $W \times Y$)	Length (m)	S_0	Design discharge (L/s)	Q_f (L/s)
AB (Pipe)	152.4 mm	3.3	0.0545	40.5	53.6
BE (Pipe)	152.4 mm	2.2	0.1737	40.5	95.6
MN (Box)	119mm×135mm	1.6	0.0715	9.3	47.7
FG (Pipe)	152.4 mm	2.2	0.0645	49.8	58.3

Note: D, diameter; W, width; Y, height; S_0, bottom slope; Q_f, free-flow capacity of each conduit.

Table 2-2 Test Program

Test case	Number of experiments	Q_1 (L/s)	Q_2 (L/s)
Benched junction	107	10 discharges from 6~40.5	6 discharges from 2~13
Rounded entrance	31	10 discharges from 15~34	4/6/8/10
No benching	30	10 discharges from 10~36	4/6/8

Note: Q_1, main flow from the inlet pipe; Q_2, lateral flow from the duct.

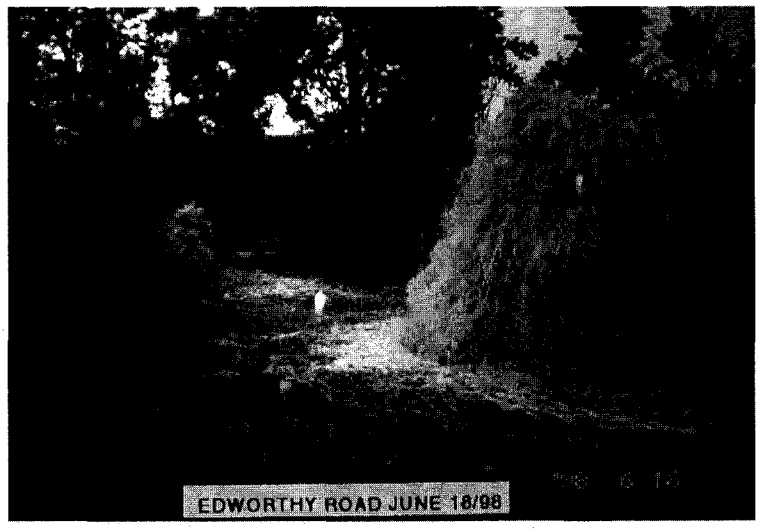

Figure 2.1 The fountain from the surcharged manhole of the Edworthy trunk in 1998 (Courtesy of the City of Calgary)

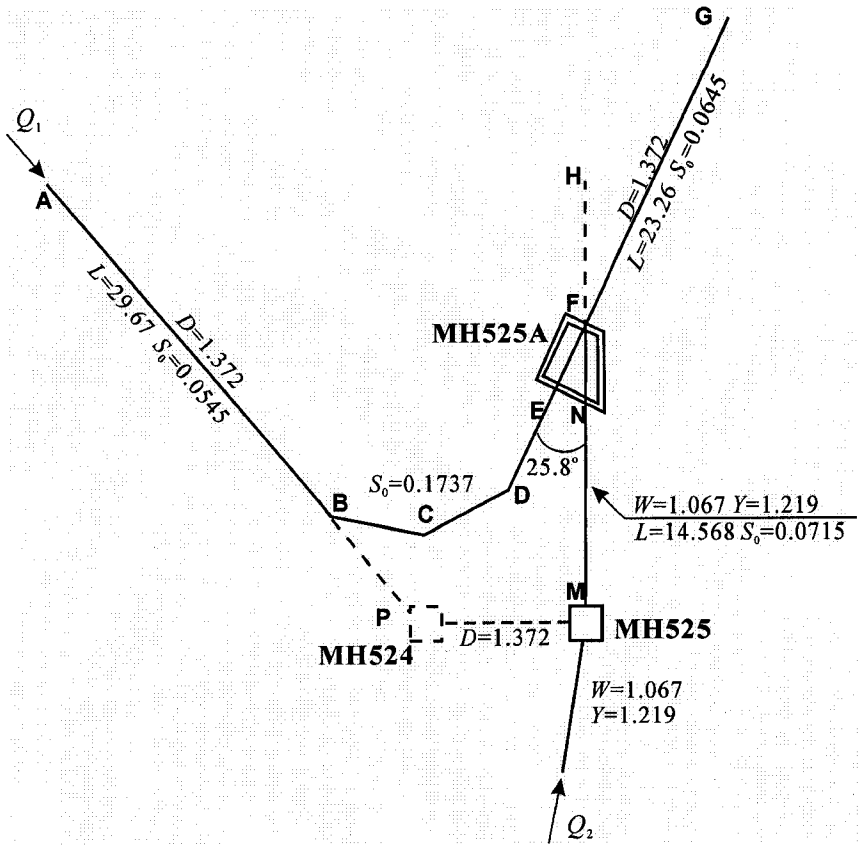

Figure 2.2 Edworthy trunk: reach of the study (All dimensions are in meters)

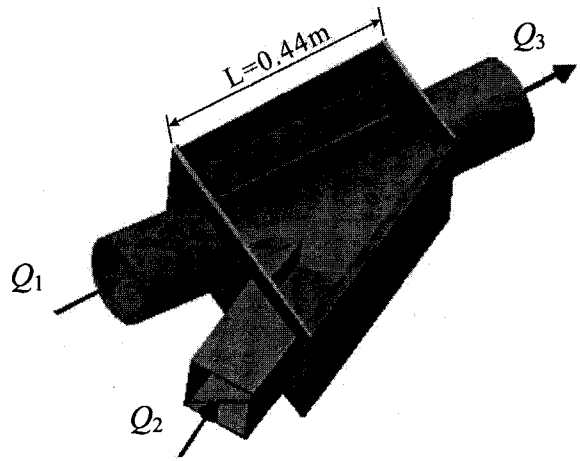

Figure 2.3 Schematic diagram of the junction chamber (MH525A)

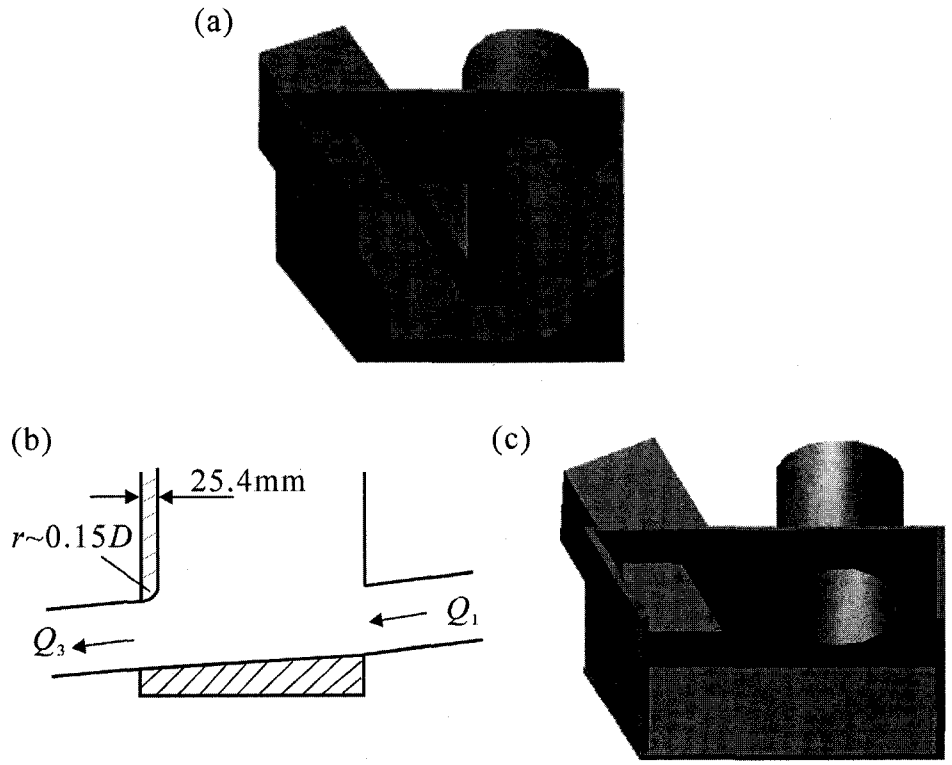

Figure 2.4 Features of tested chambers: (a) chamber with half benching (upstream view); (b) chamber with a rounded exit (side view); and (c) chamber without benching (upstream view)

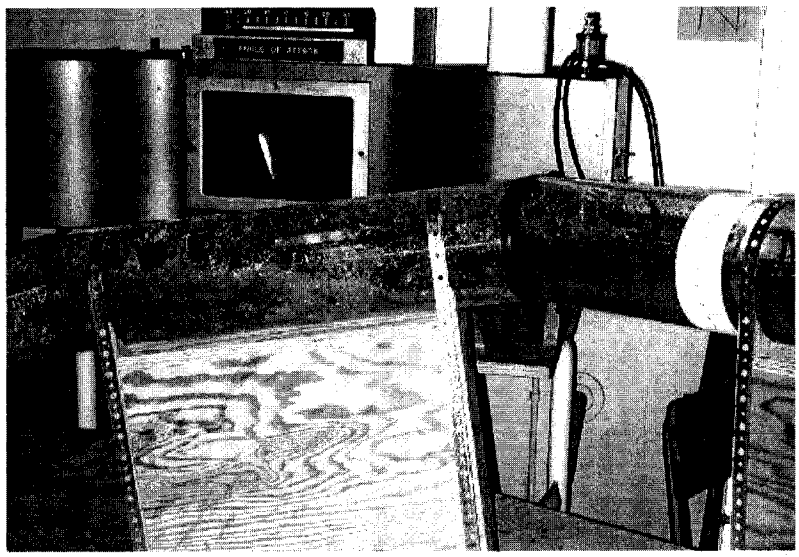

Figure 2.5 Flow in the bend diversion pipe

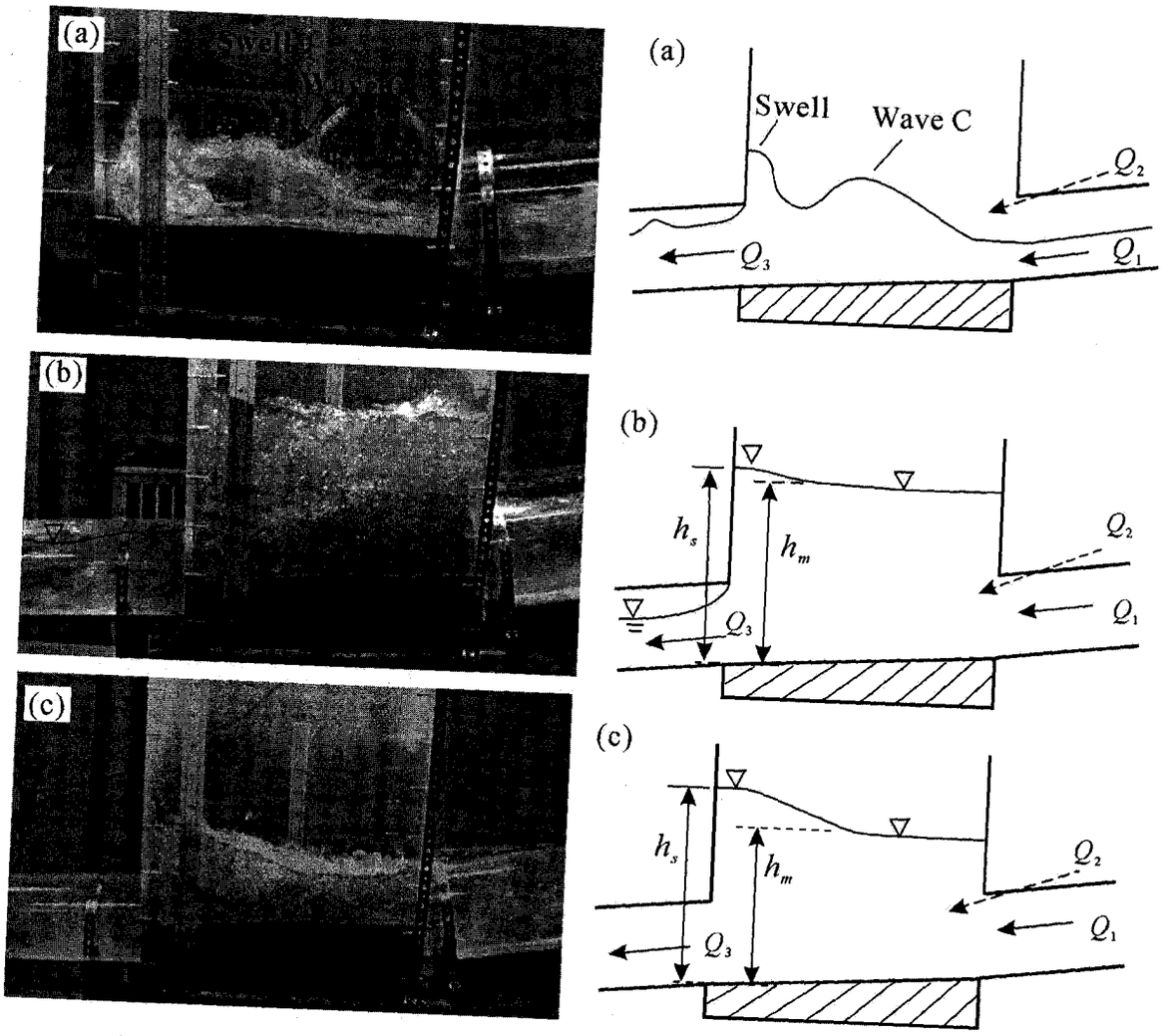

Figure 2.6 Flow regimes for Q_2 = 8 L/s: (a) Regime I (Q_1=16 L/s); (b) Regime II (Q_1=24 L/s); and (c) Regime III (Q_1=28 L/s)

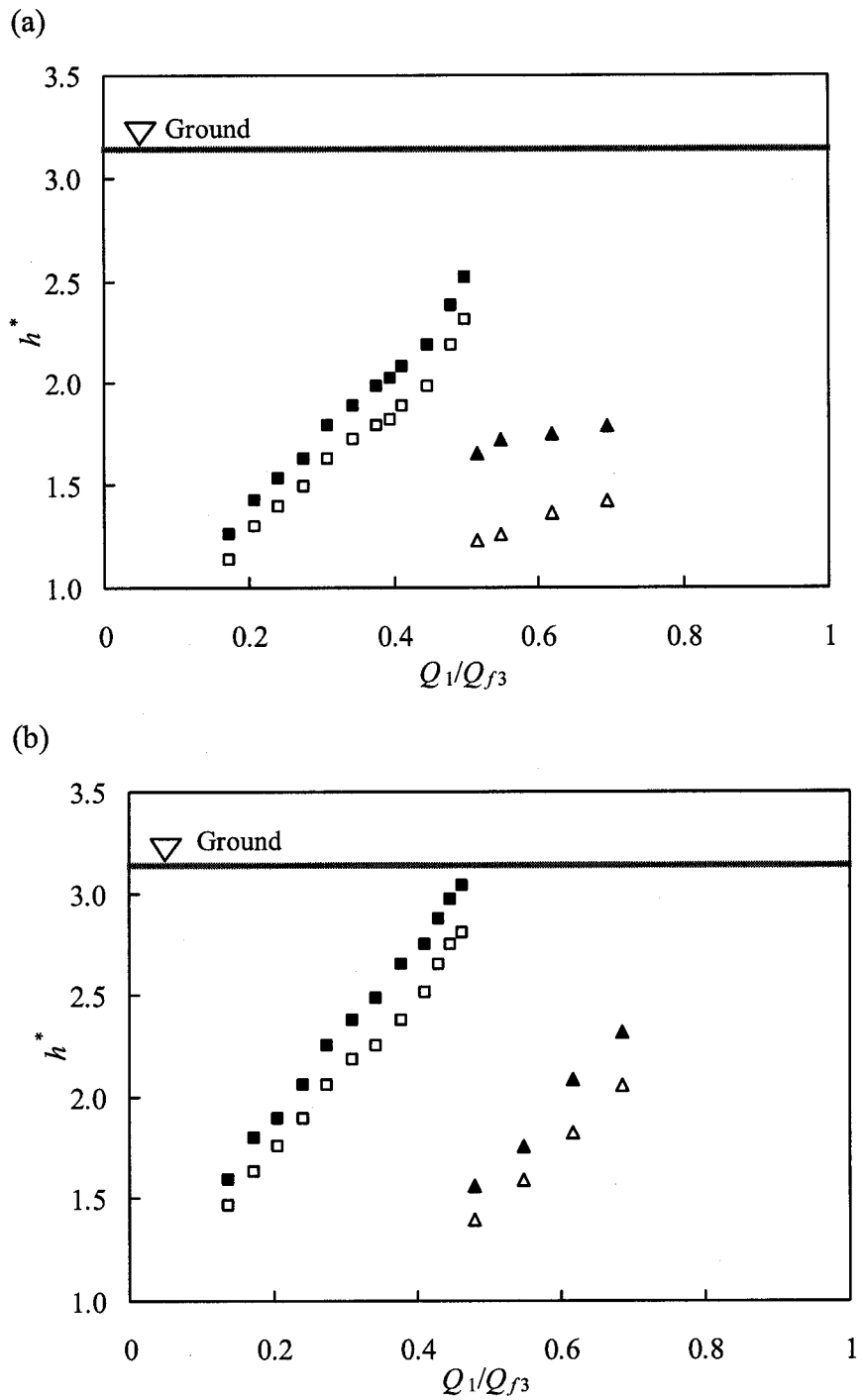

Figure 2.7 Variation of water level in the surcharged chamber with Q_1/Q_{f3} for (a) Q_2/Q_{f3} = 0.10; and (b) Q_2/Q_{f3} = 0.17: h_s in Regime II flow (■); h_m in Regime II flow (□); h_s in Regime III flow (▲); and h_m in Regime III flow (Δ)

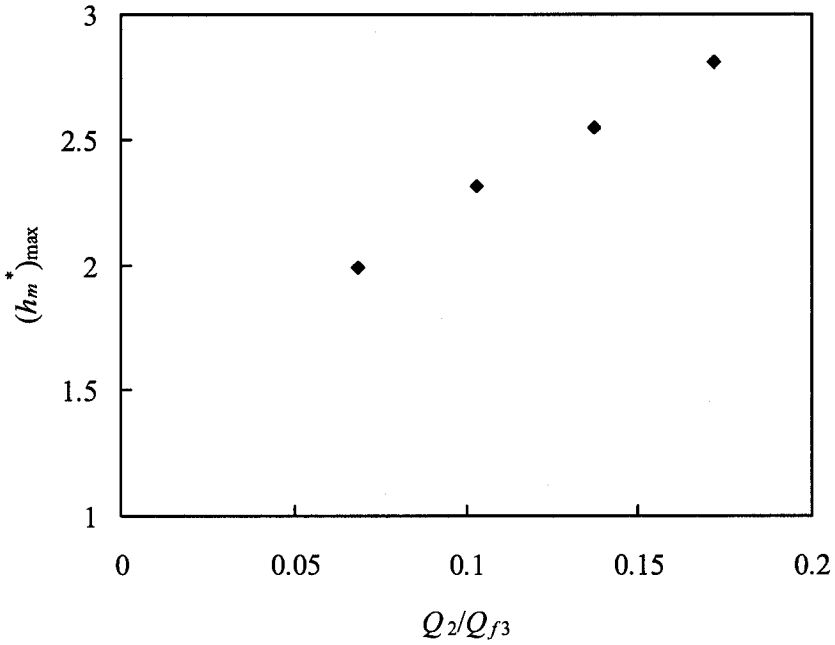

Figure 2.8 Variation of maximum depth in the surcharged chamber with lateral inflow

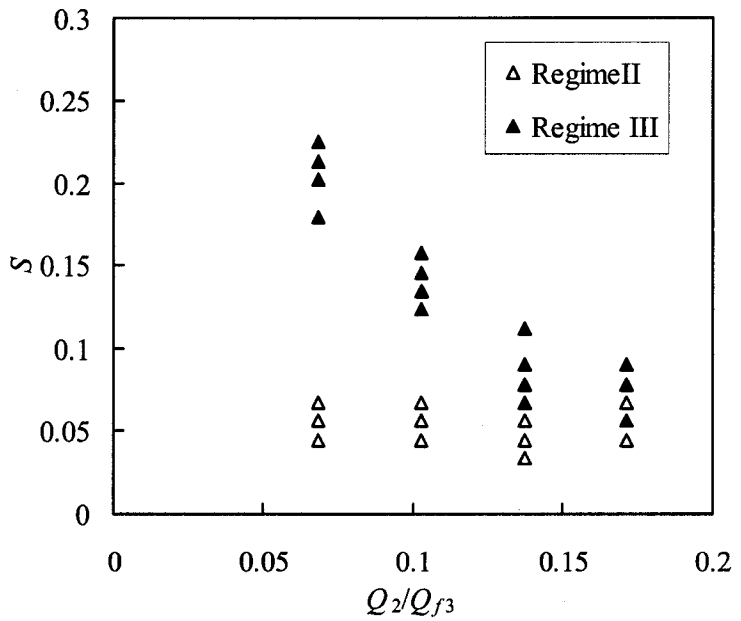

Figure 2.9 Variation of water surface slope in the chamber with lateral inflow (Q_1/Q_{f3} varies from 0.14 to 0.7)

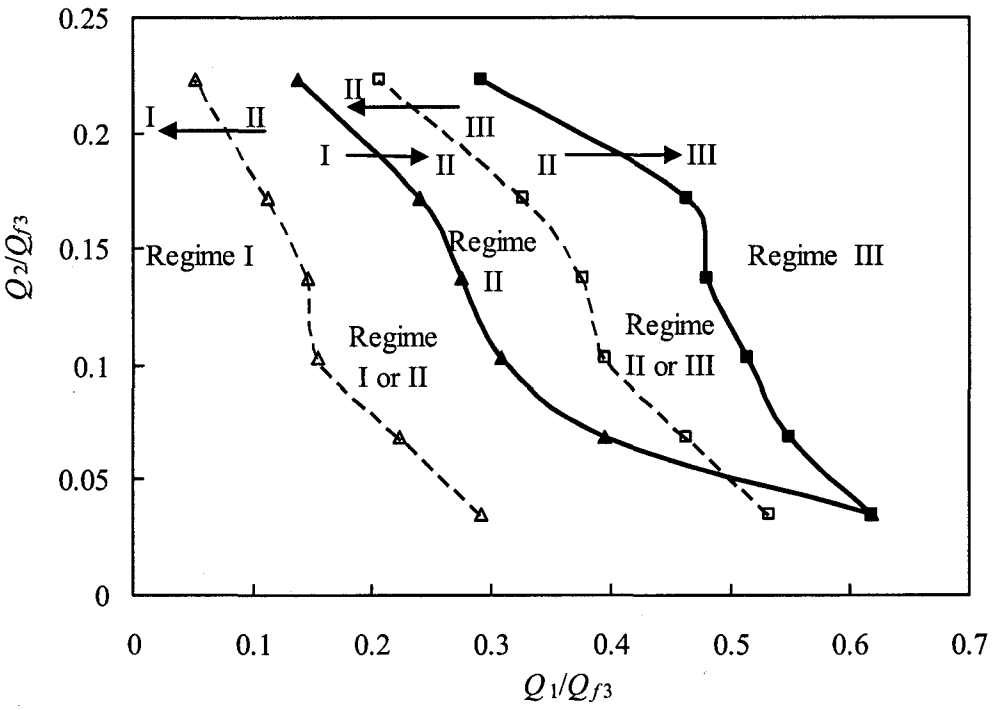

Figure 2.10 Classification of regimes

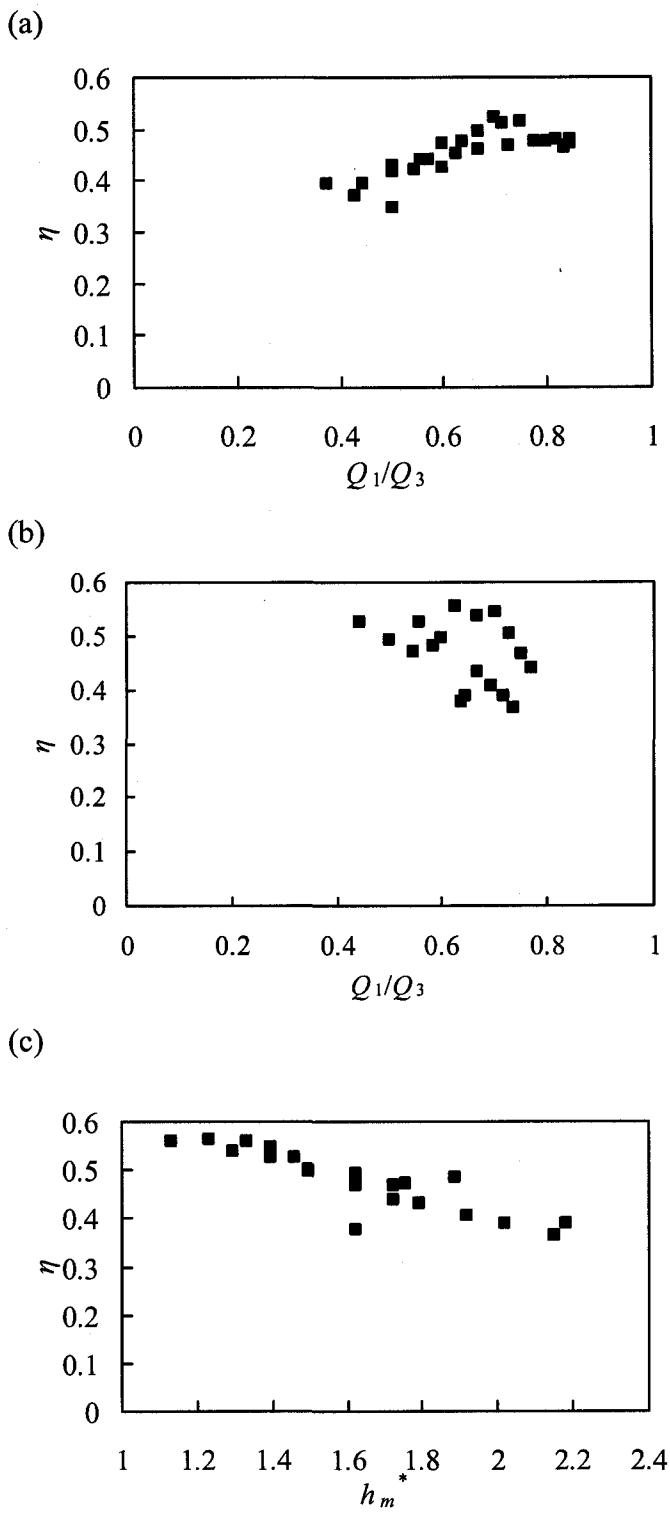

Figure 2.11 Efficiency of energy loss: (a) Regime I flow; (b) Regime II flow (η vs. Q_1/Q_3); and (c) Regime II flow (η vs. h_m^*)

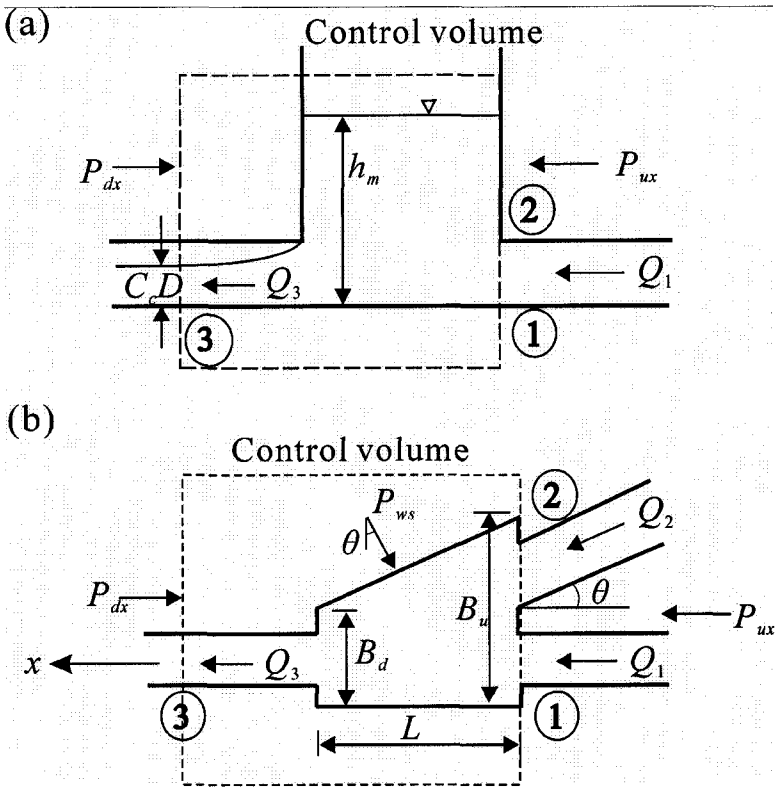

Figure 2.12 Definition of control volume for a junction manhole: (a) side view; and (b) plan view

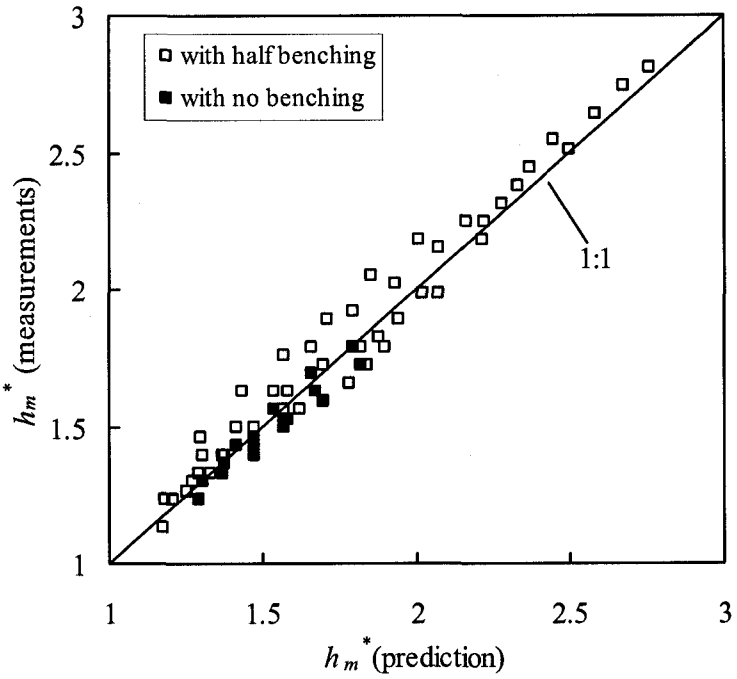

Figure 2.13 Comparison between prediction and measurement of water depth in Regime II flow ($C_c = 0.75$)

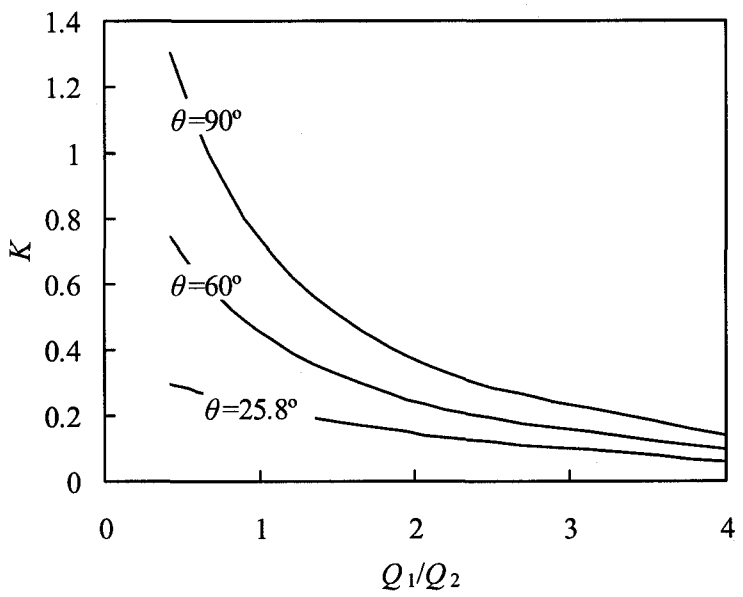

Figure 2.14 Variation of head loss coefficient (K) in combining junction manholes with inflow ratio and junction angle ($Q_2^* = 0.4$, C_c=0.75)

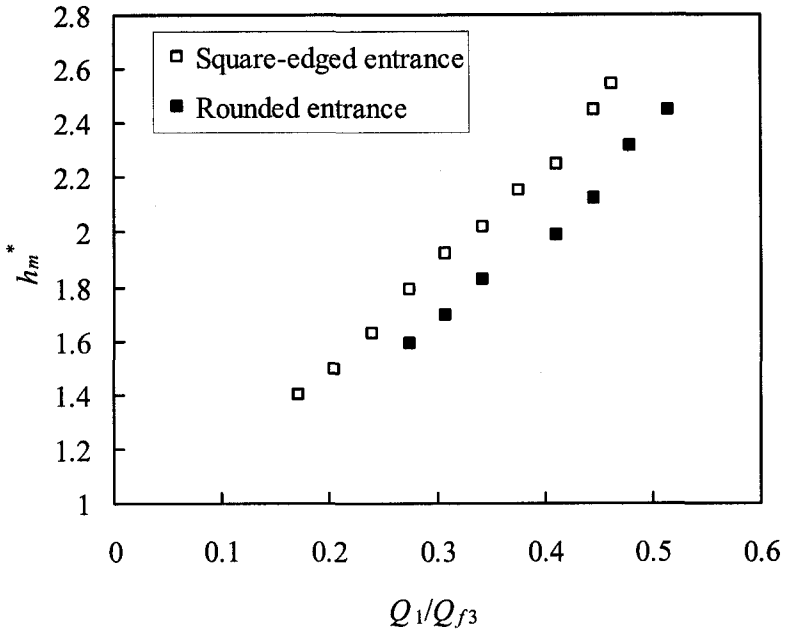

Figure 2.15 Comparison of square-edged entrance and rounded entrance of the outlet pipe in the water depth in Regime II flow ($Q_2/Q_{f3} = 0.14$)

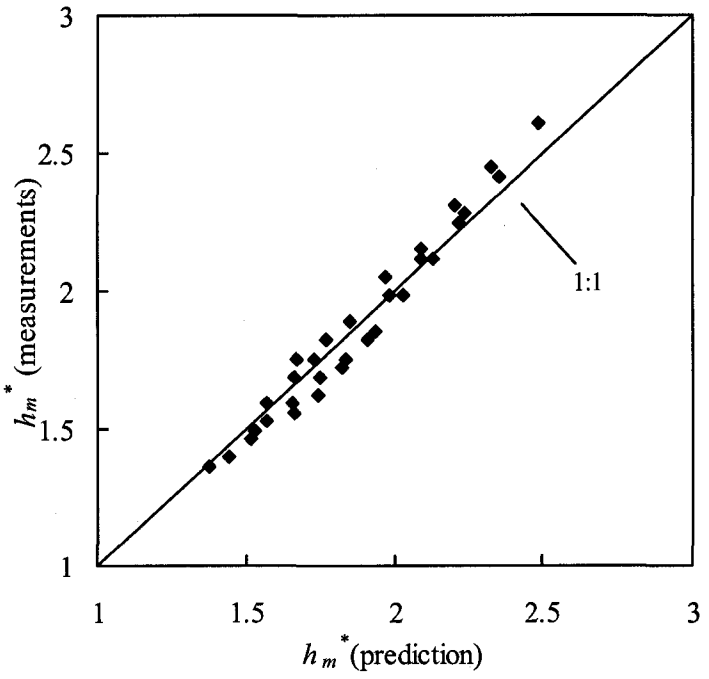

Figure 2.16 Comparison between predictions and measurements of water depth in the chamber with rounded exit in Regime II (C_c =0.85)

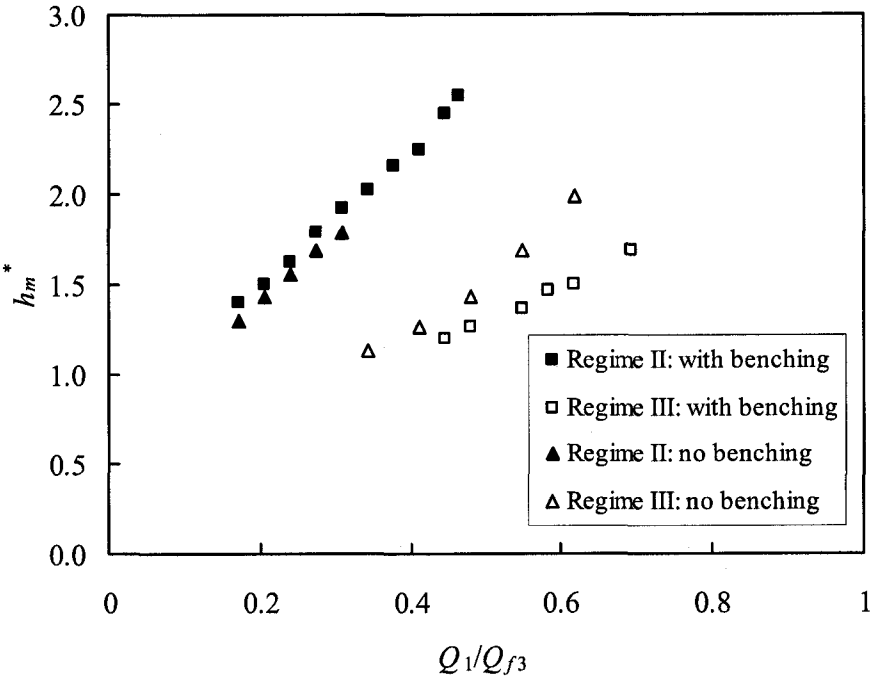

Figure 2.17 Comparison of the chambers with benching and without benching in the water depth ($Q_2/Q_{f3} = 0.14$)

References

Del Giudice, G. and Hager, W. H. (2001). "Supercritical flow in 45 degree junction manhole." *Journal of Irrigation and Drainage Engineering*, ASCE, 127(2): 100-108.

Gisonni, C. and Hager, W. H. (2002). "Supercritical flow in the 90° junction." *Urban Water*, 4(4): 363-372. *Journal of Irrigation and Drainage Engineering*, ASCE, 126(1): 48-56.

Guo, Q. and Song, C.S. (1991). "Dropshaft hydrodynamics under transient conditions. *Journal of Hydraulic Engineering*, ASCE, 117(8): 1042-1055.

Henderson, F.M. (1966). *Open Channel Flow*. Macmillan Company, New York.

Hsu, C., Lee, W. and Chang, C. (1998). "Subcritical open-channel junction flow." *Journal of Hydraulic Engineering*, ASCE, 124(8): 847-855.

Lindvall, G. (1984). "Head losses at surcharged manholes with a main pipe and a 90° lateral." *Proceedings of the Third International Conference on Urban Storm Drainage*, Göteborg, Sweden, Chamers University of Technology. Vol.1: 137-146.

Ramamurthy, A. S., Carballada, L. B. and Tran, D. M. (1988). "Combining open channel flow at right angled junctions." *Journal of Hydraulic Engineering*, ASCE, 114(12): 1449-1460.

Ramamurthy, A. S. and Zhu, W. (1997). "Combining flows in 90° junctions of rectangular closed conduits." *Journal of Hydraulic Engineering*, ASCE, 123(11): 1012-1019.

Smith, C. D. (1995). *Hydraulic Structures*. University of Saskatchewan, Saskatoon, Sask. Canada.

Zhou, F., Hicks, F. E. and Steffler, P. M. (2002). "Transient flow in a rapidly filling horizontal pipe containing trapped air." *Journal of Hydraulic Engineering*, ASCE, 128(6): 625-634.

Chapter 3

Experimental Study of Surcharged Flow at Combining Sewer Junctions*

3.1 Introduction

Sewer systems are characterized by sewer pipes joining at junctions to form a network. Normally sewer systems are designed to carry free-surface flow. Often full-pipe flows (or pressurized flows) are observed in storm/combined sewers when the flow rate exceeds the free-flow capacity of the system, which is also referred to as surcharged flow. Surcharged flow most likely begins to form at sewer junctions and may cause serious problems, such as blown-off manhole covers, sewer pipe rupture, flooding, and soil erosion. For example, in the City of Calgary, Alberta, the cover of a T-shaped combining junction manhole of the Edworthy storm sewer trunk was blown out resulting in large fountains of several meters high in 1998 (Zhao et al. 2004). Today, surcharged flow occurs more frequently in sewer systems due to a combination of urban growth, aging of the infrastructure and possibly climate change. While sewer flow in a single pipe is understood reasonably well, limited research has been conducted on sewer junctions.

At sewer junctions, subcritical or supercritical open-channel flow or surcharged flow can exist. Subcritical flow in sewer junctions has relatively small energy loss and may be described as open-channel junction flow. Detailed investigation on combining flow at open-channel junctions has been conducted recently (Hsu et al. 1998, Weber et al. 2001 and Shabayek et al. 2002). Supercritical flow at sewer junctions was studied by Del

A version of this chapter has been accepted for publication in the Journal of Hydraulic Engineering, ASCE, in March 2006.

Giudice and Hager (2001) and Gisonni and Hager (2002). Energy losses of fully surcharged sewer flow have also been investigated in straight-through junctions (Marsalek 1984 and Pedersen and Mark 1990), 90° bend junctions (Marsalek and Greck 1988) and 90° combining junctions (Marsalek 1985 and Wang et al. 1998). The word *fully* here refers to the specific situation where all incoming and outgoing pipes of the junction flow full. Yet, existing data are insufficient to develop a general description for the flow especially for the combining flow which is more common in sewer systems. Moreover, one surcharged flow pattern was omitted in previous studies in which the outgoing flow is open-channel flow while incoming pipes are full, as observed by Zhao et al. (2004).

Zhao et al. (2004) conducted a model study for a 25.8° combining junction with two inflows and one outflow, as sketched in Figure 3.1. The junction was designed to replace the problematic T-shaped junction of the Edworthy storm trunk mentioned above. In the experiment, three flow regimes were observed similar to those shown in Figure 3.2: (I) open-channel flow through the junction; (II) surcharged flow with free-surface flow in the outlet pipe; and (III) fully surcharged flow with both the inlet pipes and the outlet pipe pressurized. For the specific design of the Edworthy junction, Regime II was found to be the most critical condition as it has the maximum water depth in the chamber. In their study, the momentum equation was used for Regime II flow to analyze the variation of water depth in the junction chamber with inflow rates. Their study, however, focused on a particular design. It would be necessary and useful to extend their results for generalization and to further study Regime III flow and the transition from Regime II to Regime III.

The present study was undertaken to improve our understanding of flow regimes in sewer junctions, and in particular on surcharged junction flows. Experiments were carried out in sewer junction chambers with two incoming and one outgoing flows as such junctions are widely used in practice. The junctions studied included the 25.8° Edworthy model junction and a 90° model junction with simple geometry. Focus was given to the transition of the two surcharged flow regimes II and III to establish criteria for it. Each regime was studied experimentally and theoretically. Efforts were made to find an approach to a general description of sewer junction flows. Variations of water depth in the surcharged junction chambers were studied. Results of energy losses and velocity measurements in surcharged flow are presented. Information presented in this paper will serve as a useful guide to sewer junction design and improve our computer modeling capability of sewer flows.

3.2 Application of Momentum Equation in Junctions

The one-dimensional (1-D) momentum equation was applied to study Regime II flow in the 25.8° Edworthy sewer junction by Zhao et al. (2004). Here the approach is summarized and extended to Regime III flow. A control volume is defined in Figure 3.3 for surcharged flow in a sewer junction. Assuming hydrostatic pressure distribution, negligible friction, horizontal water surface in the junction chamber and uniform velocity distribution in the inflows, momentum equation can be written in the direction of the straight-through flow Q_1 over the control volume as:

$$\rho\left(\frac{Q_3^2}{A_3} - \frac{Q_1^2}{A_1} - \frac{Q_2^2}{A_2}\cos\delta\right) = \sum P_x \tag{3.1}$$

where ρ is water density; Q is flow rate; A is the pipe area with the subscripts 1, 2 and 3 denoting sections in the straight inlet pipe, the lateral pipe and the outlet pipe, respectively; P_x is the x component of pressure forces acting over the control volume; and δ is the average entry angle of the lateral flow. The average entry angle was discussed by Hsu et al. (1998) in open-channel junction flow and Ramamurthy and Zhu (1997) in pressurized junction flow. The angle can be expressed as $\delta = \sigma\theta$, where θ is the junction angle and σ the correction factor. The correction factor, $0 < \sigma < 1$, is dependent on various parameters including junction geometry, flow ratios, etc. To simplify our discussion, σ = 8/9 is assumed for the 90° junction according to Hager (1987) and $\sigma = 1$ for the Edworthy junction.

3.2.1 Regime II flow

As sketched in Figure 3.3(a), orifice flow exists in the outgoing pipe in Regime II flow. The water depth in the junction chamber can be derived from Eq.(3.1) as:

$$\frac{h_m}{D_3} = \frac{1}{C_c} Q_3^{*2} - \frac{A_1}{A_3} Q_1^{*2} - \frac{A_2}{A_3} Q_2^{*2} \cos\delta + \tfrac{1}{2}(C_c^{2.2} + 1) \tag{3.2}$$

where h_m is the mean water depth in the chamber measured from the invert of the outgoing pipe (diameter of D_3); D is the pipe diameter; C_c is the contraction coefficient at the outlet and C_c = 0.75 in circular pipes (Zhao et al. 2004); and the non-dimensional flow rate

$$Q_i^* = Q_i / (g D_3 A_i^2)^{1/2} \tag{3.3}$$

where subscript i = 1, 2, 3; and g is the gravitational acceleration.

The definition of the non-dimensional discharge, Eq.(3.3), was directly derived from the momentum equation. It is clear that the definition links all connecting pipes of a junction to the outlet pipe and it can be applied for junctions with non-circular inlet ducts

(e.g. the Edworthy junction). If all circular pipes are of the same diameter, the definition is essentially same to the pipe number $Q/(gD^5)^{1/2}$, which is commonly used for flow in a single pipe.

3.2.2 Regime III flow

In Regime III flow, the orifice flow vanishes and the outlet pipe flows full. Let the pressure head at section 3 (Figure 3.3b) be $p_3/(\rho g)$ and following the approach of Zhao et al. (2004), one may obtain the net pressure force

$$\sum P_x = \rho g A_3 (h_m - \frac{p_3}{\rho g}) \tag{3.4}$$

By substituting the net pressure force into Eq.(3.1), a relationship for the water depth in the chamber in Regime III flow can be obtained in the form of a submergence factor ψ as:

$$\psi = (h_m - \frac{p_3}{\rho g}) \Big/ D_3 = Q_3^{*2} - \frac{A_1}{A_3} Q_1^{*2} - \frac{A_2}{A_3} Q_2^{*2} \cos\delta \tag{3.5}$$

Equation (5) suggests that the water depth in the junction chamber is dependent on downstream condition when the outlet pipe runs full; and the submergence factor ψ is more generally applicable and is a function of flow rates only. In addition, ψ can be used as an indicator for the pressure drop in the flow through a junction chamber.

It is also interesting to see that Eq.(3.5) gives the maximum value ψ_{max} for Regime III flow at $V_1 = V_2\cos\delta$ by using $\partial\psi/\partial(Q_2/Q_3) = 0$, where $V_i = Q_i/A_i$:

$$\psi_{max} = \left(1 - \frac{A_3 \cos\delta}{A_2 + A_1 \cos\delta}\right) Q_3^{*2} \tag{3.6}$$

which indicates that the maximum submergence factor is a function of junction angle and size ratios of connecting pipes. The above predictions will be compared with the experimental results later in this paper.

3.3 Experiments

The main part of the experimental study focuses on a 90° combining junction shown in Figure 3.4. The study covers investigation of water depth and submergence factor of surcharged flows in the junction chamber, effects of slopes of the outgoing pipe, regime transitions and energy losses in Regime III flow. Additional experiments were carried out making use of Zhao et al. (2004)'s setup of the Edworthy model junction (Figure 3.1) as a special case. The measurements included submergence factor and energy losses in Regime III flow and velocity distributions in the junction chamber.

The 90° model junction was made of Plexiglas. All connecting pipes have the same diameter of D = 0.152 m. The junction chamber is a $3D \times 2D$ (length × width) rectangular box without benching. The inverts of two inlet pipes are 5 cm above the bottom of the chamber and that of the downstream pipe is 4 cm above. The junction chamber was simplified so as to make the results of the basic hydraulic features of combining sewer flow more general. The lengths of the straight inlet, the lateral inlet and the outlet pipes are 2 m, 3.8 m, and 2 m, respectively. Water was supplied by a constant head tank and inflow rates were measured using two in-line magnetic flow meters. Both the straight and the lateral inlet pipes had flow straighteners to produce a smooth approaching flow. The straighteners consist of a number of thin-walled brass pipes of $2D$ (300 mm) length and 15 mm in diameter. The outflow was drained into a reservoir through a steep (slope of about 0.1) 12-inch PVC pipe. Thus, a free outlet without

backwater effects can be assumed for the downstream pipe. Both inlet pipes were horizontal. For the outlet pipe, a zero slope (horizontal), a mild slope of 0.003 and three steep slopes of 0.014, 0.038, and 0.061, were tested. Four manometers were mounted on each pipe. The piezometric taps were spaced $2D$ apart in the inlet pipes from the chamber and located at $1.5D$, $4.5D$, $6.5D$ and $8.5D$ in the outlet pipe. Five measuring tapes were fixed in the chamber evenly spaced from the entrance to the exit along the direction of the straight pipe. These tapes were used to read the water depth in the chamber. They have an accuracy of 5 mm, but in surcharged flow the water surface was very wavy and the maximum measurement error could reach ±15 mm for the two tapes near the end wall of the chamber and about ±5 mm for the rest.

In the experiments, both inflows were varied from 0 to 40 L/s independently and 249 combinations were tested in total. Water depth in the chamber was measured when increasing the straight flow Q_1 in steps of 2 or 4 L/s for each lateral inflow Q_2. In studying regime transition, for a fixed Q_2, when Regime II flow was set up, Q_1 was increased in steps of 1 L/s until Regime III flow was formed in a stable manner. Then, Q_1 was decreased in a similar manner until a stable Regime II flow was reestablished. The process was then repeated for another value of Q_2 in steps of 2 L/s from 0 to the rate when Regime III can be formed without straight-through flow.

For the measurement of energy losses in Regime III flow, the flow ratio Q_2/Q_3 was varied from 0 to 1 for a total flow Q_3 (Note: $Q_3=Q_1+Q_2$) of 20, 30 and 40 L/s, respectively. The piezometric heads read from the first taps ($2D$ from the chamber entrance) of the both inlet pipes were used in energy calculations, because the readings of the four manometers were very close in each pipe. In the outlet pipe, the energy grade

line will not return to the friction slope for fully developed pipe flow due to the short length (15D) of the pipe. However, Serre et al. (1994) observed in a pipe junction that 80~90% of the energy loss occurred within (3~4)D from the junction. Accordingly, the piezometric head at 4.5D was used for the analysis and discussions in this paper as a compromise between covering the most local head loss and reducing effects of friction and gravity due to the pipe slope.

The Edworthy model junction consists of a straight-through circular pipe merging a rectangular duct at 25.8° (Figure 3.1). The inner diameter of the pipe is D = 0.152 m and the rectangular duct is 0.119 m wide and 0.135 m high inside. The bottom slopes (S_0) of the inlet pipe, inlet duct and outlet pipe are 0.1737, 0.0715, and 0.0645, respectively. The inlet pipe is connected to the upstream pipe with three 38° bends as shown in Figure 3.1. The length of the junction chamber is 0.44 m or 2.9D. In this study, for evaluating energy losses in Regime III (fully surcharged) flow, three piezometric taps were installed in the outlet pipe at D, 4D and 6D from its entrance. Piezometric heads of the outflow were then read using manometers while only readings at 4D were used to estimate energy losses for the reason stated above. A point gauge was used to measure the water depth near the inlet, the center and the outlet in the chamber. The submergence elevations of the junction inlets were assumed to be the piezometric heads of the inflows. In the experiments, Regime III flow was formed for a number of combinations of the straight-through inflow Q_1 from 16~42 L/s and the lateral flow Q_2 from 4~20 L/s. In addition, for a total discharge of Q_3 = 40 L/s, the flow ratio Q_2/Q_3 was varied from 0.1 to 1. Energy losses were investigated for both situations of the chamber with a half-benching and without benching.

In the Edworthy junction chamber without benching, velocities of surcharged flows were measured using a Micro acoustic Doppler velocimeter (MicroADV) manufactured by SonTek (MicroADV). The MicroADV measures 3-dimensional (3-D) flow in a cylindrical sampling volume of 4.5 mm in diameter and 5.6 mm in height. The small sampling volume is located about 5 cm from the probe and the MicroADV can measure velocities ranging from about 1 mm/s to 2.5 m/s (SonTek 1997). In the present experiment, velocity measurements were taken in a horizontal plane in the junction chamber across the center of the circular inlet pipe. Two flow regimes were tested for a flow ratio of $Q_2/Q_3 = 0.4$: (a) Regime II flow with $Q_1 = 12$ L/s and $Q_2 = 8$ L/s; and (b) Regime III flow with $Q_1 = 21$ L/s and $Q_2 = 14$ L/s. The measured plane consists of 7 sections spaced by 6~8 cm and data points of each section are spaced by 2 cm along the direction of y in Figure 3.1. The sampling rate of data acquisition was 50 Hz and the sampling time was 6 minutes.

3.4 Flow Regimes

At small inflow rates, open-channel flow was maintained through the junction (Figure 3.2a). The water surface in the junction chamber rose with the increase of flow. When the water surface exceeded the crown of the outlet, flow was choked and both inlets were submerged. In the outlet pipe, for the slopes $S_0 = 0$ and $S_0 = 0.003$, slug flow was observed with air pockets moving in the pipe. The water surface kept rising in the chamber with increasing flow rates and the outlet pipe was completely pressurized eventually. With the steep slope for the outlet pipe, orifice flow was formed (Figure 3.2b) after the flow was choked in the chamber. With increasing inflow rates, the water surface rose to a certain level and then a significant drop of the water surface was observed when

the outlet pipe primed (Figure 3.2c). These observations are very much similar to that of Zhao et al. (2004). To sum up, with the exception of the smaller slopes for the outlet pipe, the three regimes mentioned previously could be observed and classified in this experiment as: (I) open-channel flow through the junction; (II) surcharged flow with free-surface flow in the outgoing pipe; and (III) fully surcharged flow with both the inlet pipes and the outlet pipe pressurized. Regime II did not occur in the junction with smaller slopes for the outlet pipe.

Apparently, the outlet pipe performs like a culvert to some extent. However, the two types of flows are hydraulically different. First of all, while the approaching momentum is negligible in culvert flow, it plays a significant role in the junction flow. The approaching momentum reduces the required submergence for the outlet pipe to carry a given total flow; and it makes the submergence dependent of both the total discharge (Q_3) and the flow ratio (Q_2/Q_3), as discussed below.

The transition similar to that from Regime II to III may be observed in culvert flow, which is usually discussed as a change between inlet control and friction control (Hager and Del Giudice 1998). It is straight forward that, when free-flow capacity of a pipe based on friction and slope is reached, the pipe runs full and the approaching depth decreases due to the increase of carrying capacity in pipe-full flow. Nevertheless, this viewpoint might be proper for long culvert pipes only; for example, the choking limit (onset of pipe-full flow regime) presented by Hager and Del Giudice (1998) would make sense only for pipes longer than $60D$. In the present experiment, the downstream pipe is about $15D$ long and Regime III flow formed when Q_3 was about 40~60% of the free-flow capacity (by Manning's equation). Besides, no backwater in the downstream pipe was

observed in the transition from open-channel to pipe-full flow. Therefore, one cannot simply use free-flow capacity to explain the transition from Regime II to III.

The transition from Regime II to III is a quick and complicated phenomenon. The waves at the inlet of the downstream pipe might have played a significant role. In Regime II flow, a pair of symmetrical waves, starting from the entrance of the outlet pipe and clinging to the pipe wall, entered the pipe. The waves were caused by contraction of streamlines and separation and reattachment of water entering the circular inlet from the junction chamber. The wave height increased with increasing inflow rates. Obviously, these waves could block a part of the pipe area and have an impact on the air recirculation in that region, which might be crucial for stabilizing orifice flow. When the waves met at the crown of the pipe, they destroyed the orifice flow structure and converted the open-channel flow in the pipe to pipe flow, and caused the transition to Regime III. The inlet waves can be seen more clearly at a culvert inlet from a different study as shown in Figure 3.5.

The inlet waves appear to be a significant feature of supercritical flow at circular pipe inlets. It is expected that the development of the waves is independent of downstream conditions as long as supercritical flow can be formed in the pipe. Accordingly, downstream conditions should have no influence on the transition from Regime II to III flow when the downstream pipe outlet is free. This is confirmed in Figure 3.6(a) which shows the boundary of Regime II flow as Q_1^* against Q_2^* in the 90° junction. In the region above this boundary, the transition from Regime II to Regime III starts. As shown, effects of the downstream pipe slope are insignificant in the transition. In Figure 3.6(a) the broken line is the prediction of Eq.(3.2) for $h_m/D = 1$ in the 90°

junction. It is an approximation of the lower boundary of Regime II as Regime II changes to Regime I flow when h_m/D decreases to 1.

Figure 3.6(a) also shows the results of Zhao et al. (2004) from the 25.8° Edworthy junction, where the pipe slope was 0.0645. This junction is comparable with the 90° model junction in terms of size of the junction chamber and pipes, while the most significant difference is in the junction angle. Apparently, difference in the regime boundary between the two junctions is insignificant at smaller lateral flow Q_2^* in Figure 3.6(a), but it becomes noticeable at larger Q_2^* where the junction angle plays a more important role. This might be clearer in Figure 3.6(b), in which the data are re-plotted as Q_2/Q_3 against Q_2^*. The boundary for the Edworthy junction is lower than that of the 90° junction at larger Q_2^*, because the lateral inflow at smaller angles disturbs the flow only slightly in the junction chamber. Note that the disturbance might be positive for the development of the inlet waves in the outlet pipe, or for the transition from Regime II to III.

Another factor affecting the development of the inlet waves might be the submergence of the pipe inlet. Figure 3.7 shows the critical average depths, h_{mc}/D, measured in the chamber in Regime II flow on the transition boundary. When $h_m > h_{mc}$ for a given Q_2^*, Regime II flow became unstable. Note that in the present junction Regime II flow did not exist beyond Q_2^* of about 0.8, as shown in Figure 3.7, which is also clear in Figure 3.6(a).

Between Regime II and III, a transitional zone could exist in the form of slug flow in the outlet pipe. For some flow combinations, an oscillation between the two regimes existed. The water surface in the chamber fluctuated when the flow in the outlet pipe

oscillated between pipe-full and open-channel flows (with a period of 3~10 seconds). This oscillation represents essentially that the inlet waves could make the outlet pipe full at relatively small inflow rates, but the flow may not be able to produce sufficient submergence for the chamber exit in the full flow pattern. When the outlet pipe becomes full, it drains more efficiently and the water depth in the chamber decreases. With submergence of the pipe entrance being insufficient before the pattern of Regime III flow reaches a stable stage, air is sucked into the pipe. Slug flow is then formed or open-channel flow can be recovered in the outlet pipe and the flow regresses to Regime II. Thus, the flow starts oscillating. A similar oscillation was described by Smith (1995) in the discussion of drop inlet pipes. For steeper pipes, the water depth drops more in the chamber when Regime II flow changes to Regime III. Therefore, the oscillation was observed in the tests of downstream slopes of 0.038 and 0.061 but not for the slope of 0.014. Besides, the oscillation occurred more easily when Q_2 was larger than Q_1 in the transition region, as a larger Q_2 promotes the development of inlet wave and results in pipe-full flow at a smaller Q_3 which otherwise may be insufficient to maintain a stable Regime III flow.

3.5 Water Depth and Submergence Factor

Figure 3.8 shows the variation of h_m/D with the flow rate in the 90° junction chamber with different slopes for the outlet pipe. The data presented here were measured with Q_2 fixed at 4 L/s ($Q_2^* = 0.18$) in Figure 3.8(a) and at 8 L/s ($Q_2^* = 0.36$) in Figure 3.8(b). For the flat downstream slopes ($S_0 = 0$ and $S_0 = 0.003$), the water depth in the chamber keeps rising with the increase of the flow rate Q_3^*. When h_m/D exceeds 1, the flow converts to Regime III from Regime I. For the steeper slopes, Figure 3.8 clearly

shows the significant drops of the water depth in the transition from Regime II to Regime III. The drop of h_m/D in the transition is about 50% for the pipe slope of 0.061.

Effects of the slopes on h_m/D are negligible within Regime I and Regime II (Figure 3.8b). In Regime III, differences in h_m/D due to the change of the slope are expected since the change results in different conditions at the pipe outlet (e.g. elevation and pressure). Generally, the increase of the slope of the outlet pipe will reduce the water depth in the junction chamber with Regime III flow if the pressure level of the pipe outlet is kept constant. This trend is shown in Figure 3.8(b) with the exception of the data set for $S_0 = 0.061$, which overlaps the data of $S_0 = 0.031$ in Regime III.

It is clear in Figure 3.8 that, when Regime II flow exists, the water depth is larger than in Regime III flow at corresponding discharges. Therefore, for a given range of flow rates, Regime II flow can be the critical condition for the consideration of the water depth in the junction chamber, which happened to the Edworthy storm junction (Zhao et al. 2004). From another viewpoint, increasing the downstream pipe slope is not always able to reduce the water depth in a surcharged junction chamber.

For Regime II flow in the present T-shape junction of $\theta = 90°$, Figure 3.9 shows that Eq.(3.2) provides a good prediction of h_m/D comparing to the measurements. The experimental data presented in Figure 3.9 cover the measurements for all three steep slopes for the outgoing pipe. For the Edworthy junction of $\theta = 25.8°$, Zhao et al. (2004) also validated Eq.(3.2). Thus, it can be concluded that a) Eq.(3.2) can predict well the water depth in sewer junction chambers in Regime II flow; b) the water depth is a function of junction angle, pipe sizes, the total flow rate Q_3^* and the flow ratio Q_2/Q_3; and c) the variation of the depth is independent of the pipe slope once the regime is set up.

In Regime III flow, the water depth in a junction chamber will be affected by the slope of the outlet pipe, as mentioned above. Though, the submergence factor ψ, as described by Eq.(3.5), should be independent of the slope and ψ/Q_3^{*2} should be only dependent of Q_2/Q_3 for a given junction. In Figure 3.10, the measurements are presented as ψ/Q_3^{*2} against Q_2/Q_3. In the Edworthy junction (Figure 3.10a), ψ/Q_3^{*2} increases with the increase of Q_2/Q_3 until it reaches the maximum value of about 0.48 at Q_2/Q_3 of about 0.5, and then it appears to decrease slightly. Figure 3.10(a) involves experimental data in the Edworthy junction with Q_3^* of 1.45~2.33. Figure 3.10(b) covers measurements in the 90° junction for all of the tested outlet pipe slopes and Q_3^* from 0.63 to 2.33. ψ/Q_3^{*2} increases from 0.2 to about 0.85 when Q_2/Q_3 varies from 0 to 1. Obviously, the submergence factor in the 90° junction is larger than that in the 25.8° Edworthy junction and it appears independent of the downstream pipe slope.

In Figure 3.10, predicted submergence factors using Eq.(3.5) are also compared with the measurements in both junctions. The prediction for the Edworthy junction (Figure 3.10a) is good at the section of rising ψ/Q_3^{*2} but it broke down at larger Q_2/Q_3, say $Q_2/Q_3 > 0.7$~0.8. For the 90° junction, Figure 3.10(b) shows that Eq.(3.5) well describes the variation of the submergence factor. When Q_2/Q_3 decreases to 0, Eq.(3.5) predicts that ψ approaches 0, which is different from the experimental measurements as shown in Figure 3.10(b). The discrepancy is a limitation of this 1-D theoretical model due to the simplifications in the derivation.

It is interesting to note that according to Figure 3.10(a), the half benching design of the Edworthy junction has apparently no noticeable effects on the submergence factor.

In addition, one could obtain from Eq.(3.6) ψ_{max}/Q_3^{*2} of 0.49 for the Edworthy junction and 0.85 for the present 90° junction, which are coincident with the measured values.

As an implementation of the 1-D theoretical model, Figure 3.11 provides an integrated contour diagram for the variation of water depth and submergence factor of surcharged flow in the 90° junction. In this figure, the boundary of Regime II is from the best-fitting curve of the experimental data presented in Figure 3.7.

3.6 Energy Losses

Energy losses in Regime II flow were discussed by Zhao et al. (2004) by using the 1-D momentum equation discussed above. This method should also be valid for 90° junctions since we have verified Eq.(3.2) with the present experimental measurements. In this section, focus is given to Regime III flow.

For Regime III flow, energy equation can be applied to the control volume shown in Figure 3.3:

$$\rho g(Q_1 H_1 + Q_2 H_2 - Q_3 H_3) = \rho g Q_3 H_L \tag{3.7}$$

where, H_L is the head loss per-unit-weight across the junction; H_i is the total energy head at section i.

$$H_i = \frac{V_i^2}{2g} + \frac{p_i}{\rho g} + z_i \tag{3.8}$$

where, $V_i = Q_i/A_i$; p_i is the pressure; and z_i is the elevation at each section. Accordingly, energy loss coefficients may be defined respectively as:

$$K_{13} = \frac{H_1 - H_3}{V_3^2/2g};\ K_{23} = \frac{H_2 - H_3}{V_3^2/2g};\ K = \frac{H_L}{V_3^2/2g} \tag{3.9}$$

From Eq.(3.7), K can be expressed as

$$K = \frac{Q_1}{Q_3} K_{13} + \frac{Q_2}{Q_3} K_{23} \tag{3.10}$$

While K denotes the total energy loss in junction flow, the coefficients K_{13} and K_{23} indicate actually the energy change in each stream. Values of K_{13} and K_{23} could be positive or negative as energy could be lost or gained for individual streams through a combining junction.

In the experiments of the 90° junction, the coefficients for two limits of flow conditions were firstly obtained: (a) $Q_2 = 0$, which is similar to the case in straight-through manholes where $K = K_{13}$; (b) $Q_1 = 0$, which is the flow in 90° bend manholes where $K = K_{23}$. Very good linear relationships (in the form of Eq.3.9) were obtained between H_L and $V_3^2/(2g)$ with correlation coefficients over 0.99. The relationships were based on 4 measured data points for Case (a) with $V_3^2/(2g)$ ranging from 0.18 to 0.25 m, and 11 points for Case (b) with $V_3^2/(2g)$ of 0.03~0.25 m. The correlations gave $K = 0.596$ for Case (a) and $K = 1.625$ for Case (b) and as expected the downstream pipe slope has no effects on the energy loss.

For fully surcharged flow in straight-through manholes, Marsalek (1984) reported $K = 0.323$ in a square manhole of $2.26D$ in size, without benching. More energy losses in our Case (a) are expected because the pipe inverts of the present junction are slightly above the chamber bottom forming a sump (the slight bottom depression in the chamber, Figure 3.1 and Figure 3.4). For such situation in straight-through manholes, one will predict the loss coefficient $K = 0.675$ for an equivalent size to the present junction chamber ($L = 3D$) by using Pedersen and Mark (1990)'s jet theory. Although the lateral pipe in our junction provides additional space for energy dissipation, the jet theory still gives a good estimate for the present flow. For 90° bend flows, Marsalek and Greck

(1988) obtained $K = 1.73$ in a square manhole of $2.3D$ and $K = 1.52$ in a square manhole of $4.6D$, which are comparable with the present measurement in Case (b). The sump in the present junction has no significant effects in this case.

Due to the lack of experimental data for combining sewer junctions and the complexity of the flow, Yen (1986) recommended to estimate the energy loss using established charts for pipe junctions. Though, uncertainties in this approach may have considerable influence in design as the flow is strongly dependent of geometry of junction chambers. Assuming that the pieozometric heads ($p_i/\rho g + z_i$) at the two inlets (sections 1 and 2) are equal to the water level in the chamber ($h_m + z_b$ and z_b is the invert elevation of the chamber outlet), one may derive the loss coefficients from Eqs. (3.5) and (3.7~3.10):

$$K_{13} = 1 - 2\frac{A_3}{A_1}\left(\frac{Q_1}{Q_3}\right)^2 - 2\frac{A_3}{A_2}\left(\frac{Q_2}{Q_3}\right)^2 \cos\delta + \left(\frac{A_3}{A_1}\right)^2\left(\frac{Q_1}{Q_3}\right)^2 \tag{3.11a}$$

$$K_{23} = 1 - 2\frac{A_3}{A_1}\left(\frac{Q_1}{Q_3}\right)^2 - 2\frac{A_3}{A_2}\left(\frac{Q_2}{Q_3}\right)^2 \cos\delta + \left(\frac{A_3}{A_2}\right)^2\left(\frac{Q_2}{Q_3}\right)^2 \tag{3.11b}$$

$$K = 1 - 2\left(\frac{A_3}{A_1}\right)\left(\frac{Q_1}{Q_3}\right)^2 - 2\left(\frac{A_3}{A_2}\right)\left(\frac{Q_2}{Q_3}\right)^2 \cos\delta + \left(\frac{A_3}{A_1}\right)^2\left(\frac{Q_1}{Q_3}\right)^3 + \left(\frac{A_3}{A_2}\right)^2\left(\frac{Q_2}{Q_3}\right)^3 \tag{3.11c}$$

Notice that Eq.(3.11) is essentially the same as the formulas reported by Idel'chik (1993) for the loss coefficients of combining pipe junctions of type $A_1 + A_2 = A_3$, with the absence of empirical correction factors.

Figure 3.12 and Figure 3.13 present the measurements of the energy loss coefficients in the Edworthy junction and the 90° junction, respectively. For the 25.8° Edworthy junction (Figure 3.12), the energy loss coefficient of the straight-through stream, K_{13}, or of the lateral stream, K_{23} can attain negative values at Q_2/Q_3 approaching 1

or 0 respectively, which means the corresponding stream is gaining energy from the dominant one. In the 90° junction (Figure 3.13), the lateral flow can gain energy from the main flow. The energy loss in 90° junctions is more significant than that in the 25.8° junction as the coefficient K is about twice of that in the 25.8° junction.

Together with our measurements, another 4 experimental data sets from previous studies are plotted in Figure 3.13: Marsalek (1985)'s data for (1) mould M1 without benching; (2) mould M2 with half benching; (3) mould M3 with full benching; and (4) Wang et al. (1998)'s data for a junction with half benching. Both studies were conducted in 90° model junctions with 3 connecting pipes of equal diameters.

In Figure 3.13, K_{23} and K in this study compare well with data of all the other studies, but discrepancies in K_{13} are noticeable. Note the difference in the manhole geometry: Marsalek (1985) conducted the experiments in round manholes of $2.3D$ in size; Wang et al. (1998)'s data were from a round manhole of $2D$ in size; and the present investigation was for a $3D \times 2D$ rectangular chamber with a sump at the bottom. The sump in the present junction obviously had a significant impact on the results. It is expected that the sump affects the straight-through stream more than the lateral one because the discrepancies in the comparisons is significant in K_{13} and in K at small Q_2/Q_3. The effect of the sump on K vanishes when the lateral flow become significant.

In all of the junctions, good correlations between the energy loss coefficients and the flow ratio Q_2/Q_3 are clear in Figure 3.12 and Figure 3.13, coincidently with Eq.(3.11). Eq.(3.11) is compared with the experimental data in Figure 3.12 and Figure 3.13. For the 25.8° Edworthy junction, Eq.(3.11) describes the variation of the coefficients reasonably well for Q_2/Q_3 smaller than 0.7~0.8. Apparently, the limitation is from the simplification

in deriving the momentum equation as discussed above. The simplification also leads predicted K to 0 when Q_2/Q_3 approaches 0. In the 90° junction, Eq.(3.11) predicts well K_{23} in all of the junctions and K_{13} of the present study with the exception of small Q_2/Q_3, as shown in Figure 3.13. Also, the equation describes well K at larger Q_2/Q_3 when K_{23} weighs more in contributing to K (Eq.3.10).

Due to simplifications in the 1-D theoretical model, Eq.(3.11) omits effects of benching design in a junction manhole. However, by comparing the experimental data, one can find that: (1) in Figure 3.12 for the Edworthy junction, the half benching apparently has little influence on the head loss in the surcharged flow; (Note: the discrepancies at small Q_2/Q_3 are caused by the sump in the chamber without benching.) (2) in Figure 3.13 for 90° junctions, effects of the benchings of Marsalek (1985) and Wang et al. (1998) are negligible when inflows are comparable, and only fairly small influence on the head loss can be found when the lateral flow is dominant. Therefore, in surcharged flows, common benching designs for sewer junctions with straight channels and comparable discharges Q_1 and Q_2 exhibit no significant contribution to reducing the energy loss.

Based on the discussions above, Eq.(3.11) is expected to provide a good estimate for energy losses in Regime III flow in 90° sewer junctions. This theoretical model also includes the influence of pipe size ratios (A_3/A_1 and A_3/A_2) on energy losses. Comparisons between predictions of Eq.(3.11) and measurements of Wang et al. (1998) are also made in Figure 3.14 for the 90° junction with $D_1 = D_2 = 0.75D_3$ and in Figure 3.15 for $D_1 = 0.75D_3$ and $D_2 = 0.5D_3$. The predictions agree with the measurements reasonably well. The figures also show that reducing the lateral pipe size will result in significant increases

of the energy loss coefficient K: in Figure 3.13, $D_1 = D_2 = D_3$ and K is up to about 2; in Figure 3.14, $D_1 = D_2 = 0.75D_3$ and K is up to about 3.5; and in Figure 3.15, when further reducing D_2 to $0.5D_3$, K reaches about 13. Obviously, this effect of the lateral pipe size becomes significant when Q_2 becomes dominant.

3.7 Velocity Distribution in the Edworthy Junction Flow

Velocity measurements were taken at the central plane in the Edworthy model junction chamber (Figure 3.1) using a MicroADV. According to SonTek (1997), the required minimum correlation coefficient is 70% for measuring turbulent components and 40% for mean velocity. For the Edworthy junction in this experiment, the three bends (Figure 3.1) in the steep approaching pipe introduced excessive turbulence and air entrainment into the flow, and the correlation coefficient was about 40~50% at most of the measured locations. Therefore, the results of turbulence measurements were discarded and only the results of the mean velocity are presented here.

The flow in the central plane may be described with a two-dimensional flow field as the mean vertical velocity component in that plane was found to be small and fairly uniformly distributed. Figure 3.16 shows the distribution of normalized mean velocity vector ($\mathbf{V}/V_3$) in the central plane in Regime II and III flows of $Q_2/Q_3 = 0.4$. Here, $\mathbf{V} = \mathbf{U}_x + \mathbf{U}_y$ and $\mathbf{U}_x$ and $\mathbf{U}_y$ are the time-averaged axial and transverse velocity components; the coordinates x and y were defined in Figure 3.1; and V_3 is the average velocity in the outlet pipe, $V_3 = Q_3/A_3$. In Figure 3.16, the two inflow streams produce a velocity profile with two peaks at the sections near the entrance. For the tested flow combination, the maximum velocity is in the straight-through stream. The other peak in the lateral stream decays when the two inflow streams merge smoothly in the chamber. The distribution

profiles tend to be similar when approaching the chamber outlet, although the length of the chamber is only 2.9D. Apparently, the development of the profile has no significant difference between the flow regimes II and III. The merging of the two streams is completed before they leave the chamber and similar profiles are established. Figure 3.17 shows the variation of the maximum value of the plane velocity vector, $V_m(x)$. The data are presented as V_m/V_3 against x/D. As shown, along the x direction V_m/V_3 decays slightly from about 0.7 to the minimum value of about 0.55 at $x/D \sim 2.2$, or about 0.75D from the chamber outlet. Then, the flow accelerates to the chamber outlet due to the convergence of streamlines to the outlet pipe. Overall, the change of the velocity along the junction chamber is small since the chamber is short (2.9D in length) and Regime II and III flows have no noticeable difference in this variation.

To clarify the similarity of the velocity profiles when the flow approaches the chamber outlet, velocity distribution was non-dimensionalized and shown in Figure 3.18(a). Following the approach of jet studies: V_m is the maximum value of the plane velocity vector of each section; $\eta = y'/b_{0.5}$; the local coordinate y' is measured from the point where $V = V_m$ and $b_{0.5}$ is the corresponding absolute value of y' where $V = 0.5V_m$. In the non-dimensional plot, all the data points collapse to one curve that is similar to the Gaussian distribution. Note that $b_{0.5}$ could be different at the positive-y' side ($b_{0.5} = b_{+0.5}$) and at the negative-y' side ($b_{0.5} = b_{-0.5}$) because the flow field is asymmetric. Variations of $b_{+0.5}(x)$ and $b_{-0.5}(x)$ are shown in Figure 3.18(b) and the values are almost a constant around 0.4~0.6.

3.8 Summary and Conclusions

Experiments of surcharged flow were conducted in a 90° combining sewer junction with identical diameters of connecting pipes and the 25.8° Edworthy model junction. This study confirmed that three flow regimes exist in combining sewer junctions with steep downstream slopes: Regime I denotes the open-channel flow across the junction chamber; Regime II flow is partially surcharged flow, featured by orifice flow in the outlet pipe; and Regime III flow is fully surcharged flow with all connecting pipes flowing full. Once the junction chamber is choked, Regime II flow forms and the water depth in the chamber increases with increasing inflow rates. When a certain stage is reached, priming occurs in the outlet pipe and produces Regime III flow by making the pipe full, accompanied by a significant drop of water surface in the chamber. The transition from Regime II to III appears to be independent of the outlet pipe slope, or its free-flow capacity, when backwater effect is absent in the pipe. Instead, the inlet waves formed at the submerged entrance of the outlet pipe may be the trigger of the transition. The waves might be dominated by the submergence, the incoming flow ratio, turbulence of the flow in the junction chamber, and junction geometry. When the waves are sufficiently high, they destroy the structure of orifice flow in the outgoing pipe and form Regime III flow. Apparently, the two regimes of surcharged flow have no noticeable difference in the mean flow field in the junction chamber according to the velocity measurements in the Edworthy junction. The velocity measurements also showed that the surcharged combining flow might be established near the junction outlet as evidenced by the similarity of jet-like velocity profiles. Criteria for the regime transition were presented for the junctions investigated.

The 1-D theoretical model derived by Zhao et al. (2004) for Regime II flow was validated by the present measurements in the 90° junction. It was completed by extending the theory to Regime III flow. Overall, the derived equation estimates the submergence factor in Regime III flow reasonably well.

New data of the energy loss coefficients are presented for fully surcharged (Regime III) flow in the 25.8° Edworthy junction and the 90° combining sewer junction. The 90° junction data were compared with previous studies. Predictions for the coefficients were made based on the 1-D theoretical model. The derived equations are consistent with the formulas reported by Idel'chik (1993) for the loss coefficients of combining pipe junctions of type $A_1 + A_2 = A_3$. They describe reasonably well the variations of the energy loss coefficients with Q_2/Q_3 in 90° junction. For the Edworthy junction, the predicted coefficients compared very well with the experimental measurements when Q_2/Q_3 is less than 0.7 or 0.8.

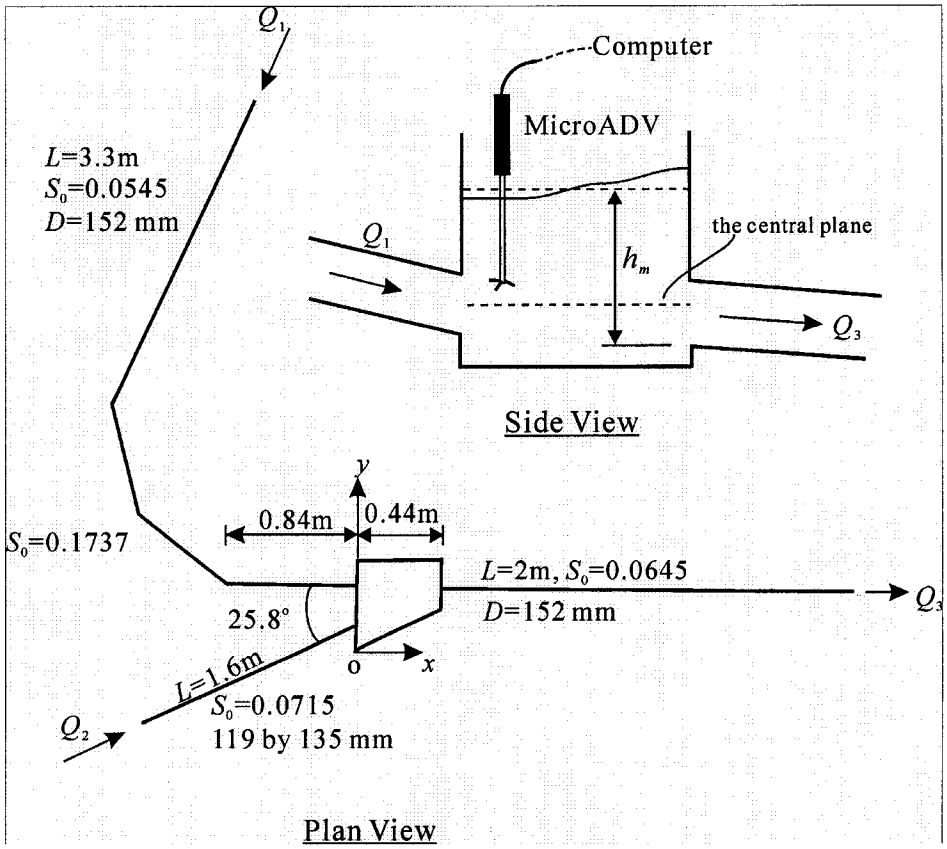

Figure 3.1 Experimental arrangement of the 25.8° Edworthy model junction

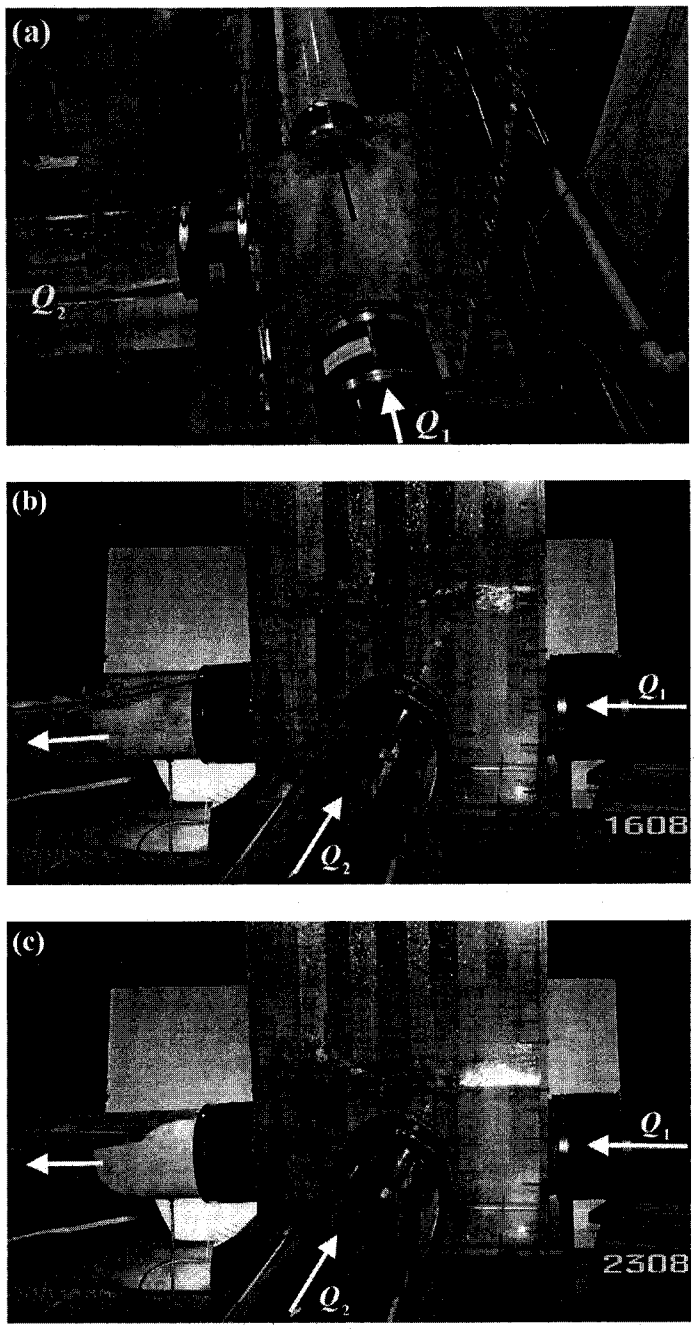

Figure 3.2 Three flow regimes in a 90° sewer junction (S_0=0.038): (a) Regime I; (b) Regime II (Q_1=16 L/s and Q_2=8 L/s); and (c) Regime III (Q_1=23 L/s and Q_2=8 L/s)

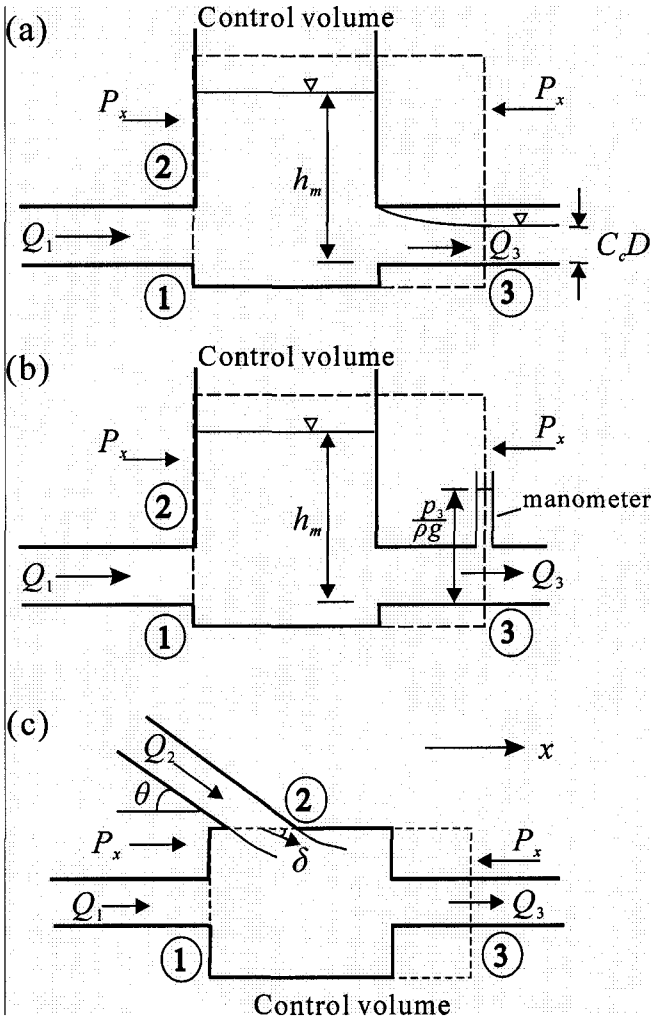

Figure 3.3 Definition of control volume for surcharged flow in a sewer junction: (a) side view of Regime II flow; (b) side view of Regime III flow; and (c) plan view

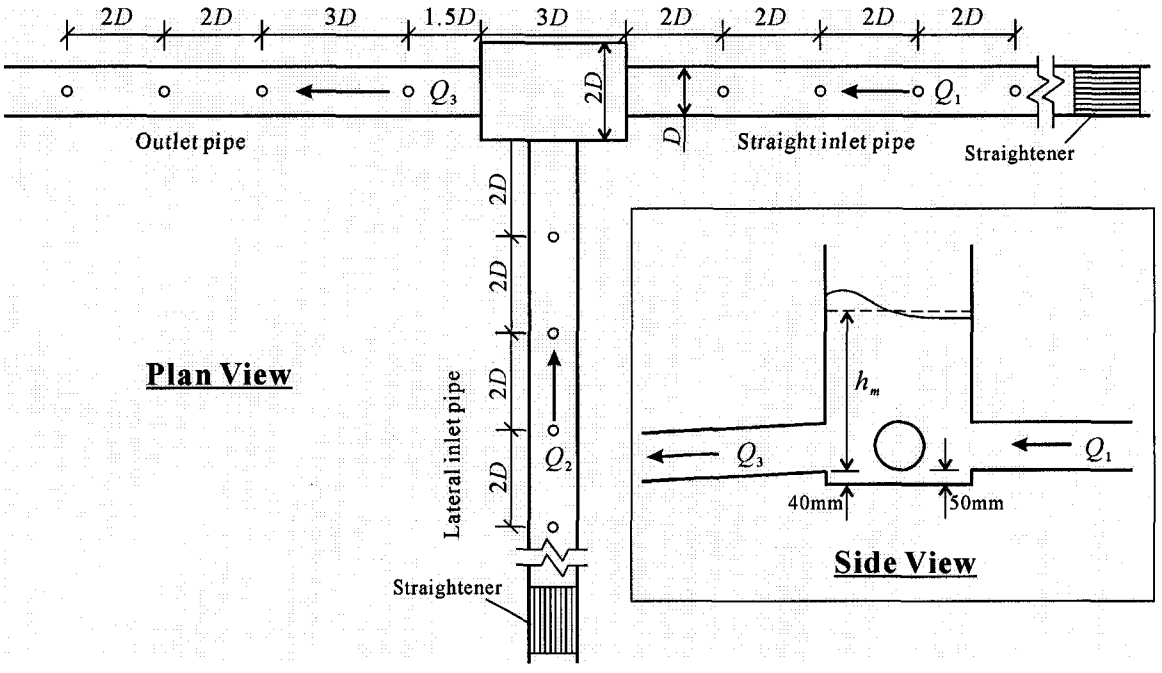

Figure 3.4 Experimental setup of a 90° sewer junction (○: piezometric taps)

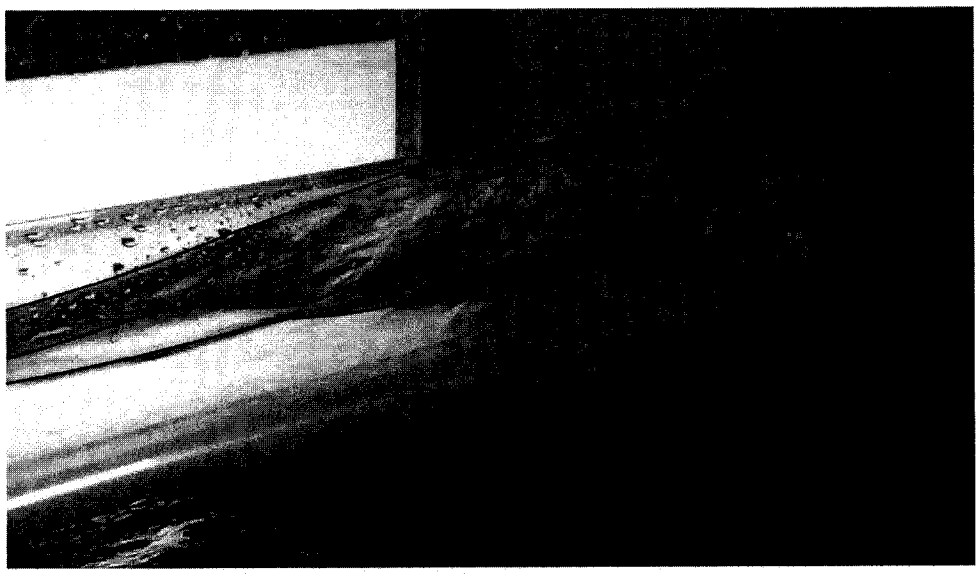

Figure 3.5 Inlet waves in a steep culvert pipe

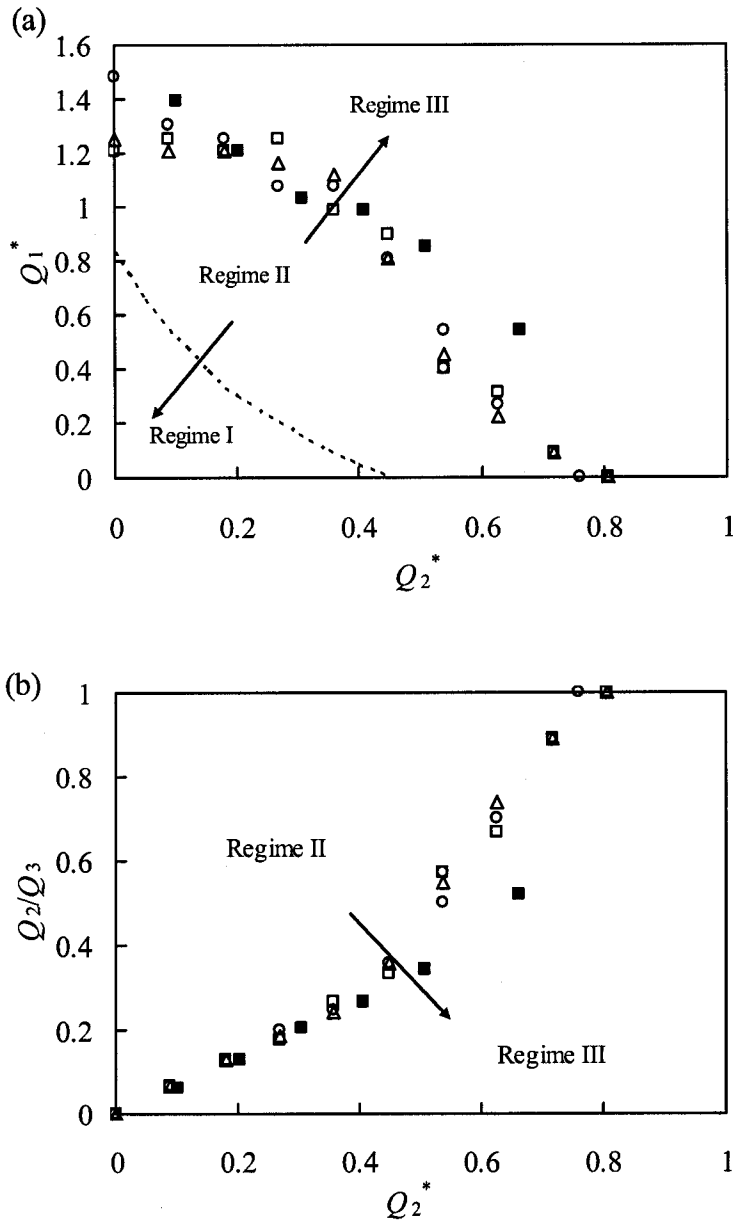

Figure 3.6 Transition from Regime II to Regime III: (a) Q_1^* vs. Q_2^* and (b) Q_2/Q_3 vs. Q_2^* for the 90° junction of S_0=0.014(Δ); 0.038(○); and 0.061(□); and the 25.8° Edworthy junction (■); lower boundary of Regime II (h_m/D=1) for the 90° junction predicted by Eq.(3.2) (--------)

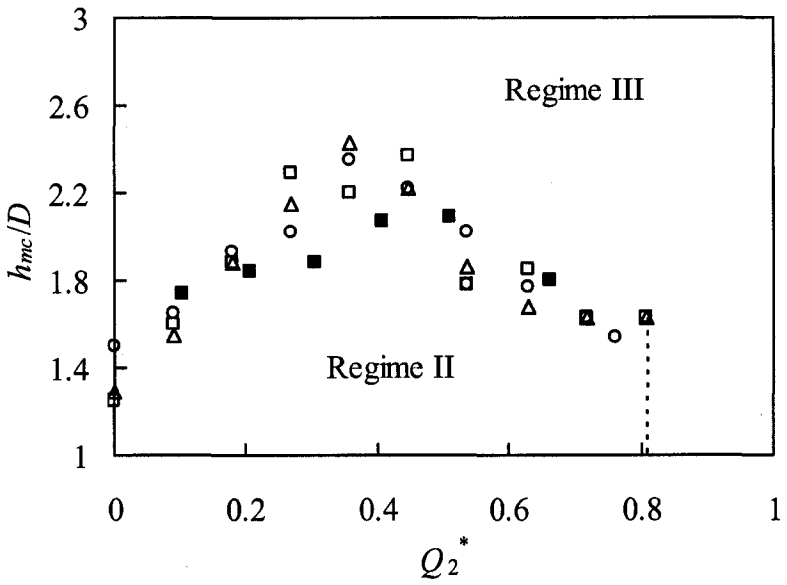

Figure 3.7 Critical water depth in the chamber at the transition from Regime II to III for the 90° junction of S_0 = 0.014(Δ); 0.038(○); and 0.061(□); and the 25.8° Edworthy junction (■)

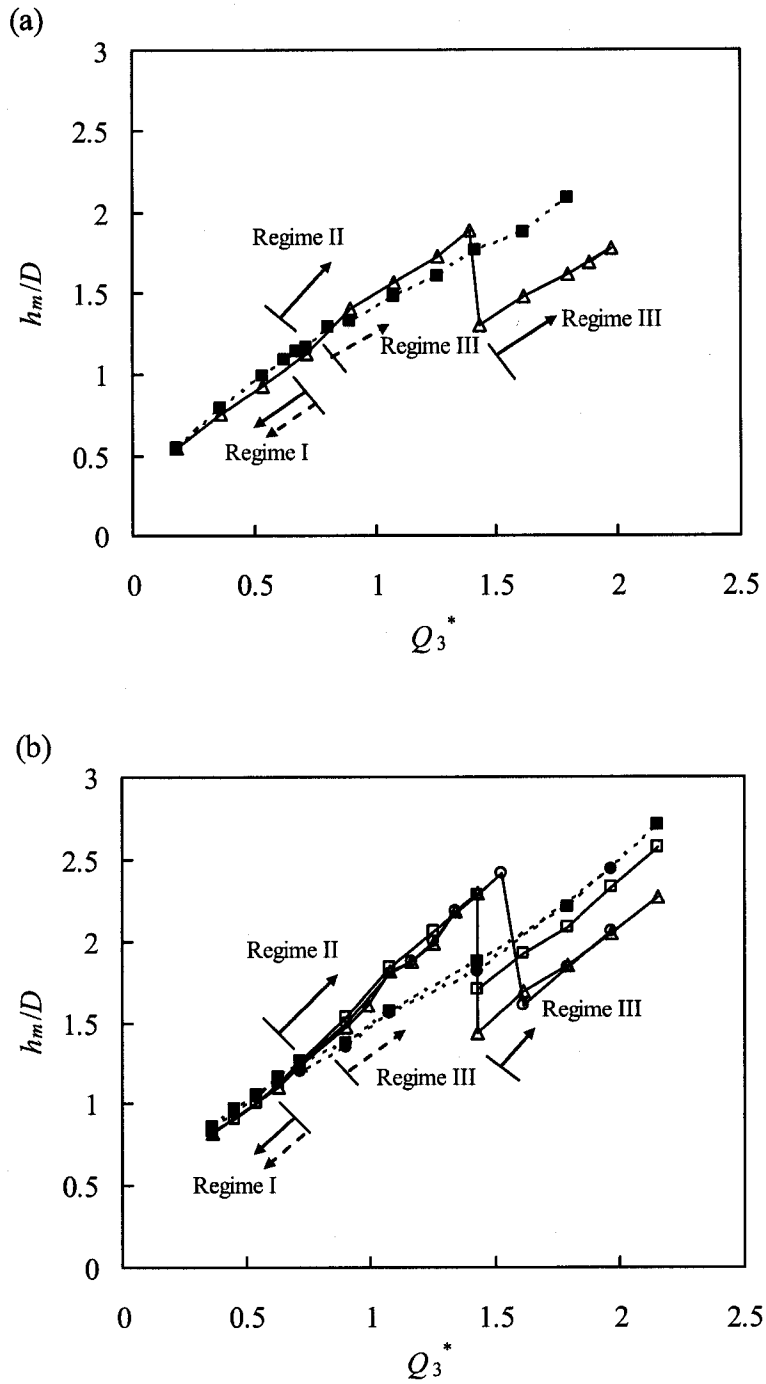

Figure 3.8 Water depth variations in the 90° junction chamber: (a) $Q_2^* = 0.18$ and (b) $Q_2^* = 0.36$ for downstream slope $S_0 = 0$ (--■--); 0.003 (--●--); 0.014 (—⊟—); 0.038 (—○—); and 0.061 (—△—)

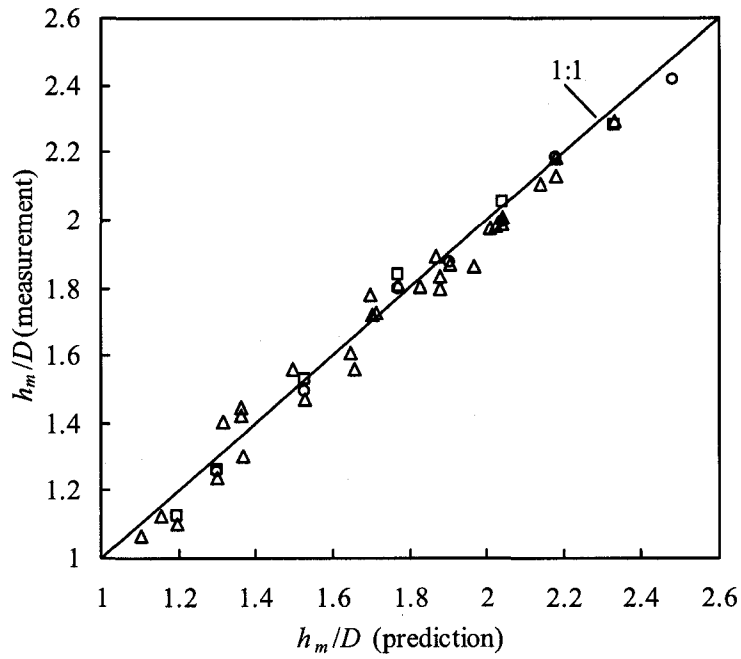

Figure 3.9 Comparison of predicted (Eq.3.2) and measured water depths of Regime II flow in a 90° junction for downstream slope S_0 = 0.014 (□); 0.038 (○); and 0.061 (Δ)

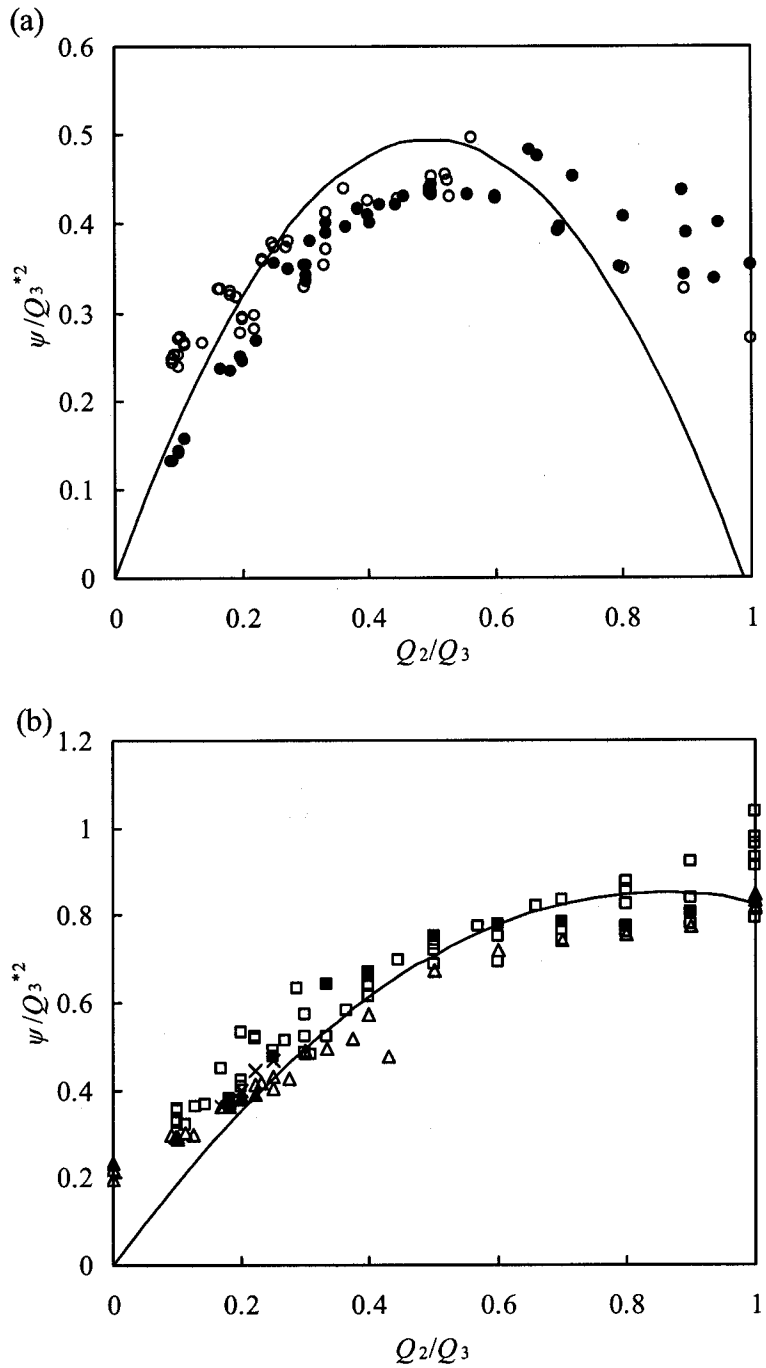

Figure 3.10 Measured submergence factors in Regime III flow:(a) the 25.8° Edworthy junction with half benching (●) and without benching (○); (b) the 90° junction for downstream slopes $S_0 = 0$ (□); 0.03 (■); 0.014 (×);0.038 (▲);0.061 (Δ); and predictions of Eq.(3.5) (——)

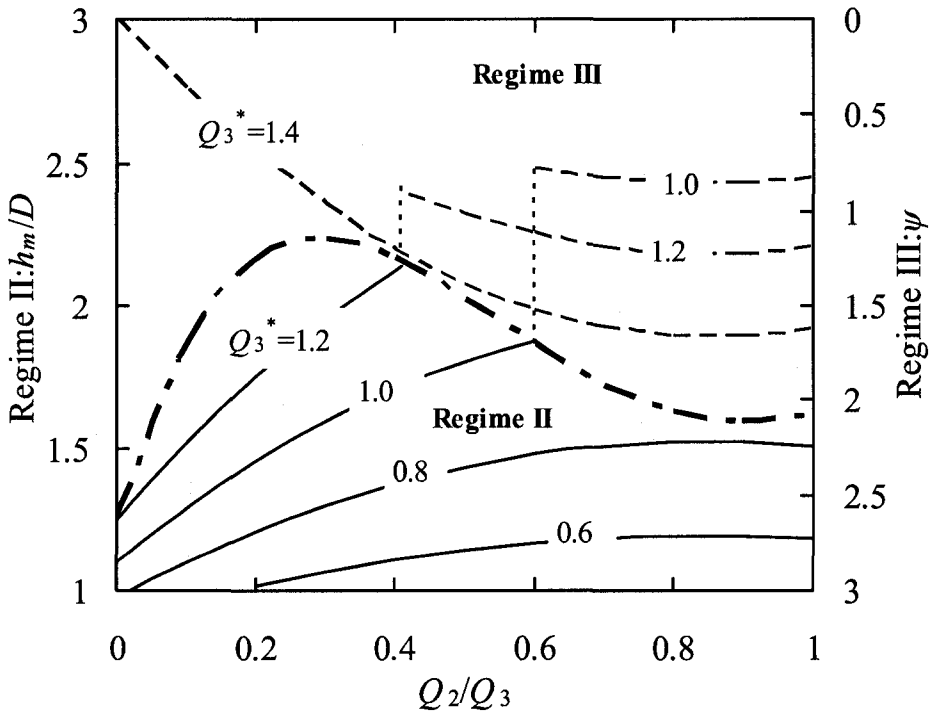

Figure 3.11 Water depth and submergence factor of surcharged flow in a 90° sewer junction: h_m/D in Regime II flow (——); ψ in Regime III flow (– – –); boundary of Regime II (—·—)

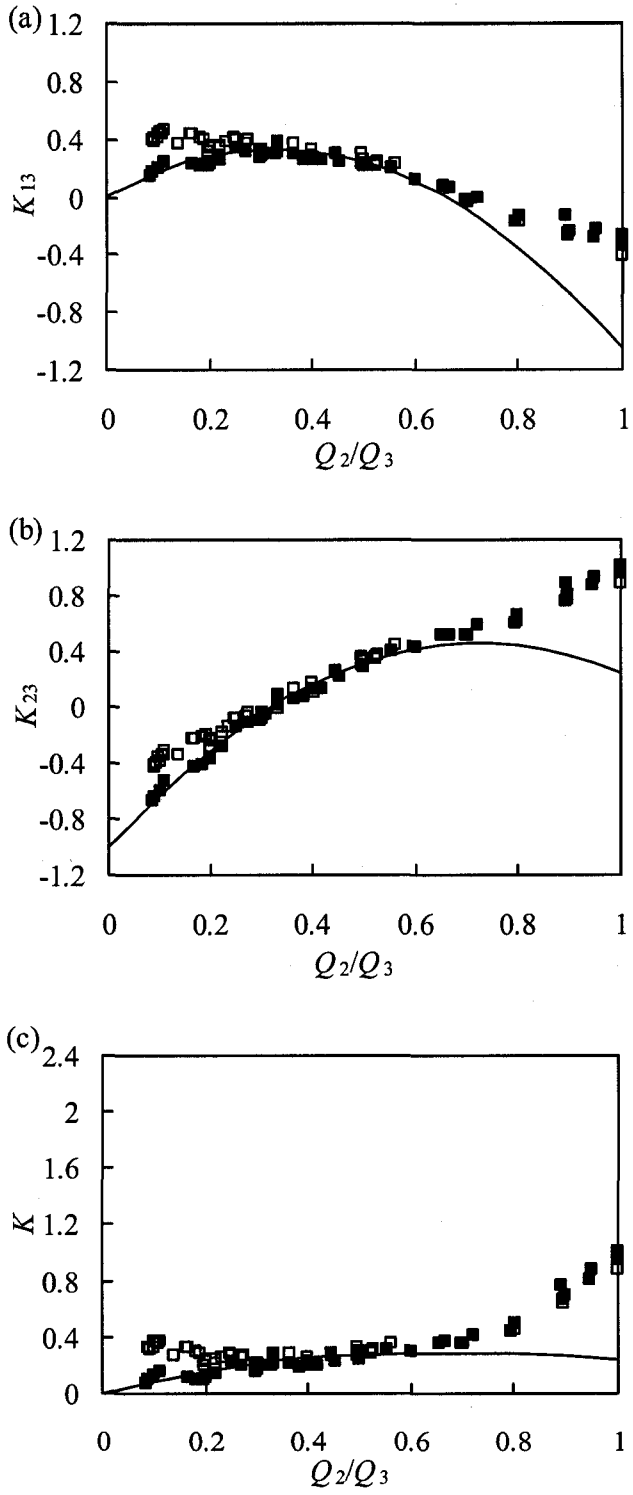

Figure 3.12 Energy loss coefficients of Regime III flow in the 25.8° Edworthy junction of (a) K_{13}; (b) K_{23}; and (c) K: measurements with half benching (■) and without benching (□); and predictions of Eq.(3.11) (——) ($Q_3^* = 1.45$~2.33)

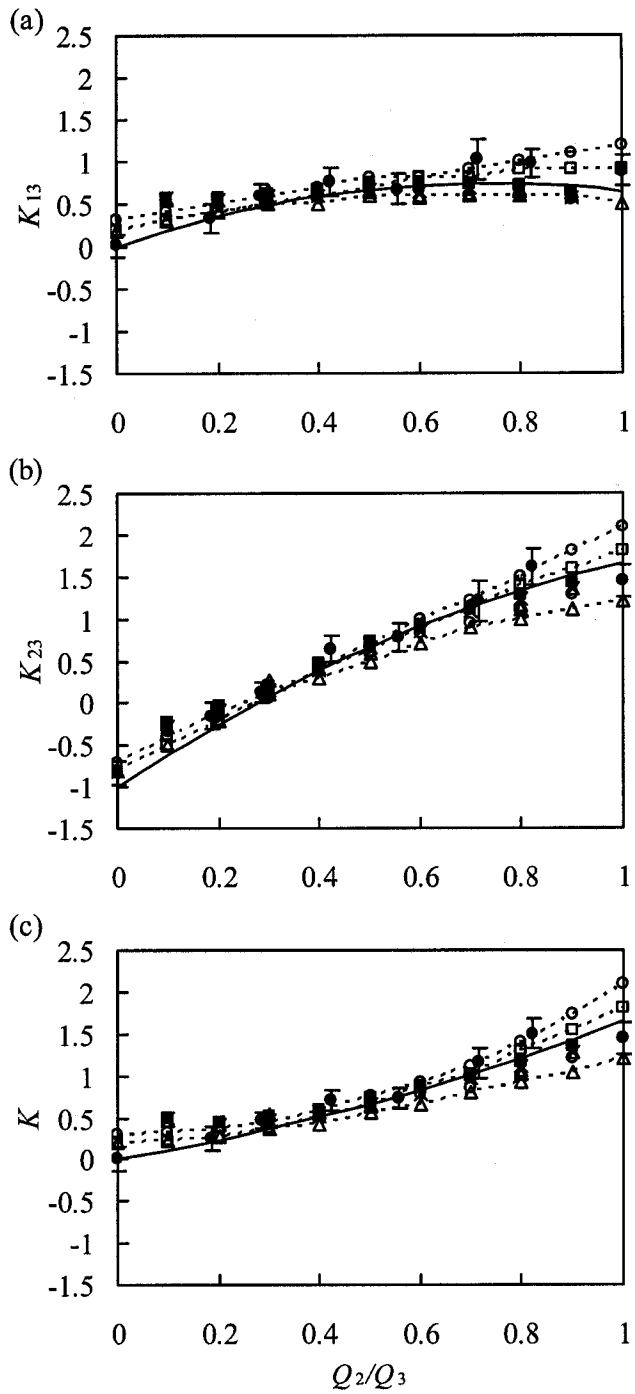

Figure 3.13 Energy loss coefficients of Regime III flow in 90° sewer junctions of (a) K_{13}; (b) K_{23}; and (c) K: the present study of $Q_3^* = 0.90$ (Δ); 1.35 (×); and 1.79 (○) with $S_0 = 0$ and $Q_3^* = 1.79$ (■) with $S_0 = 0.061$; Wang et al. (1998) (●); Marsalek (1985)'s smoothed measurements: no benching(---○---); half benching (---⊟---); and full benching (---Δ---); and predictions of Eq.(3.11) (——)

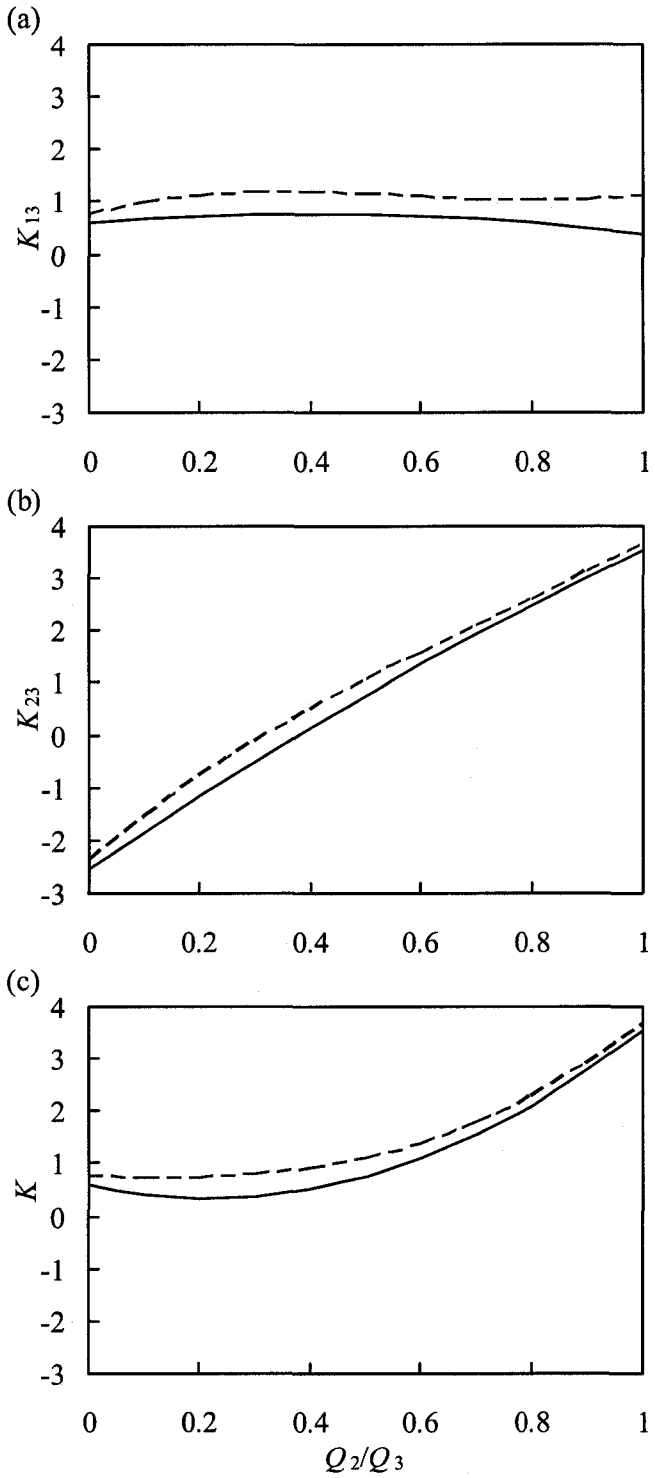

Figure 3.14 Energy loss coefficients of Regime III flow in a 90° sewer junctions with $D_1 = D_2 = 0.75D_3$: predictions of Eq.(3.11) (——) vs. smoothed measurements of Wang et al. (1998) (--------) for (a) K_{13}; (b) K_{23}; and (c) K

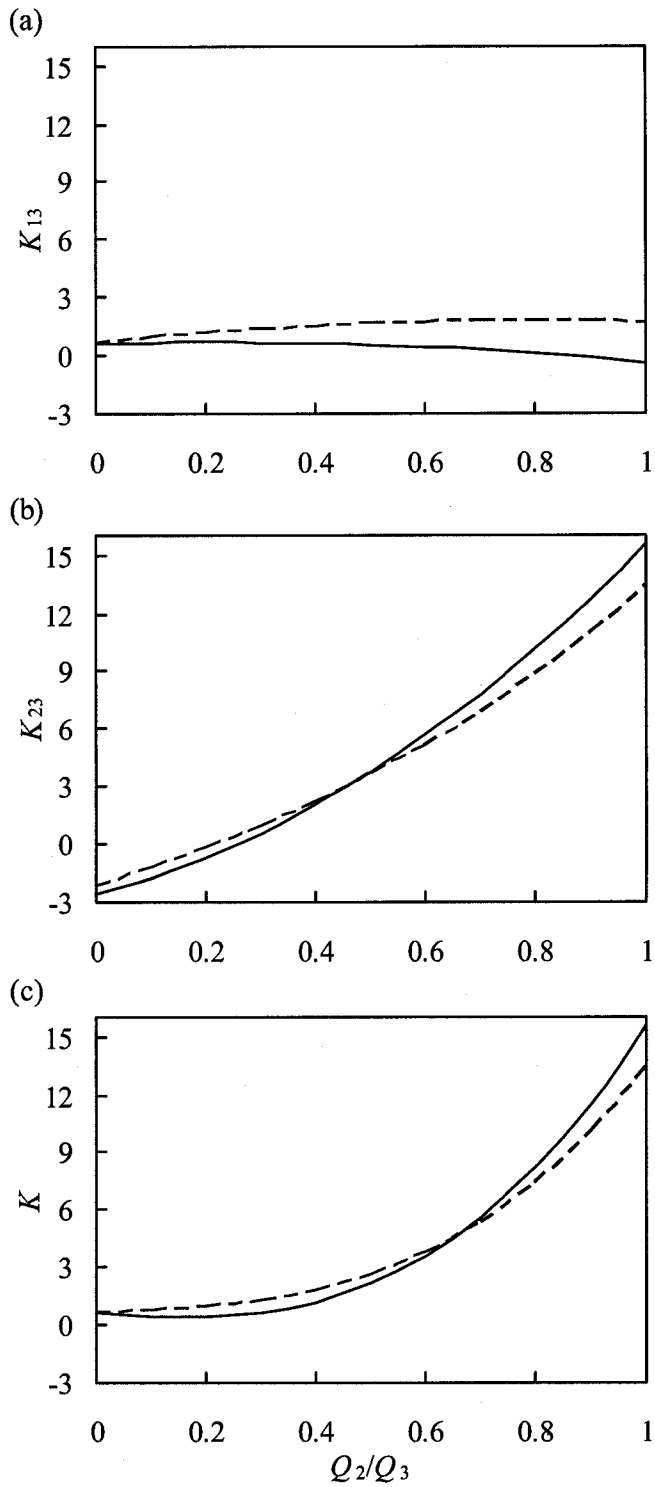

Figure 3.15 Energy loss coefficients of Regime III flow in a 90° sewer junctions with $D_1 = 0.75D_3$ and $D_2 = 0.5D_3$: predictions of Eq.(3.11) (——) vs. smoothed measurements of Wang et al. (1998) (------) for (a) K_{13}; (b) K_{23}; and (c) K

(a)

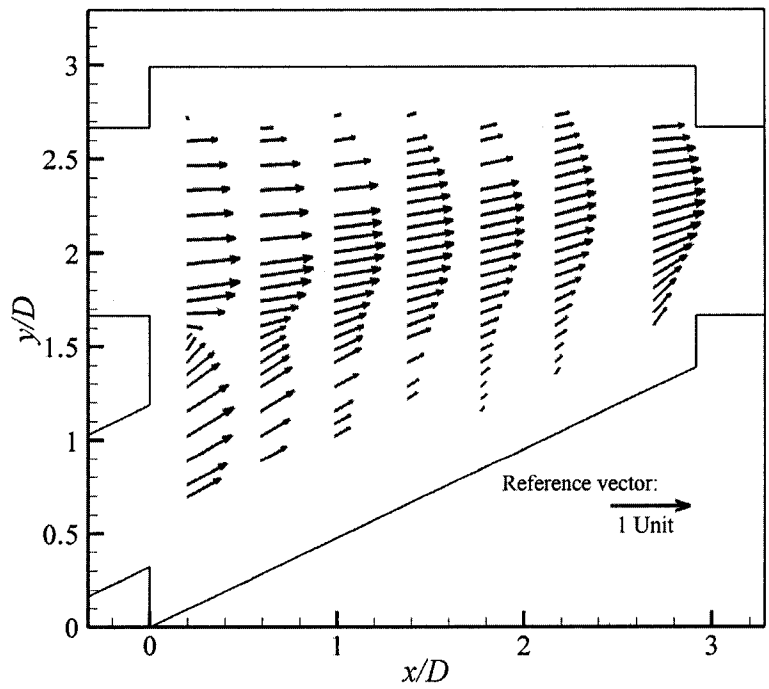

(b)

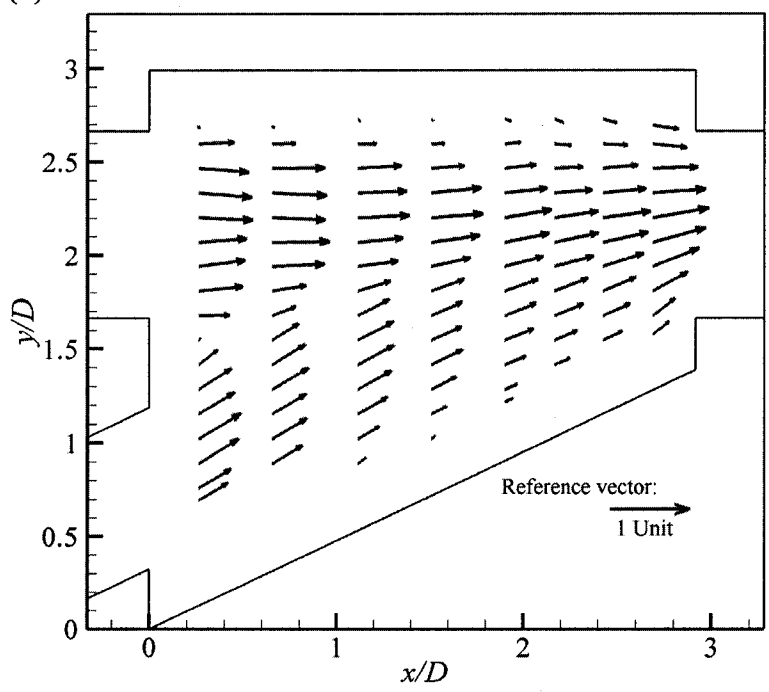

Figure 3.16 Normalized velocity ($\mathbf{V}/V_3$) distributions of surcharged flow on the central plane of the Edworthy junction for Q_2/Q_3 = 0.4: (a) Regime II (Q_3 = 20 L/s) and (b) Regime III (Q_3 = 35 L/s)

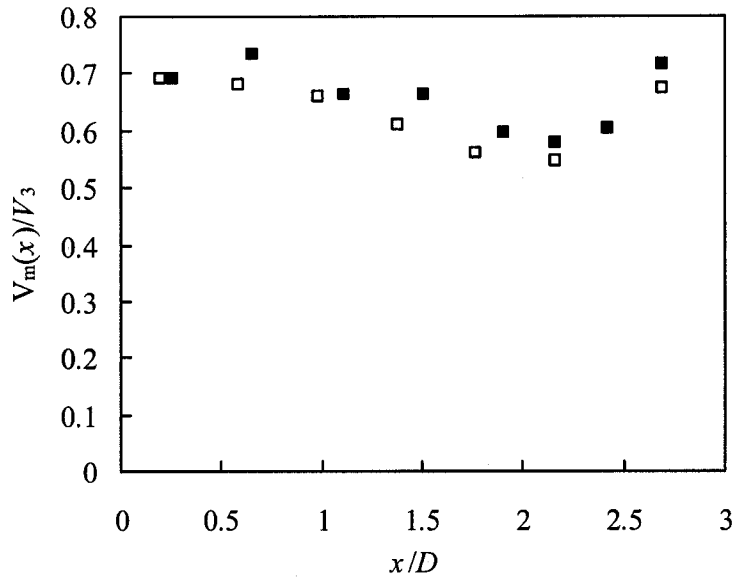

Figure 3.17 Maximum values of the plane velocity vector in the Edworthy junction for Q_2/Q_3=0.4 in Regime II flow (□) and Regime III flow (■)

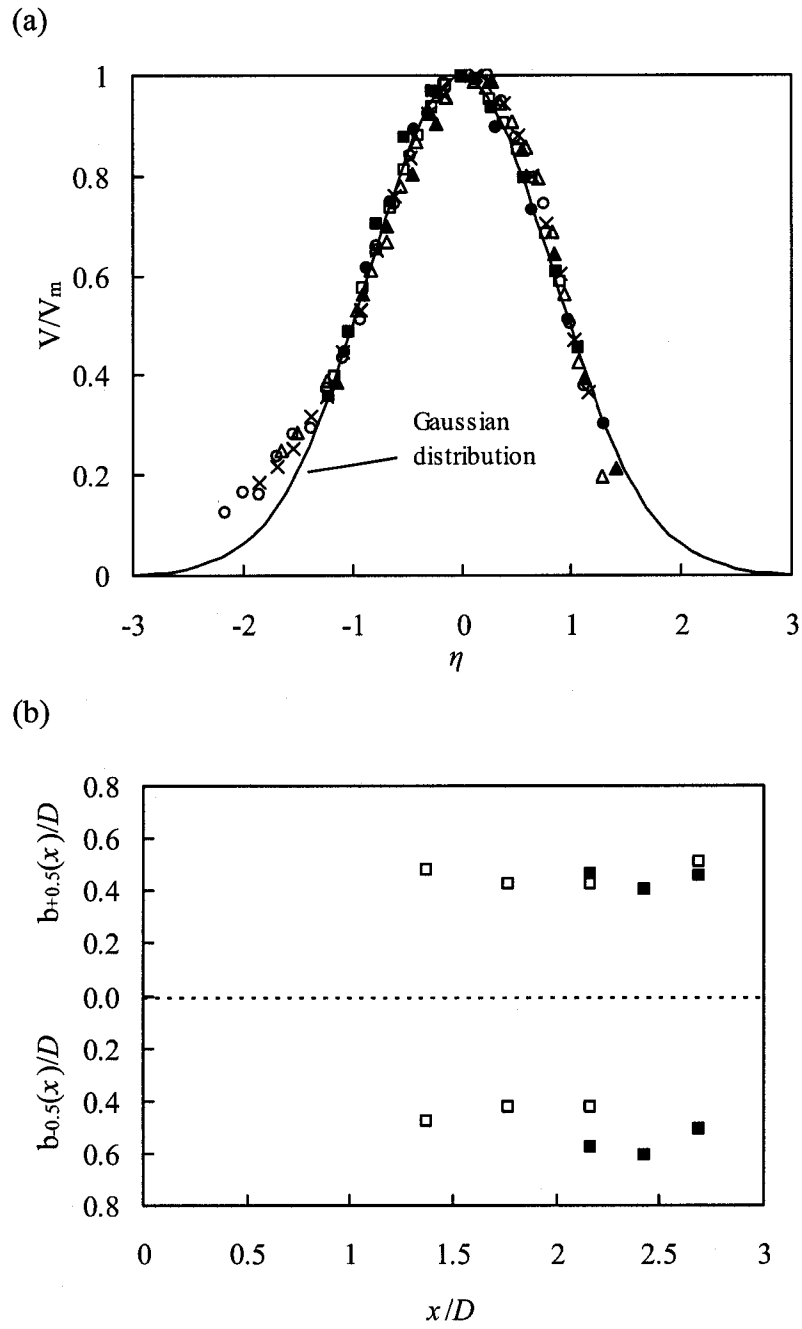

Figure 3.18 (a) Jet-like non-dimensional velocity profile in the Edworthy junction for Regime II flow at x/D=1.38 (Δ), 1.77 (○), 2.17 (×), 2.69(□); and Regime III flow at x/D=2.17 (▲), 2.43 (●), and 2.69 (■); and (b) variations of $b_{+0.5}(x)/D$ and $b_{-0.5}(x)/D$ with x/D in Regime II flow (□) and Regime III flow (■)

References

Del Giudice, G. and Hager, W.H. (2001). "Supercritical flow in 45 degree junction manhole." *Journal of Irrigation and Drainage Engineering*, ASCE, 127(2): 100-108.

Gisonni, C. and Hager, W.H. (2002). "Supercritical flow in the 90° junction." *Urban Water*, 4(4): 363-372.

Hager W.H. (1987). "Discussion to *separation zone at open-channel junctions* by Best, J.L. and Reid, I." *Journal of Hydraulic Engineering*, ASCE, 113(4): 539-543

Hager W.H. and Del Giudice, G. (1998). "Generalized culvert design diagram." *Journal of Irrigation and Drainage Engineering*, ASCE, 124(5): 271-274.

Hsu, C.-C., Lee, W.-J. and Chang, C.-H. (1998). "Subcritical open-channel junction flow." *Journal of hydraulic Engineering*, ASCE, 124(8): 847-855.

Idel'chik, I.E. (1993). *Handbook of Hydraulic Resistance*, 3rd Edition. Begell House, New York, Chapter 7: 413-428.

Marsalek, J. (1984). "Head losses at sewer junction manholes." *Journal of Hydraulic Engineering*, ASCE, 110(8): 1150-1154.

Marsalek, J. (1985). *Head Losses at Selected Sewer Manholes*. National Water Research Institute, Canada Centre for Inland Waters, Burlington, Ontario.

Marsalek, J. and Greck, B.J. (1988). "Head losses at manholes at 90° bend." *Canadian Journal of Civil Engineering* 15: 851-858.

Pedersen, F.B. and Mark, O. (1990). "Head losses in storm sewer manholes: submerged jet theory." *Journal of Hydraulic Engineering*, ASCE, 116(11): 1317-1328.

Ramamurthy, A.S. and Zhu, W. (1997). "Combining flows in 90° junctions of rectangular closed conduits." *Journal of Hydraulic Engineering*, ASCE, 123(11): 1012-1019.

Serre, M., Odgaard, A.J. and Elder, R.A. (1994). "Energy loss at combining pipe junction." *Journal of Hydraulic Engineering*, ASCE, 120(7): 808-830.

Shabayek, S., Steffler, P. and Hicks, F. (2002). "Dynamic model for subcritical combining flows in channel junctions." *Journal of Hydraulic Engineering*, ASCE, 128(9): 821-828.

Smith, C. D. (1995). *Hydraulic Structures*. University of Saskatchewan, Saskatoon, SASK., Canada, Chapter 2: 50-51.

SonTek (1997). *Acoustic Doppler Velocimeter Technical Documentation*, Version 4.0, San Diego.

Wang, K.H., Cleveland, T.G., Towsley, C. and Umrigar, D. (1998). "Head loss at manholes in surcharged sewer systems." *Journal of the American Water Resources Association*, 34(6): 1391-1400.

Weber, L.J., Schumate, E.D. and Mawer, N. (2001). "Experiments on flow at a 90° open-channel junction." *Journal of Hydraulic Engineering*, ASCE, 127(5): 340-350.

Yen, B.C. (1986). "Hydraulics of sewers." *Advances in Hydroscience*, Academic Press, New York. Vol.14: 1-122.

Zhao, C.H., Zhu, D.Z. and N.Rajaratnam (2004). "Supercritical sewer flows at a combining junction: a case study of Edworthy Trunk Junction, Calgary, Alberta." *Journal of Environmental Engineering and Science,* NRC, 3(5): 343-353.

Chapter 4

Computational and Experimental Study of Surcharged Flow at a 90-degree Combining Sewer Junction*

4.1 Introduction

Combining sewer junctions are important components in sewer networks. With more than one approaching stream at a sewer joint node, a junction chamber/manhole is usually required to provide smooth transition for stream merging and space for maintenance. Flow in these junctions presents a complicated pattern of waves, mixing, separation, turbulence and transition between or coexistence of open-channel flow and full-pipe flow. When full-pipe flow exists, the flow is also referred to as surcharged flow. Surcharged sewer flow is frequently encountered in sewer systems. While weakly surcharged flows are allowed in sewer design, as a compromise between flow carrying capacity and economy, strongly surcharged flows could produce serious problems, such as blown-off manhole covers, sewer pipe rupture, flooding, and soil erosion. Therefore, surcharged flow in sewer junctions is important in sewer design and analysis.

In sewer networks, 90° combing sewer junctions are widely used with one inlet pipe aligned with the outlet pipe and a 90° lateral inlet pipe joining. At such junctions, the flow is expected to have significant energy losses and can easily be surcharged. Zhao et al. (2004) reported a problematic 90° junction in Calgary, Alberta. The manhole cover was blown off and a large fountain formed. A review of current practice of sewer design

A version of this chapter has been submitted for publication to the Journal of Hydraulic Engineering, ASCE, in March 2006.

and construction indicates that the junction design standards are primarily based on a limited number of studies. These studies were mainly performed using physical models, empirical relationship, or one-dimensional (1-D) theoretical analysis.

Flow at sewer junctions can be subcritical or supercritical free-surface flow, or surcharged flow. Subcritical open-channel flow in sewer junctions may be described as an open channel junction. Detailed investigation on combining flow at 90° open-channel junctions has been conducted recently (Hsu et al. 1998 and Weber et al. 2001). Supercritical flow at 90° sewer junctions was studied by Gisonni and Hager (2002) focusing on wave configurations in the junction. Fully surcharged flows have relatively large energy loss and need special care in design. Experiments of energy losses in surcharged 90° sewer junctions were conducted by Marsalek (1985) and Wang et al. (1998). Yen (1986) suggested using results of pipe junction studies for sewer junction design. Zhao et al. (2006) investigated a 90° sewer junction experimentally and summarized three flow regimes at sewer junctions: free-surface flow, partially surcharged flow with free-surface flow in the outlet pipe, and fully surcharged flow. One-dimensional theoretical descriptions were also derived for surcharged flows. However, a general hydraulic description of sewer junction flows is still a challenge. This is possibly due to the complexity of the flow and details of the flow obtained in these studies being insufficient. For example, velocity fields and turbulence structure are important to better understanding of the flow, but they are difficult to obtain from traditional experimental studies.

Today, with advances in computational fluid dynamics (CFD) and computing power, CFD technology is more and more applied to hydraulics research as an alternative

and/or complementary approach to lab experiment. Examples can be found such as the 3-D simulation study for flows in open-channel junctions by Huang et al. (2002) and for flows around a submerged weir by Jia et al. (2005). In sewer junction study, computational modelling would be an effective tool to further our understanding by revealing details of the flow and to provide assistance in sewer design and analysis.

The present study is a combination of three-dimensional numerical modelling and laboratory experiments of fully surcharged flow at a 90° junction with two inflows and one outflow. At the junction, all three connecting pipes flow full with a free surface in the junction chamber. Free-surface flow models of a commercial CFD software package, Ansys CFX 10.0 (http://www.ansys.com), were employed to simulate the flow. Laboratory experiments were also carried out to provide detailed characteristics of the flow and to validate numerical simulation results. The experimental measurements include instantaneous velocity in the junction chamber, energy heads and water surface elevations. The objectives of this study are to evaluate the capability of the numerical models in study of surcharged sewer junction flow, and to provide an insight into the flow. In the following, variables of interest in the flow are briefly introduced, followed by laboratory experiments in a model junction, and fundamentals and setup of computational models. After the computational models are validated and evaluated, results and discussions are presented.

4.2 Key Variables

The present study investigates fully surcharged flow at a 90° model combining junction as shown in Figure 4.1: the junction has three connecting pipes running full and

the lateral inlet pipe is laid out at 90° to the other two pipes. The straight inflow, lateral inflow, and outgoing flow are denoted as Q_1, Q_2, and Q_3, respectively.

In the flow, variables of interest generally include water depth in the junction chamber or submergence factor, and energy coefficients. Based on a simplified one-dimensional (1-D) momentum equation, Zhao et al. (2006) derived the submergence factor ψ:

$$\psi = (h_m - \frac{p_3}{\rho g}) \Big/ D_3 = Q_3^{*2} - \frac{A_1}{A_3} Q_1^{*2} - \frac{A_2}{A_3} Q_2^{*2} \cos\delta \tag{4.1}$$

where h_m is the mean water depth in the junction chamber measured from the invert of the outlet pipe (Figure 4.1); ρ is the water density; g is the gravitational acceleration; D_3 is the outlet pipe diameter; and p_3 is the pressure at the invert of the outlet pipe cross-section right after the separation zone at the pipe entrance; A is the pipe area and $A = \pi D^2/4$; subscripts 1, 2, and 3 indicating the straight inlet, lateral inlet and outlet pipes; δ is the corrected junction angle; and the non-dimensional flow rate is defined as

$$Q_i^* = Q_i / (g D_3 A_i^2)^{1/2} \tag{4.2}$$

with subscripts $i = 1$, 2, and 3.

Energy coefficients at combining sewer junctions are usually defined as (Marsalek 1985; Wang et al. 1998; and Zhao et al. 2006)

$$K_{13} = \frac{H_1 - H_3}{V_3^2/2g};\ K_{23} = \frac{H_2 - H_3}{V_3^2/2g};\ K = \frac{H_L}{V_3^2/2g} \tag{4.3}$$

where H is the total energy head; V_3 is the average velocity in the outlet pipe and $V_3 = Q_3/A_3$; H_L is the total head loss across the junction and can be obtained using the energy equation

$$\rho g Q_3 H_L = \rho g (Q_1 H_1 + Q_2 H_2 - Q_3 H_3) \tag{4.4}$$

Apparently, K_{13} and K_{23} denote energy change in the straight and lateral streams, respectively; and K is the head loss coefficient. They are related through the equation:

$$K = \frac{Q_1}{Q_3} K_{13} + \frac{Q_2}{Q_3} K_{23} \tag{4.5}$$

4.3 Laboratory Experiments

The experimental setup is shown in Figure 4.1. The model junction was made of Plexiglas. All connecting pipes had the same diameter of D = 0.152 m. The junction chamber was a $3D \times 2D$ (length × width) rectangular box without benching. The inverts of the straight inlet and the lateral pipes were 50 mm above the bottom of the chamber and that of the downstream pipe was 40 mm above. The lengths of the straight inlet, the lateral inlet and the outlet pipes were 2 m, 3.8 m, and 2 m, respectively. Both inlet pipes were horizontal and had flow straighteners to produce a smooth approaching flow. The straighteners consisted of a number of thin-walled brass pipes of $2D$ long and 15 mm in diameter. The outlet pipe had a slope of 0.037, through which flow was drained into a reservoir directly. Inflow rates were measured using two in-line magnetic flow meters. Four manometers were mounted on each pipe. The piezometric taps were spaced $2D$ apart in the inlet pipes from the chamber and located at $1.5D$, $4.5D$, $6.5D$ and $8.5D$ in the outgoing pipe.

The coordinate system defined for the experimental setup had the positive x axis oriented in the straight inflow direction; the positive y axis in the lateral inflow direction; and the z axis pointing upward vertically. As shown in Figure 4.1, the coordinates were measured from the southwest corner with z from the invert of the outlet pipe. In the experiment, the flow ratio Q_2/Q_3 was varied from 0.2 to 0.8 while the total flow Q_3 =

0.035 m^3/s was held constant. For all of the inflow combinations, all three pipes were flowing full and the downstream pipe outlet was a free overfall. The flow conditions tested are listed in Table 4-1.

Water surface profiles were measured using a point gauge in the junction chamber. For each flow, readings were taken at about 120~240 locations, spaced 10~30 mm in the directions of x and y. Piezometric head in the connecting pipes was obtained from manometer readings to compute energy losses in the flow.

A Sontek Mirco acoustic Doppler velocimeter (MicroADV) was used to measure flow velocities. It had a sampling frequency of 50Hz. Velocity measurements were taken for flows of $Q_2/Q_3 = 0.4$, 0.5 and 0.7, at a horizontal plane in the junction chamber across the center of the outlet pipe (z = 76 mm, which is 10 mm below the inlet pipe centers as shown in Figure 4.1). A sampling time test in the junction flow of $Q_2/Q_3 = 0.5$ showed that the mean velocities and turbulent intensities hardly change for a sampling time over 360 s. Therefore, the velocity measurements were taken for 360 s at each sampling location and the locations were spaced 30 mm in the x direction and 20 mm in the y direction.

4.4 Fundamentals of Computational Modelling

At a fully surcharged sewer junction, all connecting pipes flow full, while the water surface in the junction chamber is an unknown and its position is of interest. Therefore, free-surface flow models were considered to simulate this combination of free-surface with pipe-full flows. As one case of stratified two-phase flows, free-surface flows may be simulated with Eulerian-Eulerian multiphase flow models. According to Manninen et al. (1996), computational models for multiphase flows can be classified into

homogeneous models, mixture models, and full multiphase models or inhomogeneous models. Discussions in this paper are confined to two-fluid homogeneous and inhomogeneous models with applications on free-surface flows.

4.4.1 Homogeneous Model

The homogeneous model is the simplest multiphase flow model. It assumes that all phases in the domain of interest form a mixture moving at a single velocity field with variable density and viscosity, while motions of individual components are treated in terms of diffusion within the mixture. The velocity of the mixture is solved for from a single momentum equation, while an individual continuity equation is solved for each phase to obtain its volume fraction. By volume averaging over a small control volume as shown by Wörner (2003), one can obtain the mass conservation equation for phase α:

$$\frac{\partial(r_\alpha \rho_\alpha)}{\partial t} + \frac{\partial(r_\alpha \rho_\alpha u_{mi})}{\partial x_i} = 0 \tag{4.6}$$

and the volume-averaged momentum equation for the mixture (with surface tension neglected):

$$\frac{\partial(\rho_m u_{mi})}{\partial t} + \frac{\partial(\rho_m u_{mi} u_{mj})}{\partial x_j} = \rho_m g_i - \frac{\partial p_m}{\partial x_i} + \frac{\partial}{\partial x_j}\left(\mu_m \frac{\partial u_{mi}}{\partial x_j}\right) \tag{4.7}$$

Herein, r_α is the volume fraction of phase α, and the volume conservation equation:

$$\sum_\alpha r_\alpha = 1 \tag{4.8}$$

ρ_α is the density of phase α; u_{mi} (i = 1, 2, 3) represent the mixture velocities (u,v,w) in Cartesian coordinate system (x, y, z); g_i is the gravitational acceleration in direction i; the volume-weighted mixture density ρ_m and viscosity μ_m are, as presented by Manninen et al. (1996),

$$\rho_m = \sum_\alpha r_\alpha \rho_\alpha \quad \text{and} \quad \mu_m = \sum_\alpha r_\alpha \mu_\alpha \tag{4.9}$$

where, μ_α is the viscosity of phase α; p_m is the mixture pressure; while in order to close the system, it is usually assumed that all phases share the same pressure field (Wörner 2003; Manninen et al. 1996; and Ansys 2003a), which results in the pressure constraint equation:

$$p_\alpha = p_m = p \tag{4.10}$$

where p_α is the pressure of phase α.

4.4.2 Inhomogeneous Model

The inhomogeneous model is theoretically more advanced as it fully describes the mechanics of each phase: each phase has its own velocity field and is described by an individual set of continuity and momentum equations; effects of the presence of the other phases are accounted by interphase transfer terms. However, the inhomogeneous model requires more closure relations for the interphase transfer terms, which usually involve an amount of empirical information due to limited knowledge of physics in the phase interactions. Uncertainties in the relations can make the model less reliable than simpler models.

The continuity equation of inhomogeneous models is essentially the same as Eq.(4.6) for the homogeneous model with the mixture velocity u_{mi} being replaced by the velocity of phase α, $u_{\alpha i}$. According to Drew (1992) and Wörner (2003), the momentum equation for phase α can be presented as:

$$\frac{\partial(r_\alpha \rho_\alpha u_{\alpha i})}{\partial t} + \frac{\partial(r_\alpha \rho_\alpha u_{\alpha i} u_{\alpha j})}{\partial x_j} = r_\alpha \rho_\alpha g_i - r_\alpha \frac{\partial p_\alpha}{\partial x_i} + \frac{\partial}{\partial x_j}\left(r_\alpha \mu_\alpha \frac{\partial u_{\alpha i}}{\partial x_j} \right) + M_\alpha \tag{4.11}$$

where M_α describes the interfacial forces acting on phase α due to the presence of other phases and examples include drag force, lift force, virtual mass force, turbulent dispersion force, etc. Obviously, closure relations are required for the interphase momentum transfer term M_α. Note that momentum transfer due to phase change is absent in Eq.(4.11) for free-surface flow in this study. The volume conservation equation and the pressure constraint are also used in inhomogeneous models.

4.5 Computational Approach

Both homogeneous and inhomogeneous models were applied to simulate the surcharged flows of Q_2/Q_3 = 0~1 and Q_3 = 0.035 m^3/s tested in laboratory. The simulation domain starts from 0.5 m (or 3.3D) upstream of the straight and lateral entrances of the junction chamber, as shown in Figure 4.2. The governing equations of the flow models were solved numerically in Ansys CFX 10.0 using the finite volume method.

4.5.1 Closure of the Models

To close the above equation sets for application, constitutive equations are required for turbulent (Reynolds) stress terms and the interphase momentum transfer in the inhomogeneous model. Ideally, each phase should have its own turbulence field. Based on visual observation in the experiment, it is expected that air entrainment in the flow studied is small and has insignificant impact on the water flow field. Therefore, it was assumed that air and water phases in this study share a common turbulence field, which is referred to as the homogeneous turbulence field by Ansys (2003a). In this study, the standard k-ε two-equation model (Ansys 2003a) was used. To apply k-ε model, the Reynolds number of the flow needs to be high enough for an inertial subrange to exist.

As discussed below the ADV measurements in the flow indicate the existence of an inertial subrange and thus the prerequisite can be satisfied.

For the present junction flow, the major source of the interphase momentum transfer in the inhomogeneous model is interphase drag force and closure relations need to be specified for it in Ansys CFX. In Ansys CFX interphase drag force acting on phase α due to phase β is modelled by (Ansys 2003a)

$$\mathbf{M}_{\alpha}^{D} = \frac{C_D}{8} A_{\alpha\beta} \rho_{\alpha} \left| \mathbf{u}_{\beta} - \mathbf{u}_{\alpha} \right| (\mathbf{u}_{\beta} - \mathbf{u}_{\alpha}) \tag{4.12}$$

where $\mathbf{M}^D$ is the drag force per unit volume (vector); $\mathbf{u}$ is the velocity vector; C_D is the dimensionless drag coefficient; and $A_{\alpha\beta}$ is the interfacial area density (the interfacial area per unit volume between phase α and phase β). There are several models available in Ansys CFX for C_D and $A_{\alpha\beta}$. As stated above, impacting of air on water flow is not a major concern in the present study, and we have little information for quantitatively describing the air entrainment in the flow. A free-surface transfer model was used for interfacial area density, which makes the interfacial area density equal to the absolute value of the volume fraction gradient:

$$A_{\alpha\beta} = \left| \nabla r_{\alpha} \right| \tag{4.13}$$

The relation implies that the volume integral of $A_{\alpha\beta}$ is equal to the real free-surface area (Egorov 2004). The drag coefficient C_D depends on various factors. In this study C_D = 0.44 was assumed (Manninen et al. 1996) and sensitivity analysis was conducted.

4.5.2 Boundary Conditions and Meshing

As shown in Figure 4.2 the simulation domain had two inlets where power-law velocity profiles were assigned assuming a turbulent intensity of 3.7% and an eddy length

scale of $D/4$. The downstream outlet should be a free overfall and an average static pressure equal to zero (the atmosphere pressure) was assumed over it. An "opening" boundary condition was assigned to the top of the chamber with a relative pressure equal to the atmosphere pressure, which allows the air to cross the boundary either into or out of the domain.

The simulation domain was discretized into small control volumes using a mesh generated by CFX-Mesh (Figure 4.2). The mesh had structured grids in the near-wall regions and unstructured grids inside, forming elements of tetrahedra, pyramids and wedges. A mesh sensitivity test was conducted to determine the mesh density and the convergence criteria necessary for the problem to be simulated. Five meshes were tested for the flow of $Q_2/Q_3 = 0.5$ and $Q_3 = 0.035$ m^3/s (Table.2). Convergence criteria are given by the maximum value of normalised residuals in discrete equations reaching a specified level. Results from the inhomogeneous model converged at three different levels, 10^{-3}, 10^{-4} and 10^{-5} were presented in Figure 4.3 in terms of the water depth h_m/D and the energy loss coefficient K. It is clear that changes in the results are very minor when the convergence criterion is reduced from 10^{-4} to 10^{-5}. Therefore, the convergence criterion of 10^{-4} is a good compromise between iteration accuracy and computational effort for this flow. The location of the water surface in the junction chamber did not change very much in the mesh refinement (less than 5% as shown in Figure 4.3a); while the energy loss coefficient K decreased about 9% from Mesh 2 to Mesh 3 and became almost constant in further refinement (Figure 4.3b). Accordingly, Mesh 3 was used in this study, which had 452,399 elements constructed by 139,970 nodes with a maximum spacing of 16 mm

(0.1D). Simulations were carried out on computers with dual 2.8 GHz Xeon processors and 4 GB RAM and one run of the simulation takes about 2~3 days.

4.6 CFD Model Validation and Results

The homogeneous and inhomogeneous models described above are validated and evaluated with comparisons of simulation results and experimental measurements at the 90° model junction.

4.6.1 Flow Pattern and Bulk Variables

Figure 4.4 shows the water surface profiles in the junction chamber obtained from the experiments and simulated by the numerical models for Q_2/Q_3 of 0.4, 0.5 and 0.7. In the experiment for $Q_2/Q_3 = 0.4$, the water surface was flat and fairly calm (Figure 4.4a) and the depth h_m/D was about 2. A small amount of air bubbles were entrained intermittently by occasional surface rolling. A portion of the bubbles was released back to the air and the rest was carried into the outlet pipe. When Q_2/Q_3 was increased to 0.5 (Figure 4.4b), water rose up at the northeast corner of the chamber and formed a swell with plunging. Air was entrained by the plunging and was partly driven into the outlet pipe. The mean water depth h_m/D was 2.35. The path of the bubbles clearly showed a vortex from the surface into the outlet pipe. The vortex was somewhat similar to intake vortices discussed by Hecker (1987). At $Q_2/Q_3 = 0.7$ (Figure 4.4c), the swell at the surface was significant and $h_m/D = 2.6$. More air was entrained and a considerable portion was carried into the outlet pipe as the vortex became stronger.

In the comparisons in Figure 4.4, the inhomogeneous model predicted the water surface profiles well for all the three flows. The homogeneous model performed reasonably well for $Q_2/Q_3 = 0.4$ and 0.7, but it produced a flat surface when $Q_2/Q_3 = 0.5$

and missed the swell. Note that in CFX, the water volume fraction $r_w = 0.5$ (= the air volume fraction) is usually assumed at water surface (Ansys 2003b) such that the surface was determined. Simulation of the air entrainment in the flow will be discussed later.

Simulated variations of mean water depths (h_m/D) with the flow ratio Q_2/Q_3 are compared with experimental results in Figure 4.5 with Q_3 = 0.035 m^3/s (or Q_3^* =1.57). When the two inflow rates were close (Q_2/Q_3 ranging from 0.4~0.6), the results of the inhomogeneous model compare with the measurements very well and better than those of the homogeneous model. Other than that, both of the models predicted reasonably well the location of the water surface. It is believed that the discrepancies between the homogeneous and inhomogeneous models are due to the different manner in which the models are dealing with the air flow field, which will be discussed later.

In Figure 4.6 and Figure 4.7 simulated submergence factors (ψ) and energy coefficients (K_{13}, K_{23} and K) are compared with experimental results. The submergence factor is presented as ψ/Q_3^{*2}, in Figure 4.6, which is a function of the flow ratio Q_2/Q_3 according to Eq.(4.1). The prediction from Eq.(4.1) is also shown in the figure. Eq.(4.1) describes the variation trend well in comparison with experimental results but it fails to predict the value when Q_2/Q_3 is approaching 0 due to simplifications in deriving the 1-D momentum equation (Zhao et al. 2006). On the other hand, the homogeneous and inhomogeneous models produced satisfactory results. They also predict the energy coefficients reasonably well in Figure 4.7. To show the consistency of the comparison, Figure 4.7 also includes a set of data from Zhao et al. (2006) measured in the same setup and data from Marsalek (1985) measured in model junctions with a chamber size of 2.3D with no benching. Overall, both these bulk variables could be well predicted with either

the homogeneous or inhomogeneous models. The discrepancies in the comparisons may be acceptable considering uncertainties in the measurements.

4.6.2 Velocity Field in the Central Plane in the Junction Chamber

In Figure 4.8 simulated mean velocity distributions at the central plane of the chamber are compared with the MicroADV measurements. The three mean velocity components (U, V, W) were normalized by V_3 in the plots as (U^*, V^*, W^*). In Figure 4.8(a), $Q_2/Q_3 = 0.4$ and both of the homogeneous and inhomogeneous models predicted well all three velocity components. For $Q_2/Q_3 = 0.5$ (Figure 4.8b), the inhomogeneous model compares well with the measurements, while the results of the homogeneous model are somewhat disappointing especially in the predictions of the transverse component V. For the vertical component W in Figure 4.8(b-3), both models gave fairly consistent results, but at the southeast corner of the chamber they did not agree very well with the measurements. One possible reason is that: for flows $Q_2/Q_3 \geq 0.5$, a cloud of air bubbles entrained from the water surface can be observed in this region and the bubbles could cause noticeable errors in the ADV measurements. The homogeneous model predicted the air volume fraction up to 0.5% in this region for the flow of $Q_2/Q_3 = 0.5$. According to Liu et al. (2002), such a fraction level might cause the MicroADV to underestimate the velocity components in a horizontal plane by 10%. For the vertical component W^*, a larger error is expected considering buoyancy effects. In Figure 4.8(c) for $Q_2/Q_3 = 0.7$, both models appear to work well; exceptions are: the section close to the chamber exit where the MicroADV might suffer from the influence of air bubbles again; the section at the center of the lateral entrance ($x/D = 1.48$) where the homogeneous model under-predicted the transverse velocity V^*.

Based on all the above discussions, one may conclude that, overall, the inhomogeneous model performed better than the homogeneous model in simulating the water surface and the velocity field of the flow in the junction chamber.

Some turbulence characteristics of the flow were obtained from the ADV measurements. Figure 4.9 shows typical power spectra $G_u(f)$, $G_v(f)$ and $G_w(f)$ for the corresponding velocity components u', v', and w', where f is the frequency; (u', v', w') denotes fluctuation components in the directions of (x, y, z); $(u', v', w') = (u, v, w) - (U, V, W)$; (u, v, w) represents instantaneous velocity. The plot in Figure 4.9 is in logarithmic scale and the power spectra is normalized using the root-mean square (RMS) of the turbulent velocity fluctuation such as $G_u(f)/(u_{rms})^2$. An inertial subrange can be clearly seen in the figure as marked by the existence of the -5/3 slope. In the inertial subrange, energy transfer from large eddies (low frequency) to small eddies (high frequency) takes place with no viscous dissipation. As mentioned previously, the existence of the inertial subrange is the foundation of the k-ε turbulence model.

The turbulent kinetic energy was calculated using the measured instantaneous velocity:

$$k = \tfrac{1}{2}(u_{rms}^2 + v_{rms}^2 + w_{rms}^2) \tag{4.14}$$

For the flow of $Q_2/Q_3 = 0.4$, the distribution of k at the central plane is presented in Figure 4.10(a) as $k^{1/2}/V_3$, with the normalized Reynolds stress $-\overline{u'v'}/V_3^2$ in Figure 4.10(b). The broken lines in these figures depict the stream line in the central plane that is the divide between the two incoming streams.

The normalized turbulent kinetic energy $k^{1/2}/V_3$ in Figure 4.10(a) represents the turbulent intensity of the flow. As shown, the distribution is fairly uniform across the first

2/3 of the central plane ($x/D < 2$) as the turbulent intensity profiles do not change very much in the direction of x. Over each cross-section the value varies from about 0.03 to 0.15. Apparently, the higher turbulent intensity is caused by wall effects and the interaction between the two incoming streams. The most turbulent part is at the downstream of the lateral entrance ($x/D > 2$) and the turbulent intensity is up to 0.45 at the chamber exit. In this region, the two streams start to mix; stream lines converge when approaching to the exit; and the intake vortex dives into the outlet pipe through the southeast region of the chamber. A similar pattern can be found in Figure 4.10(b) for $-\overline{u'v'}/V_3^2$. The Reynolds stress is noticeable at the stream divide. In the region of x/D <2 it has a maximum value of 0.01, but the most significant value, 0.015, appears at the region close to the chamber exit.

Simulation results of the inhomogeneous model for k and the Reynolds stress are also plotted in Figure 4.10 for comparison. The numerical model predicted the distribution of $k^{1/2}/V_3$ fairly well when $x/D < 2$ (Figure 4.10a). At the chamber exit region, the model underestimates the value of k. The most significant discrepancy appears at the southeast corner at the exit. Again, one should be aware that air bubbles there impacted on the accuracy of the MicroADV. The Reynolds stress $-\overline{u'v'}/V_3^2$ is also significantly underestimated at some locations by the inhomogeneous model. However, the pattern of its distribution at the central plane is described reasonably well. Overall, in simulating the turbulence part of the flow, the inhomogeneous model does not perform as well as in simulating the mean flow. No noticeable difference was found between the homogeneous and inhomogeneous model in simulating the turbulent components.

4.6.3 Flow Structure

The flow at a surcharged combining junction is highly three dimensional and complex. Using the validated inhomogeneous model, details of the flow at the junction were obtained and presented.

To clarify the patterns of the incoming flow interaction, mean velocity distributions at the central plane computed by the inhomogeneous model are presented in Figure 4.11 as the normalized plane velocity (U^*—V^*) vector field with the contour of normalized vertical velocity W^*. Some plane stream lines are also presented on the plane. The stream line AB indicates the approximate stream divide at the central plane. The figure shows three flow scenarios of $Q_2/Q_3 = 0.4$, 0.5 and 0.7.

As shown in Figure 4.11(a), when the straight incoming stream Q_1 is dominant, it is slightly deflected by the lateral stream Q_2 at the central plane. On the other hand, Q_2 gains momentum in the x direction to rush out of the chamber. At the side north to the straight stream, a long and narrow eddy is formed along the wall and the flow rises up when approaching the end wall. The vertical velocity is significant at some spots, but along the streams it is fairly uniform and small (close to zero).

When the two streams are equal in Figure 4.11 (b), Q_1 is significantly deflected as if it is weaker. This was surprising but it is consistent with experimental measurements. It may be explained as follows: the large eddy at the central plane is concentrated in the northwest region of the chamber; although there is an eddy on the other side of Q_1 (the southwest side of the chamber), the counterbalance between the two streams makes it weak; therefore, the pressure at the north side might be slightly lower and the straight incoming stream thus withdraws. Apparently, when Q_1 is reaching the chamber walls, it

rises up at the northeast region; rolls over the lateral stream; and dives back from the southeast region into the outlet pipe.

In Figure 4.11 (c), the lateral stream is prevailing. It cuts off the straight incoming stream; impinges on the side wall with little deflection; and then spreads out. On the left side, it produces a substream along the side wall like a wall jet. The velocity is considerable toward upstream and a large circulation is formed between the substream and Q_1 at the central plane. The straight incoming stream is cut off. Most of the water rises up on both sides while a small part gets over the lateral stream from the bottom.

3-D velocity structure for $Q_2/Q_3 = 0.4$ is examined in Figure 4.12 at $z/D = 0.25$, 0.75, 1.1 and 1.9. At $z/D = 0.25$ and 0.75, the patterns of U^*—V^* vector fields are similar to that of the central plane where $z/D = 0.5$. Differences are seen in the distribution of W^*. At $z/D = 0.25$ (Figure 4.12a), the vertical velocity is downward (negative) when the two streams meet and upward (positive) when the flow is approaching the exit; at $z/D = 0.75$ (Figure 4.12b), it is reversed. In Figure 4.12(c) at the plane of $z/D = 1.1$ (slightly above the pipe crown), water is dragged toward the end wall by the two incoming jets underneath. The flow produced by the straight incoming stream merges well with that produced by the lateral stream while a combined jet profile tends to be formed. The flow is accelerating while merging at the plane. The plane of $z/D = 1.9$ in Figure 4.12(d) is very close to the water surface (about $0.1D$ below). The flow there apparently originates at the northeast corner of the chamber and moves toward the straight and lateral inlets. The distribution of W^* is fairly uniform and upward.

4.7 Discussions on Air Entrainment and Chamber Geometry

4.7.1 Air Entrainment

Air entrainment in combining sewer junction flows is a concern to designers/engineers. In surcharged flow, air is entrained in the junction chamber and a portion is carried into the outlet pipe. Excess air in the pipe is unfavourable because it may reduce the pipe carrying capacity, and produce problems such as pressure surge due to sudden release of pressurized air.

Air entrainment was observed in the experiment as mentioned previously. When the flow ratio Q_2/Q_3 was small and the exit of the junction chamber was just slightly submerged, the straight incoming stream impinged on the chamber end wall and resulted in a wavy and rough water surface in the chamber. Air bubbles were entrained at the region close to the chamber exit from the surface into the outlet pipe. The water depth increased in the chamber with increasing Q_2/Q_3, and when the surface calmed down the air entrainment almost ceased. When Q_2/Q_3 reached about 0.4~0.5, entrainment happened only intermittently with occasional surface rolling and plunging at the northeast corner of the chamber; and most of entrained bubbles escaped back to the water surface. The intake vortex drove a small portion into the outlet pipe (Figure 4.4). When Q_2/Q_3 was further increased, more air was entrained by plunging at the surface. The vortex became stronger and brought more entrained bubbles into the outlet pipe. Overall, the air entrainment in the flows tested was not significant based on visual observations. As part of entrained air was released back to the atmosphere, the net entrainment flow (Q_a, the air flow carried into the outlet pipe) ratio (Q_a/Q_3) appeared to be small.

The air flow was simulated by CFX. However, as discussed previously, some important assumptions and constitutive relations are used in the multiphase models, thus

simulation results need to be examined carefully. The homogeneous and inhomogeneous models solve the air flow field in different ways, which might be the cause of the differences in the simulation results presented above.

The homogeneous model assumes that air shares the flow field of water, which could be a good assumption for very small air bubbles carried by water. In the present study, entrained air bubbles observed in the junction chamber were fairly large, with equivalent diameters up to 20 mm. In such cases, the relative velocity between air bubbles and ambient water could be significant, and some entrained bubbles could escape from the water. The homogeneous model may exaggerate the amount of air entrainment in the flow due to the velocity assumption. However, a reasonable estimate might be obtained from the simulation as shown in Figure 4.13 and Figure 4.14.

In Figure 4.13, the homogeneous model shows the transport of entrained air into the outlet pipe, which is consistent with experimental observations. The vectors presented in the figure are for air flow superficial velocities (air flow velocity times the air volume fraction), which indicate the local air fluxes. In Figure 4.14, simulated net entrainment rates (Q_a/Q_3) are plotted against the inflow ratio Q_2/Q_3 along with the variation of the water depth in the chamber. Q_a/Q_3 is about 0.02 at small h_m/D close to 1 and decreases to a very small value with the increase of h_m/D. When the flow becomes more turbulent due to the increasing lateral flow rate, the rate of air entrainment increases but stays at a small level due to the increase of water depth. When Q_2 becomes more and more dominant, more air is entrained although the water depth is still increasing. This variation is reasonable and consistent with experimental observations. In the quantitative aspect, the entrainment rate Q_a/Q_3 stays below 0.03 in the whole range simulated. Note that the real

net entrainment might be less than the simulated results because the homogeneous model neglected the drift and release of entrained bubbles.

It was found in the validation that the homogeneous model did not perform as well as the inhomogeneous model for the present flow. Some of discrepancies in the comparisons conducted previously may be attributed to the assumption of the common flow field of the homogeneous model. One example is the poor performance of the model in simulating the water surface in some flows. In the model, once air bubbles are entrained, they attain the same velocity as the ambient water. A hypothesis is that, the entrained air is trapped; and when transported to some low-velocity circulation regions in the junction chamber, the bubbles rise up approaching the water surface but cannot get out from the water. Evidence is that the homogeneous model usually produces a blurred interface between air and water. In some flows studied, the transition layer from pure water (the air volume fraction $r_a = 0$) to pure air ($r_a = 1$) could have a thickness of more than 1/3 of the water depth that was determined by defining water surface with $r_w = r_a = 0.5$. Thus, the definition of water surface may be debatable. The situation might affect the simulation accuracy the most at around $Q_2/Q_3 = 0.5$ when most entrained air in the experiment was released. Note that the blurred interface cannot be attributed to numerical diffusion because a mesh refinement at the interface did not show noticeable improvement.

The inhomogeneous model, on the other hand, produced clear and well-defined interfaces in this study. As mentioned, the inhomogeneous model is superior to the homogeneous model depending on closure relations for air-water interactions. With the free-surface interphase transfer model (Eq. 4.12 and Eq. 4.13) used in the present study,

entrained air might be pushed back to the atmosphere in the inhomogeneous model as the model produced almost no net entrainment. This should not be attributed to the uncertainty in the drag coefficient C_D. As mentioned by Manninen et al. (1996), the value of C_D decreases with the increase of the particle Reynolds number and approaches a constant of 0.44 when the Reynolds number is sufficiently large. In a sensitivity test, C_D was increased from 0.44 to 24 for the flow of $Q_2/Q_3 = 0.7$ and only an extremely small entrainment rate Q_a/Q_3 of 0.0003 was obtained. However, given that the air entrainment is insignificant in the junction flow studied, the inhomogeneous model is still a good choice for simulating the flow and it produced satisfactory results other than air entrainment.

4.7.2 Effects of Junction Chamber Size on Energy Loss

Geometry of a junction chamber may impact on energy loss in the flow. In practice, rounded barrels or square boxes are the most common types of sewer junction chambers. Marsalek (1985) found no noticeable difference in energy loss between rounded and square chambers of 90° junctions, but chamber size may be an important parameter. In his experiments, chambers of 2.3D and 4.6D were tested and the larger chamber tended to result in larger energy losses. In this study, the $3D \times 2D$ rectangular junction chamber may be equivalent to a square chamber of sides of 2.45D. To test the effects of chamber size, the inhomogeneous model was launched for $Q_2/Q_3 = 0.5$ and $Q_3 = 0.035$ m^3/s with the rectangular chamber being replaced by square chambers of (2~5)D. The computed energy loss coefficient K is presented in Figure 4.15(a), along with that of the rectangular chamber (equivalent size: 2.45D). The simulated variation of K against the chamber size (D_M/D) agrees very well the measurements of Marsalek (1985). It is

clear in the figure that K increases from 0.59 to 0.81 with the increase of the chamber size from $2D$ to $3D$, but further increase in the chamber size to $5D$ only results in an increase of 5% in the value. Therefore, one may conclude that the chamber size of a 90° junction has negligible effects on energy losses in the flow when it exceeds $3D$. Variation of the mean water depth h_m/D with chamber size is presented in Figure 4.15(b). The variation is consistent with that of K. It is obvious that the increase of the chamber size results in a larger energy loss and a higher water level in the chamber; but when the chamber size exceeds $3D$, the change of h_m/D is negligible.

4.8 Summary and Conclusions

Three-dimensional computational simulations were carried out for surcharged flow at a 90° combining sewer junction using a commercial CFD code, Ansys CFX 10.0. The junction studied had a $3D \times 2D$ rectangular chamber, two inlet and one outlet pipes with identical diameters. A homogeneous and an inhomogeneous two-phase free-surface flow models were employed with a k-ε turbulence model. At the same time, detailed measurements were conducted at a physical model junction, including 3-D instantaneous velocity measurements, water surface mapping and measurements of energy coefficients. The experimental measurements were used to validate the computational models. It was found that both the homogeneous and inhomogeneous models predicted the bulk variables of the flow well, including the mean water depth in the junction chamber, the submergence factor, and the energy coefficients. The inhomogeneous model showed better performance in simulating flow details such as mean velocity distributions and shape of the water surface in the chamber.

Some turbulent characteristics of the junction flow were obtained from the instantaneous velocity measurements using a MicroADV. The measurements proved the existence of the inertial subrange in the flow. Velocity distributions in the junction chamber simulated by the inhomogeneous model were presented to gain an insight into the flow structure. The validated inhomogeneous model was applied to test the effect of chamber size on energy loss in the flow. For a square chamber, the energy loss increases with the increase of chamber size, but the effect is negligible when the chamber size exceeds $3D$.

Air entrainment in the flow was discussed based on the simulation results. Theoretically, the inhomogeneous model is superior to the homogeneous model in handling phase interactions. The accuracy of the inhomogeneous model, however, relies on closure relations for the phase interaction. Knowledge of air entrainment in the flow studied was not sufficient to set up a reliable closure relation. A free-surface transfer model was used in this study, but it did not simulate the air entrainment. On the other hand, the homogeneous model based on the assumption of air and water moving at same velocities showed some features of the air entrainment. The path of air bubbles in the chamber and the variation of entrainment rate obtained from the homogeneous model are reasonable in comparison with experimental observation. It was found that the relative net air entrainment rate, Q_a/Q_3, is related to the flow ratio Q_2/Q_3 and the mean water depth h_m/D. It is expected that the rate Q_a/Q_3 for the flows studied is no more than 0.03 and its impact on the water flow is negligible.

Table 4-1 Experimental Flow Conditions

$Q_3(m^3/s)$	Q_2/Q_3	ADV Measurement
0.035	0.2	
0.035	0.4	√
0.035	0.5	√
0.035	0.7	√
0.035	0.8	

Table 4-2 Meshing Schemes

	Mesh 1	Mesh 2	**Mesh 3**	Mesh 4	Mesh 5
#Nodes	47,747	86,874	**139,970**	212,263	287,135
#Elements	139,365	259,957	**452,399**	710,296	1,017,077
Max. Body Spacing (mm)	24	20	**16**	14	12

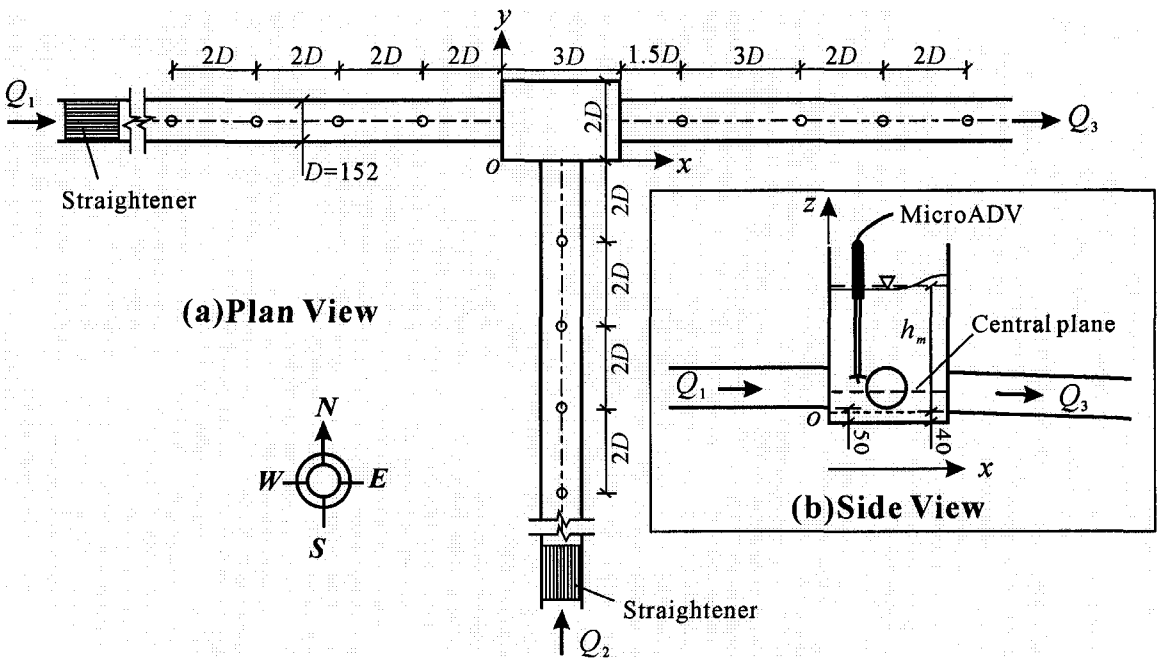

Figure 4.1 Experiment setup of a 90° model junction (○: piezometric taps; all dimensions are in millimeters)

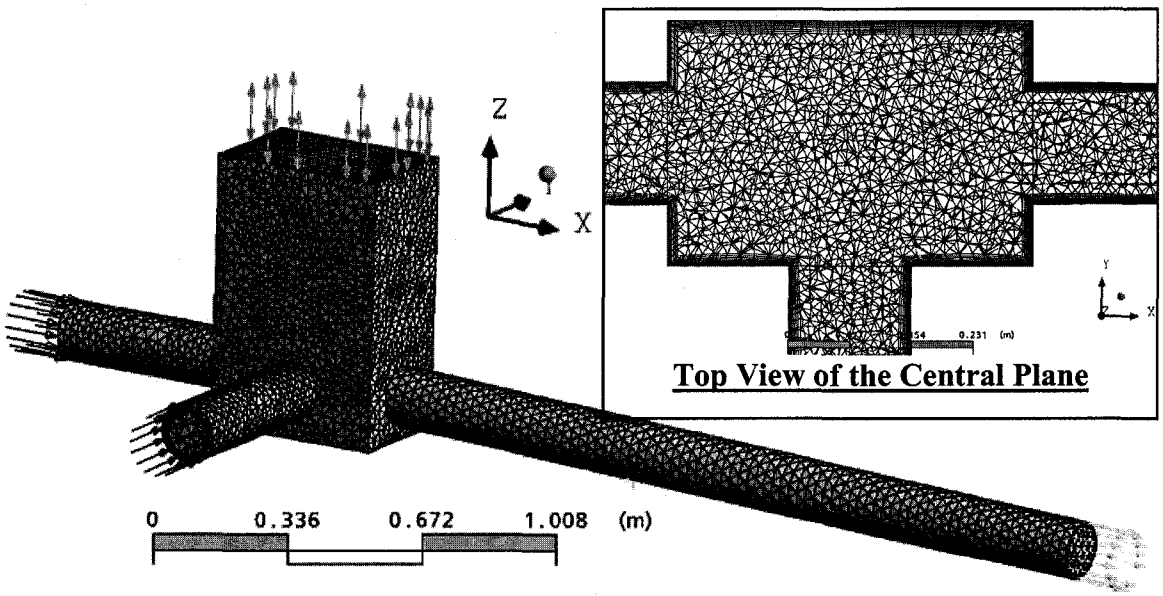

Figure 4.2 Simulation domain of the 90° junction

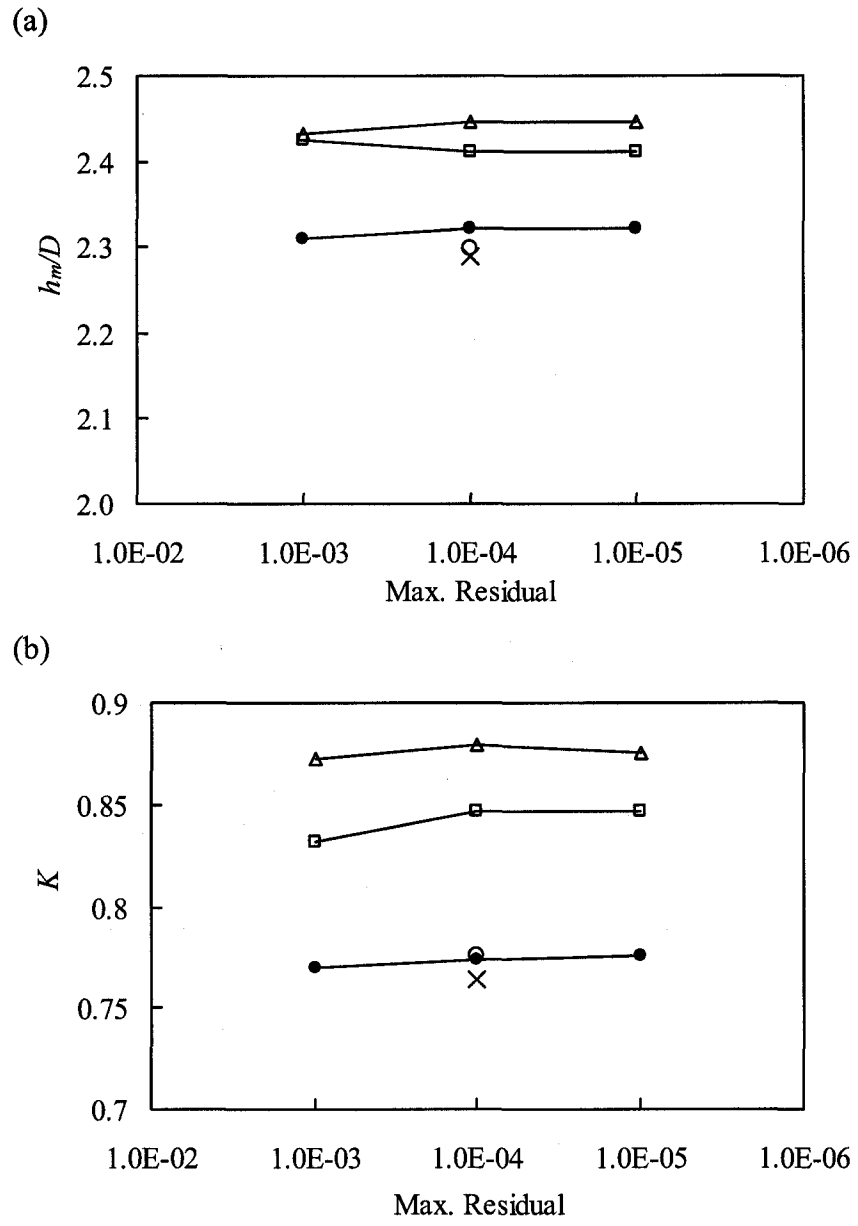

Figure 4.3 Mesh refinement in the inhomogeneous model with $Q_2/Q_3 = 0.5$ and $Q_3 = 0.035$ m^3/s: (a) mean water depth in the chamber h_m/D at different convergence levels; and (b) energy loss coefficient K at different convergence levels. Mesh 1 (—△—); Mesh 2 (—⊟—); Mesh 3 (—●—); Mesh 4 (○); and Mesh 5 (×)

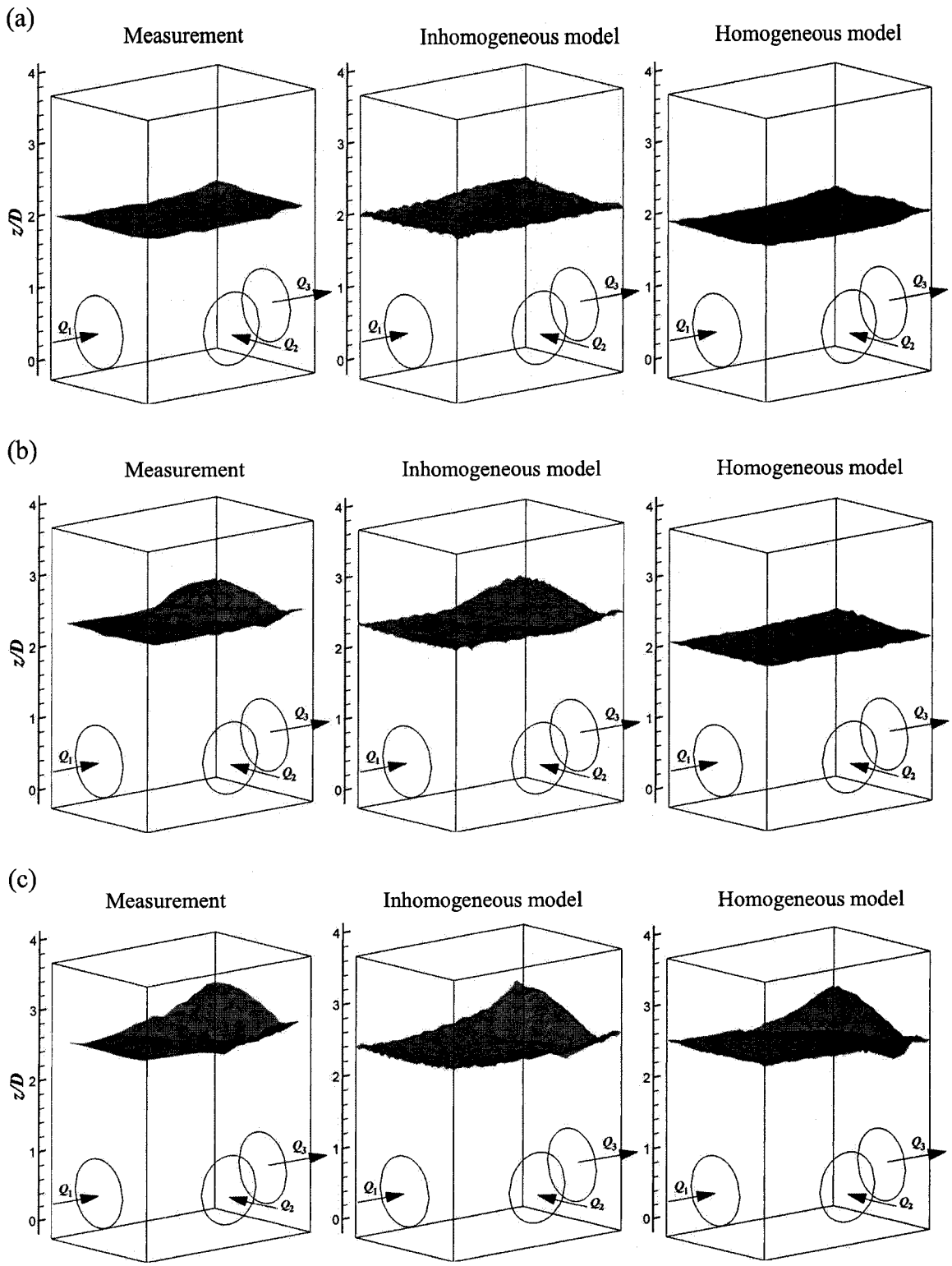

Figure 4.4 Comparison of water surface profile measurements and simulations by the homogeneous and inhomogeneous models for (a) $Q_2/Q_3 = 0.4$; (b) $Q_2/Q_3 = 0.5$; and (c) $Q_2/Q_3 = 0.7$

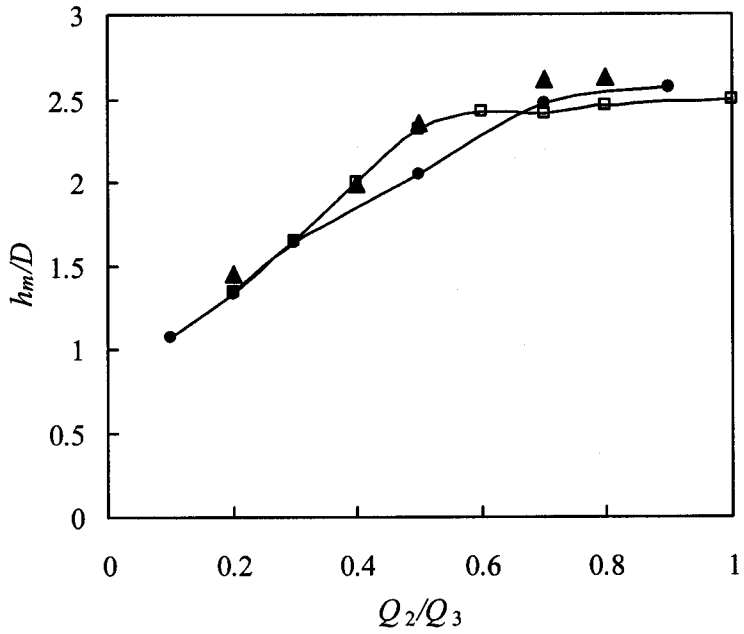

Figure 4.5 Comparison of simulated mean water depths (h_m/D) in the junction chamber with measurements: measurements (▲); the inhomogeneous model (—⊟—); and the homogeneous model (—●—)

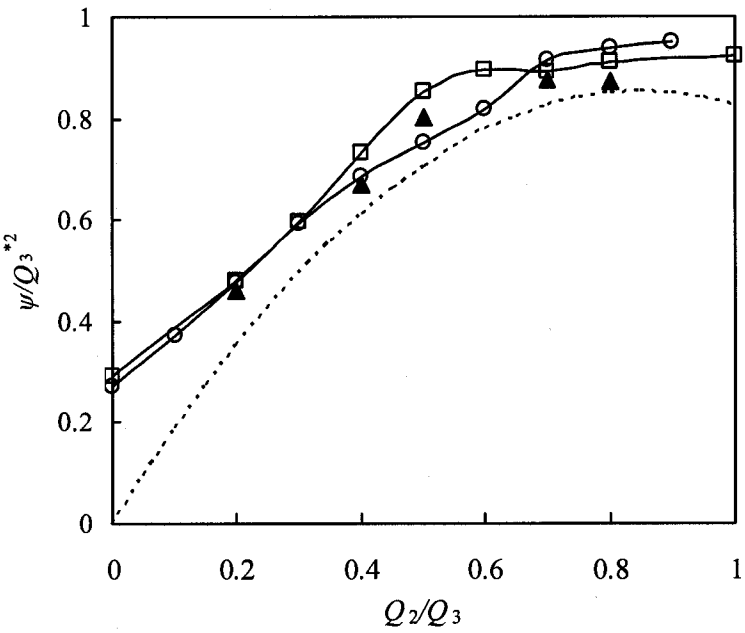

Figure 4.6 Comparison of simulated submergence factors (ψ) with measurements: measurements (▲); the inhomogeneous model (—⊟—); the homogeneous model (—⊙—); and Eq.(4.1) (--------)

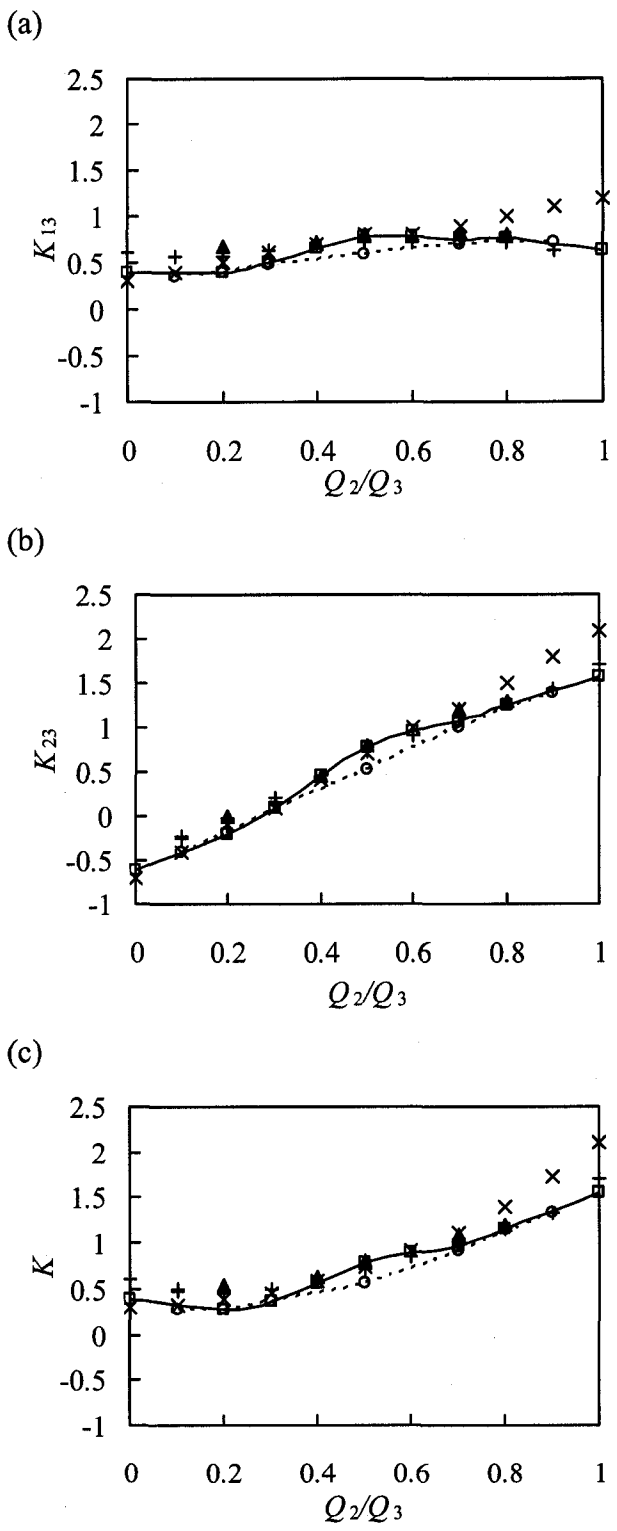

Figure 4.7 Comparisons of simulated energy coefficients with experimental results: (a) K_{13}; (b) K_{23}; and (c) K. The inhomogeneous model (—⊟—); the homogeneous model (----⊖----); the present experiment (▲); Zhao et al. (2006) (+); and Marsalek (1985) (×)

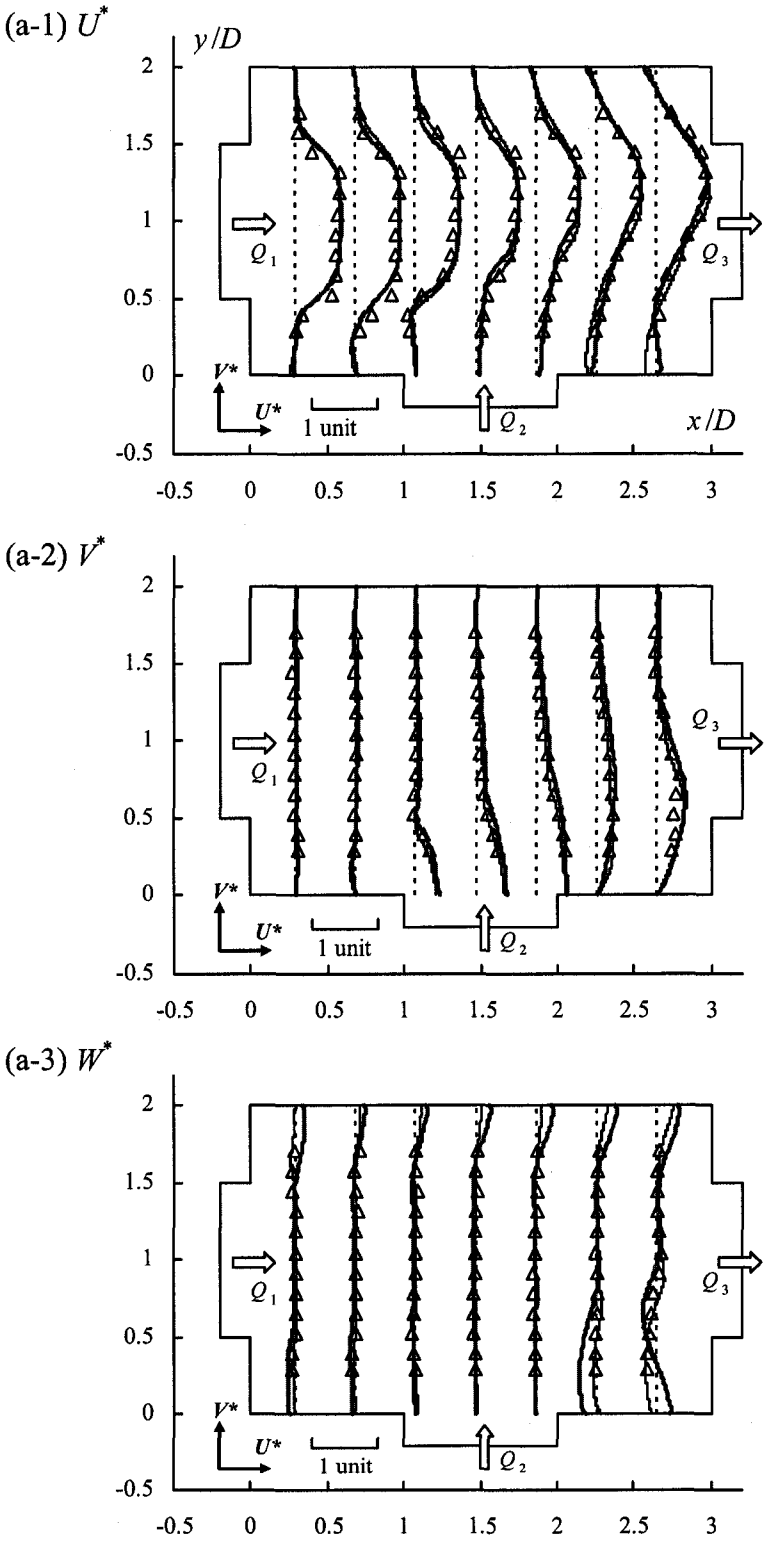

Figure 4.8 (a-c) Comparisons of simulated mean velocities at the central plane with experimental measurements: (a) $Q_2/Q_3 = 0.4$. The inhomogeneous model (———); the homogeneous model (———); and measurements (Δ)

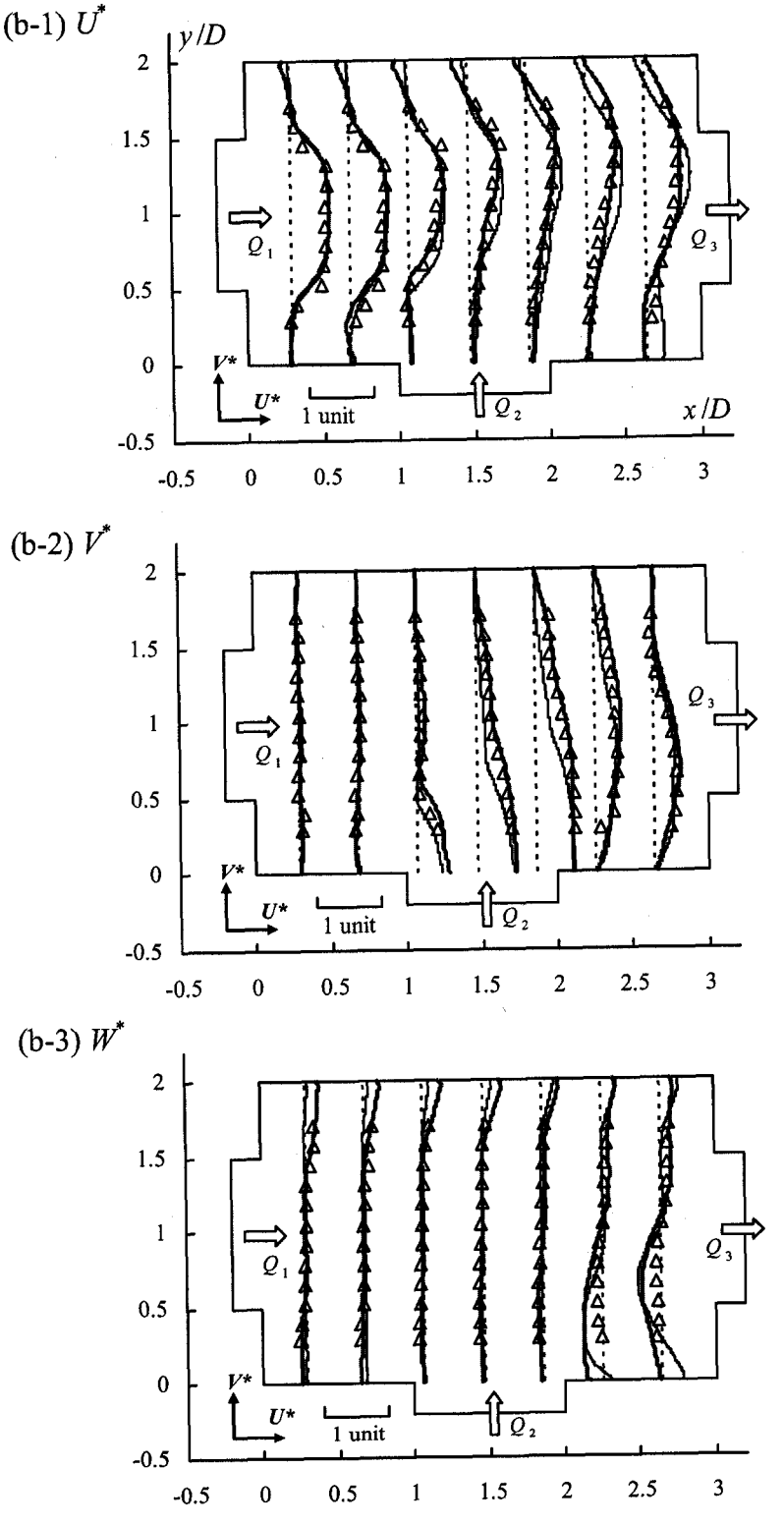

Figure 4.8 (a-c) Comparisons of simulated mean velocities at the central plane with experimental measurements: (b) $Q_2/Q_3 = 0.5$. The inhomogeneous model (———); the homogeneous model (———); and measurements (Δ)

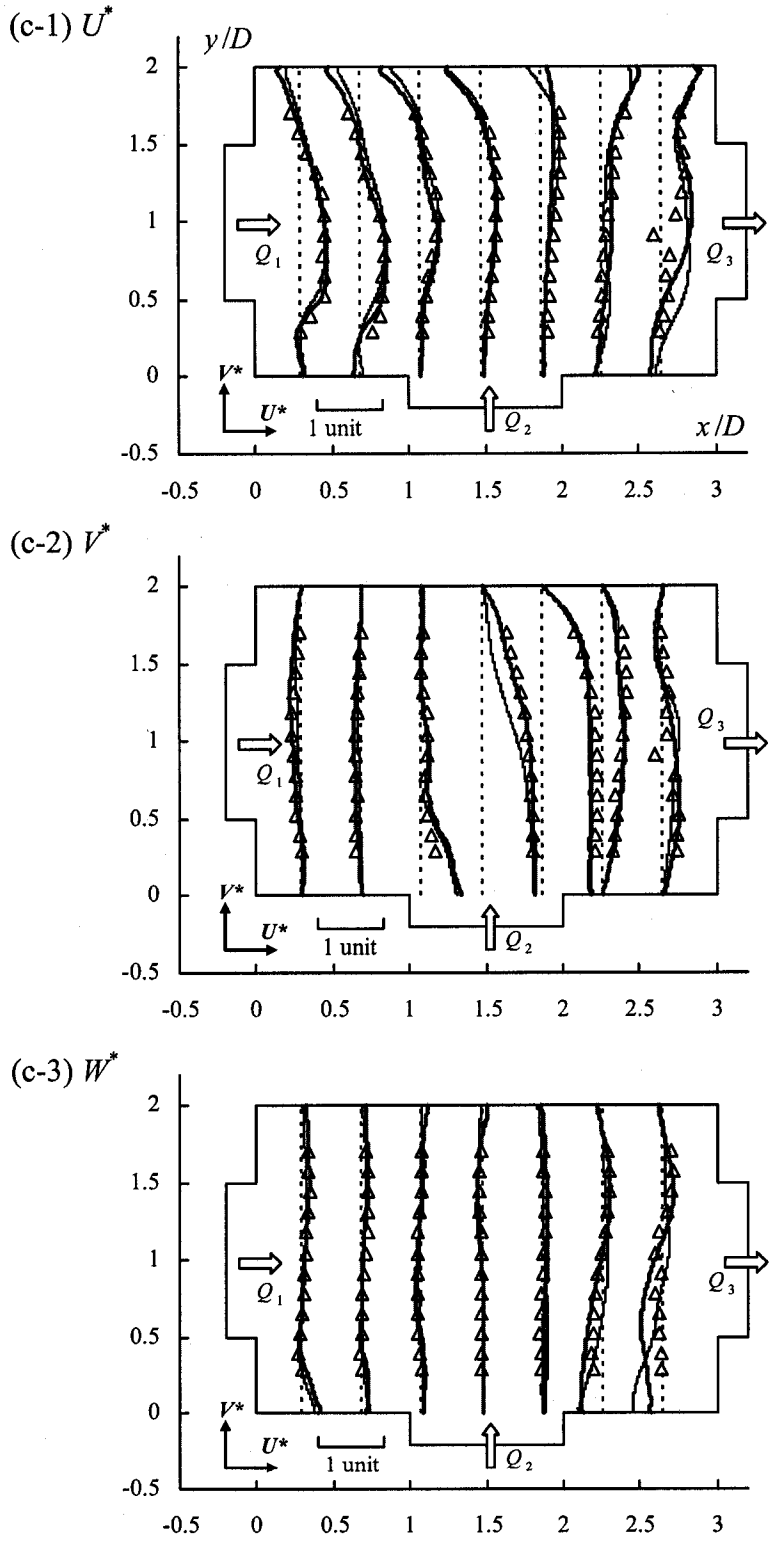

Figure 4.8 (a-c) Comparisons of simulated mean velocities at the central plane with experimental measurements: (c) Q_2/Q_3 = 0.7. The inhomogeneous model (———); the homogeneous model (———); and measurements (Δ)

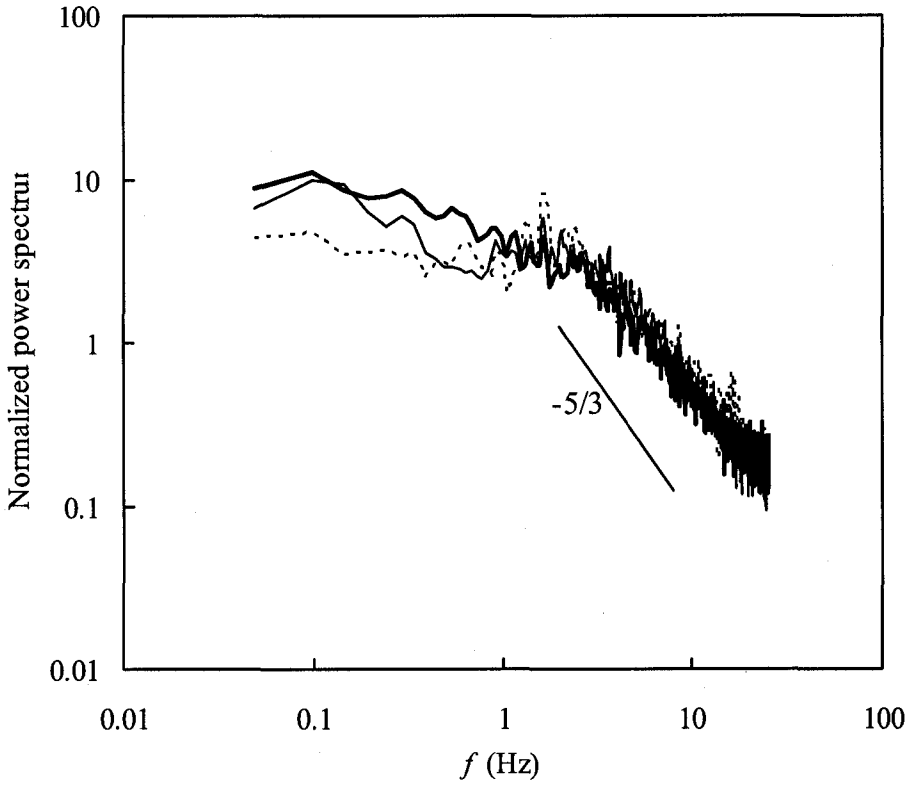

Figure 4.9 Normalized velocity power spectrum at $x/D = 1.87$ and $y/D = 1.05$ at the central plane for $Q_2/Q_3 = 0.4$. $G_u(f)/(u_{rms})^2$ (——);$G_v(f)/(v_{rms})^2$ (--------);$G_w(f)/(w_{rms})^2$ (———)

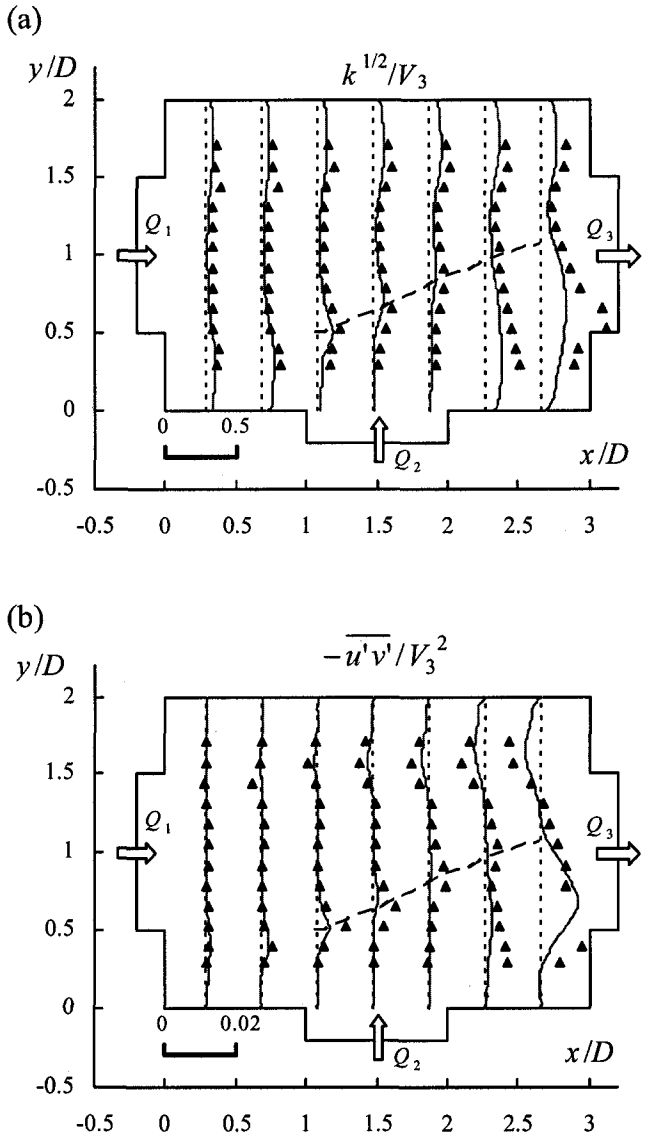

Figure 4.10 Distribution of normalized (a) turbulent kinetic energy ($k^{1/2}/V_3$) and (b) Reynolds stress at the central plane for $Q_2/Q_3 = 0.4$: measurement (▲); the inhomogeneous model (———); and the stream divide (– – –)

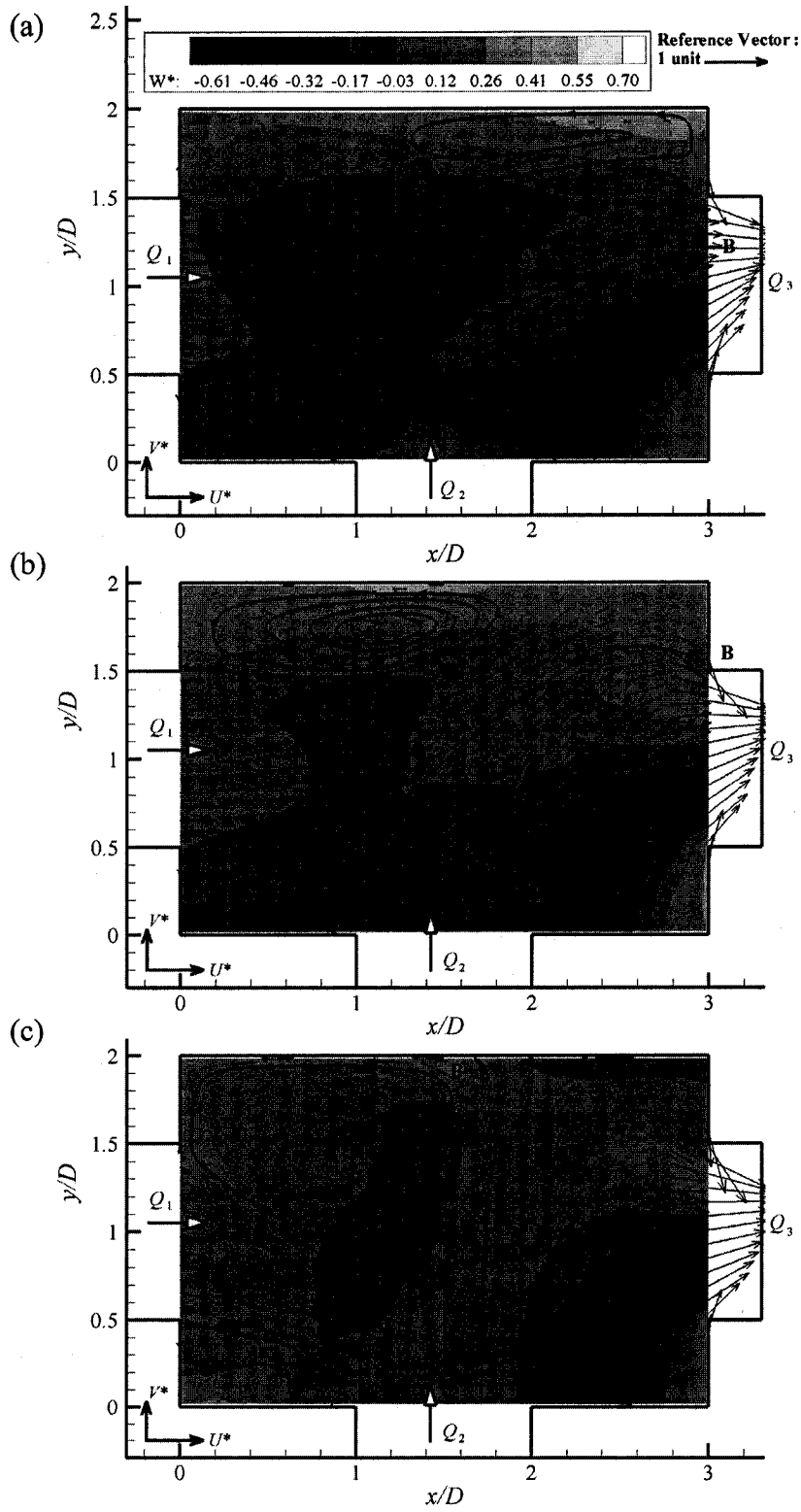

Figure 4.11 Normalized mean velocity distribution at the central plane simulated by the inhomogeneous model for (a) $Q_2/Q_3 = 0.4$; (b) $Q_2/Q_3 = 0.5$; and (c) $Q_2/Q_3 = 0.7$

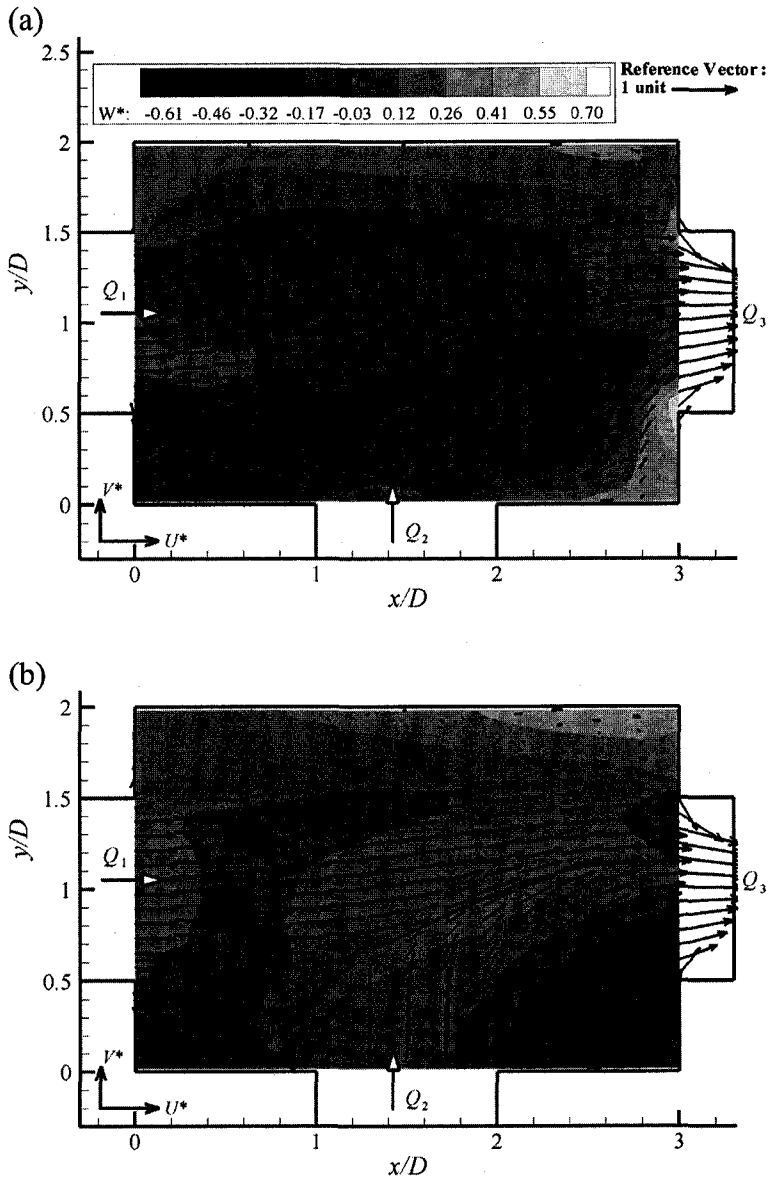

Figure 4.12 (a-d) Simulated mean velocity distributions for $Q_2/Q_3 = 0.4$ at planes of (a) z/D=0.25 and (b) $z/D = 0.75$

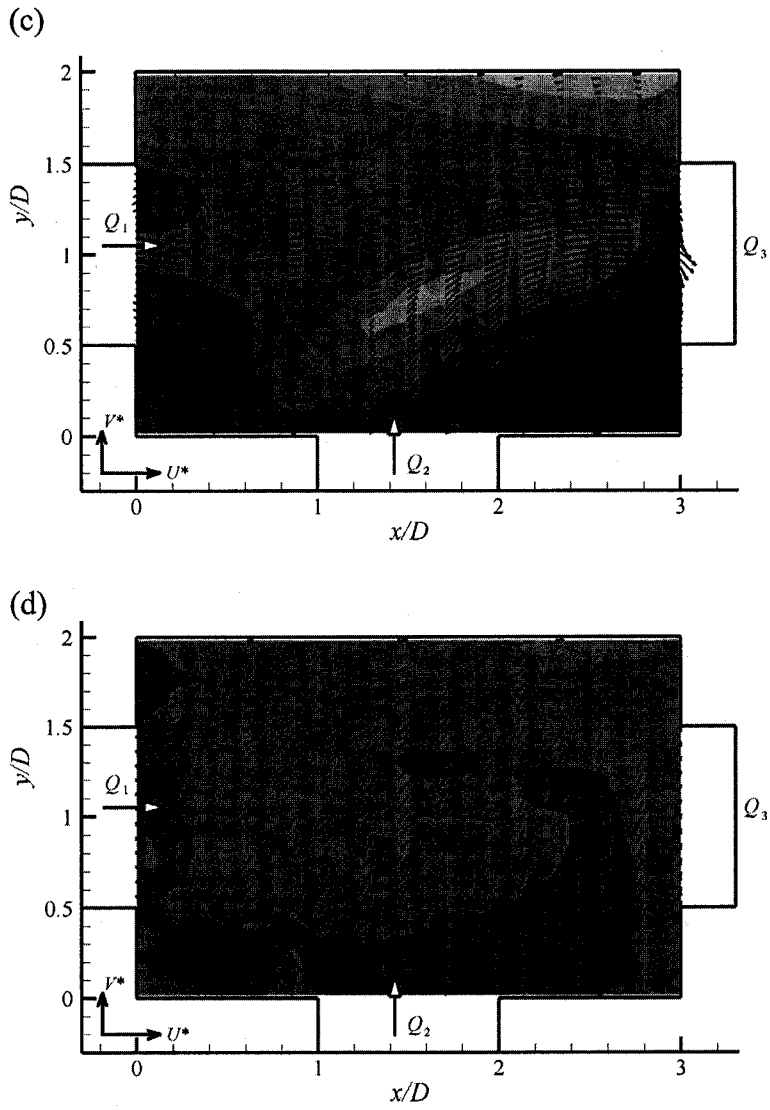

Figure 4.12 (a-d) Simulated mean velocity distributions for $Q_2/Q_3 = 0.4$ at planes of (c) $z/D = 1.1$ and (d) $z/D = 1.9$

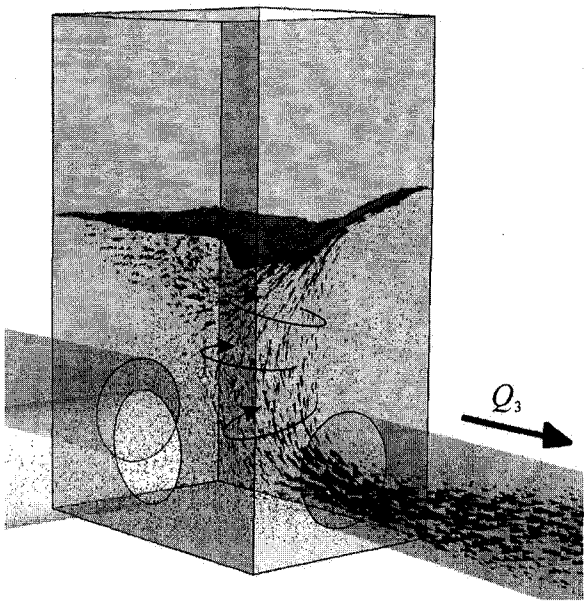

Figure 4.13 Air entrainment simulated by the homogeneous model for $Q_2/Q_3 = 0.7$

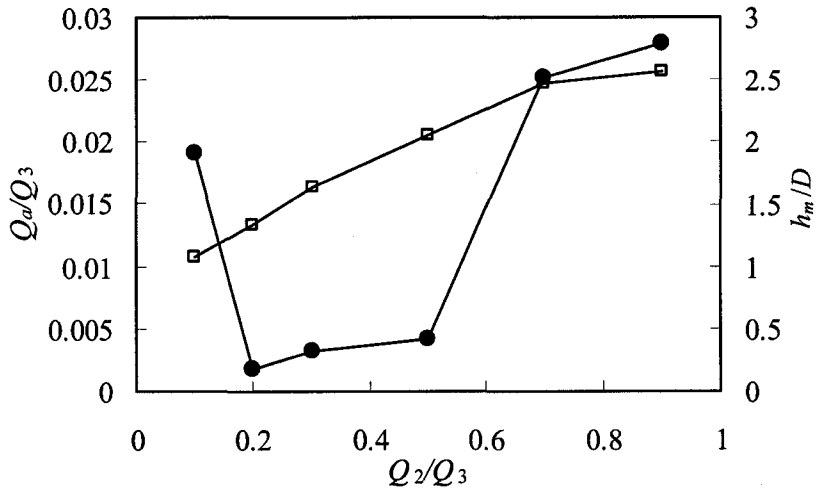

Figure 4.14 Simulated variation of net air entrainment flow ratio (Q_a/Q_3) against inflow ratio (Q_2/Q_3) and water depth in the junction chamber (h_m/D) for $Q_3^* = 1.57$: Q_a/Q_3 against Q_2/Q_3 (—●—); and h_m/D against Q_2/Q_3 (—⊟—)

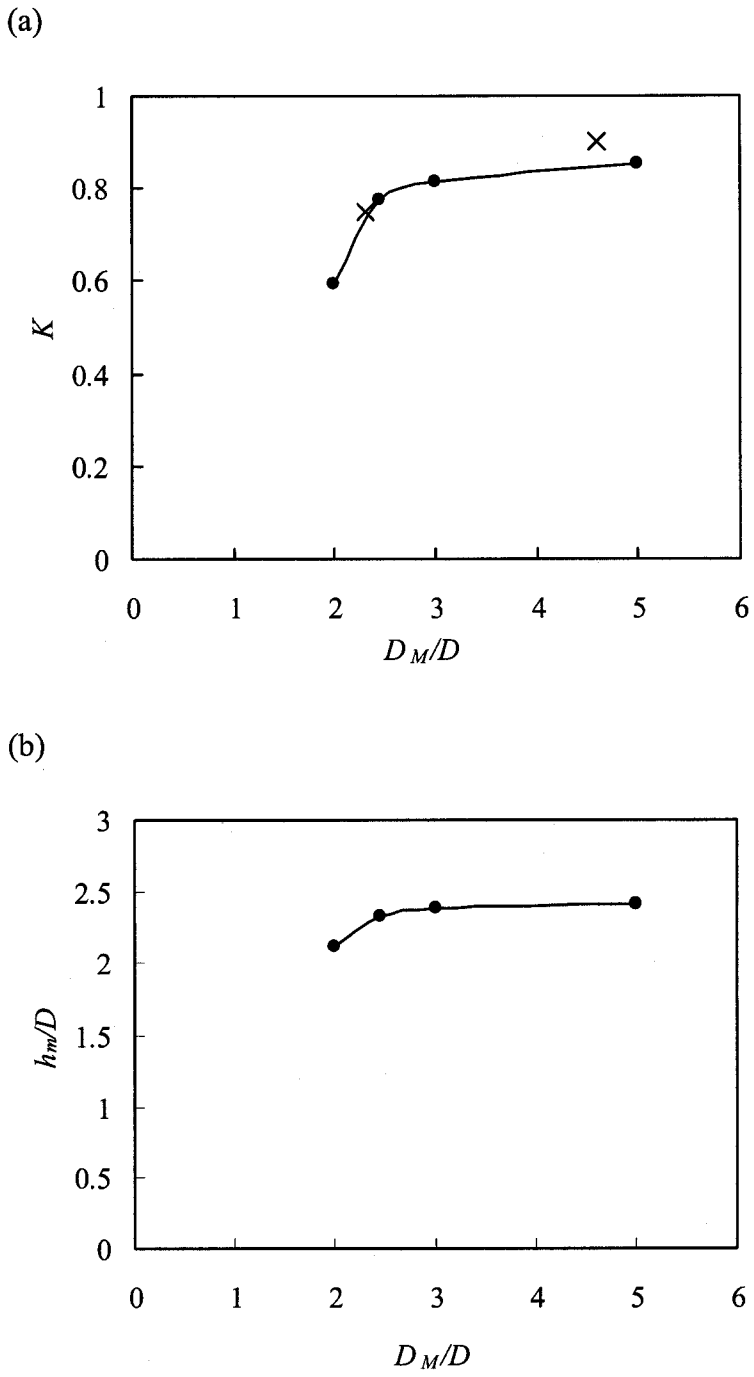

Figure 4.15 Effects of junction chamber size: (a) energy loss coefficient K against the chamber size D_M/D; and (b) mean water depth h_m/D in the chamber against D_M/D: the inhomogeneous model (—●—) and Marsalek (1985) (×)

References

Ansys (2003a). *CFX-5 Solver Theory*. ANSYS Canada Ltd.

Ansys (2003b). "Tutorial 7: free surface flow over a bump." *CFX-5 Tutorials*. ANSYS Canada Ltd.

Drew, D. A. (1983). "Mathematical modelling of two-phase flow." Annual Reviews of Fluid Mechanics, 15:261-291.

Egorov, Y. (2004). "Validation of CFD codes with PTS-relevant test cases." ECORA Report: EVOL-ECORA-D07. http://domino.grs.de/ecora/ecora.nsf

Gisonni, C. and Hager, W. H. (2002). "Supercritical flow in the 90° junction." *Urban Water*, 4(4): 363-372. *Journal of Irrigation and Drainage Engineering*, ASCE, 126(1): 48-56.

Hecker, G.E. (1987). "Chapter 2: Fundamentals of vortex intake flow." *Swirling Flow Problems at Intakes*. Edited by Jost Knauss. A.A. Balkema, Netherlands.

Huang, J., Weber, L. J., and Lai, Y. G. (2002). "Three-dimensional numerical study of flows in open-channel junctions." *Journal of Hydraulic Engineering*, ASCE, 128(3): 268-280.

Hsu, C. C., Wu, F. S., and Lee, W. J. (1998). "Flow at 90° equal-width open-channel junction." *Journal of Hydraulic Engineering*, ASCE, 124(2): 186-191.

Jia, Y., Scott, S., Xu, Y., Huang, S. and Wang, S. S. (2005). "Three-dimensional numerical simulation and analysis of flows around a submerged weir in a channel bendway." *Journal of Hydraulic Engineering*, ASCE, 131(8):682-693.

Liu, M., Zhu, D.Z., and Rajaratnam, N. (2002). "Evaluation of ADV measurements in bubbly two-phase flow." *Proc., Conf. of Hydraulic Measurements and Experimental Methods 2002*, Estes Park, Colo. (CD ROM).

Manninen, M., Taivassalo V., and Kallio S. (1996). *On the Mixture Model for Multiphase Flow*, Espoo, Technical Research Center of Finland, VTT Publications 288. Finland.

Marsalek, J. (1985). *Head Losses at Selected Sewer Manholes*. National Water Research Institute, Canada Centre for Inland Waters, Burlington, Ontario.

SonTek (1997). *Acoustic Doppler Velocimeter Technical Documentation*, V. 4.0, San Diego.

Wang, K.H., Cleveland, T.G., Towsley, C. and Umrigar, D. (1998). "Head loss at manholes in surcharged sewer systems." *Journal of the American Water Resources Association*, 34(6): 1391-1400.

Weber, L.J., Schumate, E.D. and Mawer, N. (2001). "Experiments on flow at a 90° open-channel junction." *Journal of Hydraulic Engineering*, ASCE, 127(5): 340-350.

Wörner, M. (2003). *A Compact Introduction to the Numerical Modeling of Multiphase Flows*, Forschungszentrum Karlsruhe GmbH, Karlsruhe, Germany.

Yen, B.C. (1986). "Hydraulics of sewers." *Advances in Hydroscience*. Edited by B. C. Yen, Academic Press, New York. Vol.14: 1-122.

Zhao, C.H., Zhu, D.Z. and N.Rajaratnam (2004). "Supercritical sewer flows at a combining junction: a case study of Edworthy Trunk Junction, Calgary, Alberta." *Journal of Environmental Engineering and Science,* NRC, 3(5): 343-353.

Zhao, C.H., Zhu, D.Z. and N.Rajaratnam (2006). "Experimental study of surcharged flow at combining sewer junctions." Accepted by *Journal of Hydraulic Engineering*, ASCE, in 2006 March.

Chapter 5

General Analysis and Discussion on Sewer Flow at Junctions

5.1 Introduction

In previous chapters, sewer flow at a 25.8° and a 90° junctions was studied. The investigation covered detailed flow structure, flow regimes, water depth variation, energy loss, and effects of pipe slopes, benching, and junction chamber size. In this chapter, an attempt is made to develop a comprehensive picture of sewer flow at three-way combining junctions.

All the junctions studied and presented previously have an inlet pipe aligned in a straight line with the outlet pipe. In practice, both inlet pipes can have a deflection angle to the outlet pipe. One extreme arrangement is that the two inlet pipes are aligned in a straight line to produce opposing incoming flows, while the outlet pipe is on the lateral. Such junctions, referred to as T-shaped colliding junctions here, is not uncommon in cities with structured blocks (e.g. the City of Edmonton, Alberta). This type of junction was investigated experimentally in this chapter to complete the observation of angle effects.

Sewer junctions with two inflows combining at an acute angle are also commonly used and need to be studied. Although the 25.8° Edworthy model junction was studied, the junction has some considerable site-specific features as a particular retrofit design. Especially, predictions for Regime III flow based on the one-dimensional (1-D) theoretical model were not satisfactory. Therefore, Regime III flow in a 45° combining

junction was simulated and analyzed numerically using the three-dimensional (3-D) inhomogeneous free-surface flow model in Ansys CFX 10.0.

In this chapter, details of study methodology for the two types of junctions are presented. Then, general discussions on sewer flow at junctions are carried out based on results from all junctions studied. Additionally, benching was installed into the 90° model junction studied in Chapters 3 and 4 and its effects are tested and discussed. Some flow features of the T-shaped colliding junction and the 45° junction are also presented.

5.2 Experiments of a T-shaped Colliding Junction

The experimental setup of a T-shaped colliding model junction is shown in Figure 5.1. The model junction was made of Plexiglas. All connecting pipes had the same diameter of D = 0.152 m. The junction chamber was a $2.5D \times 2.5D$ square box with a height of 1 m. The pipe inverts were 25 mm above the bottom of the chamber. The lengths of the straight inlet, the lateral inlet and the outlet pipes were 2 m, 2.2 m, and 2 m, respectively. Both inlet pipes were horizontal and had flow straighteners to produce a smooth approaching flow. The outflow was drained into a reservoir through a big pipe with a relatively steep slope. The total flow rate (Q_3) and one inflow rate (Q_1) were measured using two in-line magnetic flow meters. Four manometers were mounted on each pipe. The piezometric taps were spaced $2D$ apart in the inlet pipes from the chamber and located at $1.5D$, $4.5D$, $6.5D$ and $8.5D$ in the outlet pipe.

In the experiments, the outlet pipe was first laid horizontally and then at a slope of 0.056. Observations of flow regimes in the junction were conducted. When all flow regimes were identified, measurements were taken in the respective regimes.

When the outlet pipe was horizontal, one inflow Q_2 (Figure 5.1) was held constant and the other (Q_1) was increased from 0 to 0.040 m^3/s to observe flow regimes. Four Q_2 values ranging from 0~0.010 m^3/s were tested. When Q_1 was small, subcritical flows were formed in the inlet pipes. They merged in the junction chamber and then freely went into the outlet pipe. With the increase of the flow rate, the water depth in the junction chamber increased; eventually submerged the two inlets and the outlet and made all pipe full. Slug flow could be observed in the outlet pipe during the transition from free-surface flow (Regime I) to full-pipe flow (Regime III) when the chamber outlet was just slightly submerged. When the slope of 0.056 was put on the outlet pipe, a similar test procedure was carried out. With the increase of the flow rate (Q_1), three flow regimes were observed in the sequence: Regime I, free-surface flow across the junction; Regime II, partly surcharged flow with orifice flow in the outlet pipe; and Regime III, fully surcharged flow with all pipes running full. The observations were the same as the flow patterns in a 90° model junction observed previously.

Then, Regime II and Regime III flows at the T junction were investigated in the experiment. Regime III flow was studied in the junction with the horizontal outlet pipe. The total flow Q_3 was held constantly at 0.030 m^3/s, while the flow ratio Q_2/Q_3 was increased from 0 to 1 at a step of 0.1. Manometer readings and measurements of water depth in the junction chamber were taken for each flow combination. Once the measurement results confirmed that the experiment setup was symmetrical, further experiments were conducted by varying the flow ratio Q_2/Q_3 from 0~0.5 and results were extended to the ratio range of 0.5~1 by mirroring. To test the consistency of the experiment, another Q_3 of 0.04 m^3/s was tested with varying Q_2/Q_3 from 0~0.5. A Sontek

Mirco acoustic Doppler velocimeter (MicroADV) was used to measure flow velocities. The velocimeter had a sampling frequency of 50Hz. Velocity measurements were taken for flows of $Q_2/Q_3 = 0.2$ and 0.5 with $Q_3 = 0.03$ m^3/s, at a horizontal plane in the junction chamber across the center of the outlet pipe (Figure 5.1). A sampling time test in the junction flow of $Q_2/Q_3 = 0.5$ showed that the mean velocities and turbulent intensities hardly change for a sampling time over 360 s. Therefore, the velocity measurements were taken for 360 s at each sampling location and the locations were spaced 25 mm in the plane.

Regime II flow was set up in the junction with the outlet pipe at the slope of 0.056. The flow ratio Q_2/Q_3 was held at a constant while the total flow Q_3 was increased at a step of 0.002 m^3/s until Regime III flow was formed. Variation of the water depth in the chamber was measured. Six flow ratios (Q_2/Q_3) from 0~0.5 were tested and the results were mirrored into the range of Q_2/Q_3 of 0.5~1.

5.3 Numerical Simulation for a 45° Junction

An inhomogeneous free-surface flow model was set up using Ansys CFX 10.0 and used to simulate Regime III flow in a 90° junction in Chapter 4. The model was validated with satisfactory performance in predicting mean flow velocities, submergence factors and energy coefficients in the flow. Here, the numerical model was used to predict Regime III flows in a 45° combining junction. The simulated junction is shown in Figure 5.2, which has a straight inlet (Q_1) and a lateral inlet (Q_2) joining at 45°. All three pipes are horizontal and have a diameter of D = 152 mm. The two inlet pipes are 0.5 m long and the outlet pipe is 2 m long. The junction chamber is a $3D \times 3D$ square box with a height of 0.6 m. The junction was discretized into 570,092 small control volumes using a

mesh generated by CFX-Mesh (Figure 5.2). The mesh had structured grids in the near-wall regions and unstructured grids inside, forming elements of tetrahedra, pyramids and wedges. The maximum spacing between the grids is 16 mm. The mesh is supposed to have the same resolution with that for the 90° junction in Chapter 4, which was sufficient to eliminate the sensitivity of simulation results to mesh size.

In the present study, a total flow $Q_3 = 0.035$ m^3/s was maintained while five flow combinations were simulated with Q_2/Q_3 ranging from 0.1~0.9. Power-law velocity profiles were assigned at both inlets and a turbulent intensity of 3.7% and an eddy length scale of $D/4$ were assumed there. An average static pressure equal to zero (the atmosphere pressure) was assumed over the downstream outlet. An "opening" boundary condition was assigned to the top of the chamber with a relative pressure equal to the atmosphere pressure, which allows the air to cross the boundary either into or out of the simulation domain.

5.4 Characteristics of Flow at Sewer Junctions

At combining sewer junctions, three flow regimes can exist:

Regime I: free-surface flow (subcritical/supercritical) through the junction;

Regime II: partly surcharged flow with (supercritical) free-surface flow in the outlet pipe;

Regime III: fully surcharged flow (all connecting pipes are running full.).

5.4.1 Regime I flow

Regime I flow occurs at relatively small flow rates. When benching exists, the flow is channeled all the way through the junction chamber. For subcritical flow, energy loss in the flow is relatively small (Marsalek 1985) and the flow may be analyzed based

on studies of open-channel junction flow by, e.g., Ramamurthy (1988), Hsu et al. (1998), Weber et al. (2001) and Shabayek et al. (2002).

For junctions with no benching, a pool is formed in the chamber. The momentum carried by the incoming subcritical flows may become relatively small when the flow approaches the chamber outlet. Its impacts on the flow in the junction chamber may be neglected. Thus, the outlet pipe may perform similar to an unsubmerged culvert. A relation between the total flow rate (Q_3) and the depth in the junction chamber could be found in the form of that for weir-type flow as

$$Q_3^+ = \frac{Q_3}{(gD_3^5)^{1/2}} = C_d\left(\frac{h_m}{D_3}\right)^{3/2} \tag{5.1}$$

where g is the gravitational acceleration; D_3 is the outlet pipe diameter; C_d is the discharge coefficient; and h_m is the mean depth in the junction chamber, measured from the invert of the outlet pipe. Figure 5.3 presents measurement results obtained in the experiment of a 90° junction of Chapter 3 and in the T-shaped colliding junction. The data covers flow ratios Q_2/Q_3 ranging from 0.33 to 1 and slopes of the outlet pipe from 0~0.061 for the 90° junction and 0 and 0.056 for the colliding junction. C_d = 0.4 was found to be the best fit for the data. Apparently, the arrangement of inlet pipes (junction angle) has no noticeable impacts on the depth-discharge relation for sewer junctions. When h_m/D_3 exceeds 1 with increasing flow rates, Regime I ends and the flow moves to the next regime (Regime II or III).

If incoming flows are supercritical, approaching momentum is significant and the analysis mentioned above may not be applicable. Supercritical flow at junctions is featured by shock waves due to interactions between inflows and chamber walls. Water

surface profile in junction chambers is dominated by the waves. A depth-discharge relation may not exist. Del Giudice and Hager (2001) and Gisonni and Hager (2002) investigated wave configurations of supercritical flow in sewer junctions, and one could find choking limits (where Regime I ends) for the junctions from their observations. However, it should be understood that the wave patterns may be dependent strongly on the geometry of junction chambers (e.g., chamber size, shape, benching design, and junction angle). Further studies may be needed to develop a criterion of regime change for supercritical sewer junctions.

5.4.2 Regime II Flow

Regime I ends when the chamber outlet of a junction is choked or the depth $h_m/D > 1$ at a certain flow rate. If the slope of the outlet pipe is steep enough to form supercritical flow in the pipe for the flow rate, Regime II flow will be present. The inlet pipes are running full and the chamber outlet is submerged. Orifice flow exists in the outlet pipe. The flow can be described by the 1-D momentum equation derived previously. Here, in a more general form for a junction shown in Figure 5.4, the equation is presented as:

$$\frac{h_m}{D_3} = \frac{1}{C_c} Q_3^{*2} - \frac{A_1}{A_3} Q_1^{*2} \cos(\sigma_1 \theta_1) - \frac{A_2}{A_3} Q_2^{*2} \cos(\sigma_2 \theta_2) + \tfrac{1}{2}(C_c^{\,2.2} + 1) \tag{5.2}$$

$$Q_i^* = Q_i / (g D_3 A_i^{\,2})^{1/2} \tag{5.3}$$

where ρ is water density; Q is flow rate; A is the pipe area with the subscripts 1, 2 and 3 denoting sections in inlet pipe 1, inlet pipe 2, and the outlet pipe, respectively; θ is the junction angles; and σ is correction factors accounting for deflection of incoming streams and maybe simplifications made in the derivation of the equation (e.g. assumptions of

hydrostatic pressure distribution and horizontal water surface); D is the pipe diameter; C_c is the contraction coefficient at the outlet; and subscripts i = 1,2 and 3.

Eq. (5.2) predicts well the water depth of Regime II flow in junction chambers when proper values of the contraction coefficient (C_c) and the angle correction coefficients (σ_i) are used. The values of C_c used in this study are: C_c = 0.75 for sharp-edged outlets and C_c = 0.85 for rounded outlets of junction chambers. For other chamber outlet types, one may refer to literature of orifice (gated) flow in closed conduits (such as culverts).

The angle correction coefficients might be a function of flow ratios and junction angles, and may be affected by pipe size and chamber size. Calibration may be needed to determine the proper values for particular junctions. In this study, the following values were used: $\sigma_1 = \sigma_2 = 1$ for the acute-angle junctions (the Edworthy junction and the 45° junction); and $\sigma_1 = 1$ and $\sigma_2 = 8/9$ for the 90° junction. For the measurements in the T-shaped colliding junction, a good fit was found using the following relation:

$$\sigma_i = 1-(1-Q_i/Q_3)^2 \tag{5.4}$$

As predictions of Eq.(5.2) are not very sensitive to the correction coefficients, the 1-D theoretical model can also produce satisfactory predictions with Eq.(5.4) for all other junctions studied. Therefore, Eq.(5.4) may be recommended for junctions with various angles and comparable size to the junctions studied.

Comparisons of predicted and measured h_m/D in junctions are presented in Figure 5.5. Eq. (5.2) slightly overestimates the water depth in the T-shaped colliding junction, but the predictions are still within a reasonable range. For the 25.8° Edworhy junction and the 90° junction, the depth can be predicted very well.

5.4.3 Regime III Flow

Regime III flow has full-pipe flow in all connecting pipes of a junction. As the outlet pipe is full, different from Regime II flow, the water depth in the junction chamber is dependent on the downstream condition, or pressure in the outlet pipe, but not only on inflow conditions. Coupling the depth with the pressure in the outlet pipe is a general way to describe the characteristics of Regime III flow in a junction chamber. This leads to the definition of submergence factor:

$$\psi = (h_m - \frac{p_3}{\rho g}) \Big/ D_3 \tag{5.5}$$

where ψ is the submergence factor; p_3 is the pressure at the invert of section 3 in Figure 5.4c that is supposed to be right after the separation zone at the pipe entrance. Variation of the submergence factor with inflow conditions was derived in the 1-D theoretical analysis as follows:

$$\psi = Q_3^{*2} - \frac{A_1}{A_3} Q_1^{*2} \cos(\sigma_1 \theta_1) - \frac{A_2}{A_3} Q_2^{*2} \cos(\sigma_2 \theta_2) \tag{5.6}$$

The angle correction coefficients (σ_1 and σ_2) can be obtained from Eq.(5.4). For given flow rates in practice, one may predict ψ using the equation above and estimate p_3 by using pipe flow theory, such as Darcy-Weisbach equation, in the outlet pipe with a known pressure at downstream. When p_3 is known, the water depth in the junction chamber, h_m, can be obtained from Eq.(5.5).

As discussed in Chapter 3, Eq.(5.6) predicts the submergence factor reasonably well for the 90° junction and the 25.8° Edworthy junction with comparable inflows. However, the equation underestimated the submergence factor for lateral flow ratios (Q_2/Q_3) approaching 0, and for the Edworthy junction with large Q_2/Q_3. In Figure 5.6,

Eq.(5.6) is compared with measurements in the T-shaped colliding junction and simulated results for the 45° junction. The predictions for the T-shaped colliding junction are satisfactory with small discrepancies at highly uneven inflow ratios (Q_2/Q_3 close to 0 or 1). For the 45° junction, Eq. (5.6) predicts the variation trend of ψ very well, but it underestimates the values. The limitations of the 1-D theoretical model come from likely the simplifications made in the derivation, such as the hydrostatic pressure distribution in junction chambers. It is believed that improvements could be obtained for the model by introducing empirical correction factors with further calibrations when more data are available. For practical use, Figure 5.7 summaries data of the submergence factor variations in all junctions studied, which shows essentially effects of flow rates and junction angles on the submergence factor.

5.5 Onset of Regime

In practice, Regime I is the normal operation condition of sewer junctions. However, surcharged regimes may not be avoidable for design flows and some rare events. With subcritical inflows, water depth in the junction chamber may be determined according to the discussion above; and the depth $h_m/D > 1$ can be regarded as the onset of surcharged regimes. For supercritical flow, choking of the chamber outlet due to standing waves in the junction may suggest the break of Regime I. However, as impacts of junction geometry on free-surface flow may be significant, further study on the choking criteria may be necessary, especially for supercritical flow.

At the break of Regime I (free-surface) flow, Regime II flow will occur if the outlet pipe is steep, i.e. its slope is larger than the critical slope for the choking flow rate. Otherwise, Regime III flow may be formed. For example, the criterion for the onset of

surcharged flow regime can be assumed as $h_m/D = 1$ for the 90° junction studied in Chapter 3; and the choking flow rate Q_{3c}^+ is equal to C_d according to Eq.(5.1). For the flow rate, one could find the critical slope (S_c) for the outlet pipe using Manning's equation and the definition of the Froude number (F_r) equal to 1 as follows:

$$Q_{3c} = \frac{1}{n} A R_h^{2/3} S_c^{1/2} \tag{5.7}$$

$$F_r = Q_{3c} / (A\sqrt{gA/T}) = 1 \tag{5.8}$$

where, A is flow area; R_h is hydraulic radius, and T is top width of the open-channel flow. For the 90° junction, $C_d = 0.4$ and assuming Manning's $n = 0.009$ for the Plexiglas pipe, S_c can thus be solved from Eq.(5.1), Eq.(5.7) and Eq.(5.8) and $S_c = 0.0043$. Therefore, for the junction, if the slope of the outlet pipe $S_0 > S_c$, Regime II flow can be expected. In fact, Regime II flow was observed in the experiments of Chapter 3 when S_0 was 0.014 and larger, but not when $S_0 = 0$ and 0.003.

In Regime II flow, with supercritical flow in the outlet pipe, a pair of inlet waves exists at the junction chamber outlet. The waves are expected to have impacts on the stability of Regime II flow. The transition from Regime II to Regime III flow with increasing inflow rates may be related to the development of the inlet waves: if they are violent, they may cause priming in the outlet pipe and result in the onset of Regime III.

Figure 5.8 presents the criteria for the regime transitions in junctions studied as a function of the total flow rate Q_3^* against the velocity ratio V_2/V_3, where V is the average velocity and $V_i = Q_i/A_i$. Data points in the figure are essentially the maximum flow rate that can pass a junction in Regime II at a given flow ratio, which form the upper boundary of Regime II. When the flow rate exceeds the upper boundary, Regime III will form. Data points obtained in the 25.8° Edworthy junction and in the 90° junction may be

represented by the same trend line when $V_2/V_3 \leq 0.3$, i.e. the straight inflow is dominant. Small difference is seen at larger lateral inflow rates, which may be attributed to effects of junction angle. As the experiment of the Edworthy junction tested flow ratios only up to 0.6 of V_2/V_3, the trend line for its upper boundary of Regime II flow in Figure 5.8 is just an approximation. However, one could still expect that the difference between the boundaries for the 25.8° junction and the 90° junction is fairly small. Note that in Figure 5.8 the velocity ratio is used instead of the flow rate ratio Q_2/Q_3 with the intent to consider effects of pipe size ratios; however, care should be taken that in the experiments, the 90° junction and the T-shaped colliding junction have identical sizes for connecting pipes, and the 25.8° Edworthy junction of which the lateral conduit was a rectangular duct with $A_2/A_3 = 0.88$.

In Figure 5.8, the upper boundary of Regime II flow for the T-shaped colliding junction is symmetrical about $V_2/V_3 = 0.5$ because of the symmetrical arrangement of the junction. At $V_2/V_3 > 0.5$, the data points fall on the same trend line for the 90° junction. On the other side of $V_2/V_3 < 0.5$, the difference between the two junctions indicates effects of the inflow angle of Q_1. (Note: for the 90° junction, $\theta_1 = 0$ and $\theta_2 = 90°$; and for the colliding junction, $\theta_1 = \theta_2 = 90°$)

Lower boundaries of Regime II flow are also shown in Figure 5.8. Across the boundary, Regime II flow changes into Regime I flow with decreasing flow rates. The lower boundaries were obtained using Eq.(5.2) for the mean depth $h_m/D = 1$. Effects of junction angles on the boundary are presented in a similar pattern with those on the upper boundary discussed above.

5.6 Energy Loss in Fully Surcharged Flow

In design and analysis of sewer junctions, energy methods are usually used. For fully surcharged flow (Regime III), energy coefficients could be derived from the 1-D theoretical mode as follows:

$$K_{13} = 1 - 2\frac{A_3}{A_1}\left(\frac{Q_1}{Q_3}\right)^2 \cos(\sigma_1\theta_1) - 2\frac{A_3}{A_2}\left(\frac{Q_2}{Q_3}\right)^2 \cos(\sigma_2\theta_2) + \left(\frac{A_3}{A_1}\right)^2\left(\frac{Q_1}{Q_3}\right)^2 \tag{5.9a}$$

$$K_{23} = 1 - 2\frac{A_3}{A_1}\left(\frac{Q_1}{Q_3}\right)^2 \cos(\sigma_1\theta_1) - 2\frac{A_3}{A_2}\left(\frac{Q_2}{Q_3}\right)^2 \cos(\sigma_2\theta_2) + \left(\frac{A_3}{A_2}\right)^2\left(\frac{Q_2}{Q_3}\right)^2 \tag{5.9b}$$

$$K = \frac{Q_1}{Q_3}K_{13} + \frac{Q_2}{Q_3}K_{23} \tag{5.9c}$$

As the equations are primarily based on Eq.(5.6), limitations of the model discussed above in predicting submergence factor also exist in predicting the energy coefficients for sewer junction flow. As other junctions were discussed in previous chapters, here predicted energy coefficients are compared with experimental measurements for the T-shaped colliding junction in Figure 5.9 and with numerical simulation results those for the 45° junction in Figure 5.10. Eq.(5.9) works reasonably well for both junctions with comparable inflows. In sewer junction design, Eq.(5.9) could be a first estimate, and again, it would be needed to introduce empirical corrections for a good prediction.

Figure 5.10 also compiles some experimental measurements in a 90° junction and the 25.8° Edworthy junction to show effects of junction angles. From the comparison, it may be said that: (1) when the straight inflow is dominant (small Q_2/Q_3), effects of junction angles are insignificant; and (2) energy loss in the 45° junction is much smaller than that in the 90° junction at relatively large Q_2/Q_3, but further reducing the junction angle from 45° to 25.8° shows only limited reduction of energy loss.

5.7 Considerations of Other Factors

Some other factors in sewer junction design that may have impacts on flow are briefly discussed in this section, including pipe slopes, size of junction chambers and benching design.

5.7.1 Pipe Slopes

Pipe slopes are expected to have significant impacts on free-surface flow. They determine whether the flow is supercritical or subcritical. As discussed above, the slope of the outlet pipe impacts on the onset of flow regimes in a sewer junction. If the outlet pipe has a sufficiently steep slope, supercritical flow will occur and Regime II flow can exist in the junction. However, once surcharged flow is set up, including Regime II and Regime III, pipe slopes do not matter. As discussed in Chapter 3, in Regime II flow, water depth in a junction chamber for given inflow rates, is independent of the slope of the outlet pipe. Also, the slope does not affect the transition criteria for Regime II to III. A steeper outlet pipe could result in smaller depth in the junction chamber in Regime III flow; however, the slope change has no impacts on submergence factor and energy loss coefficients in the flow.

5.7.2 Junction Chamber Size

Chamber size determines the room for flow interaction and mixing in a sewer junction. Regime I flow may not be affected by chamber size if it is subcritical; but if inflows are supercritical, different chamber size may result in differences in wave locations and wave heights in sewer junctions, and thus may impact on criteria of regime transition.

For Regime II flow, the stability of the orifice flow in the outlet pipe may be affected by inflow momentum (especially that from the lateral) approaching the chamber outlet. If a junction chamber is too large, the momentum that reaches the outlet will be weak, and the transition from Regime II to Regime III is expected at larger flow rates. As all tests of the transition were conducted in junctions with comparable chamber size (all junction chambers have an equivalent diameter of about 2.5D), the statement here is just a hypothesis and further studies will be needed to discuss impacts of the chamber size on the regime transition.

The effect of chamber size on energy loss in Regime III flow was investigated in Chapter 4. It was found that larger chamber can cause larger energy loss, but the effect may be negligible when the chamber size exceeds 3D.

5.7.3 Benching

Two types of benching are commonly used in sewer junction design: half benching and full benching. As shown in Figure 5.11, half benching is a half-circle channel at the bottom of a junction chamber, leading the inflow through the junction; and full benching is a U-shaped channel with a height of D. Both benching types were tested experimentally in the 90° model junction presented in Chapters 3 and 4.

For Regime II flow, benching designs make no noticeable difference in water depth in junction chambers. Eq.(5.2) is applicable for junctions with and without benching. However, benching apparently helps to stabilize the flow pattern. Regime II flow can be maintained at larger flow rates in junction chambers with benching than those without benching. Figure 5.12 shows impacts of benching on the transition from Regime II to III observed in the 90° junction. As shown, the most significant impact

appears when one of the inflows is dominant. When two inflows are comparable, benching effects are relatively small as interaction of inflows is dominant. In Regime III flow, traditionally benching is regarded as a way to reduce energy loss. However, as discussed in Chapter 3, effects of benching on reducing energy loss in Regime III flow are limited and only noticeable when one inflow is dominant.

5.8 Surcharged Flow Structures of the Colliding Junction and the 45° Junction

5.8.1 Mean Velocity Distribution in the Colliding Junction

To improve understanding of the inflow interaction in the T-shaped colliding junction, mean velocity distributions of Regime III flow were measured at the central plane by the MicroADV. The distributions are presented in Figure 5.13. The velocities were normalized with the average velocity in the outlet pipe (V_3) and are presented in Figure 5.13. The figure shows the normalized plane velocity (U^*—V^*) vector fields with the contours of normalized vertical velocity W^*. In the figure, the coordinates x and y are measured from the chamber center with x positively pointing at the outgoing flow direction (Figure 5.2).

In Figure 5.13(a), Q_2/Q_3 = 0.2 and Q_1 is the primary flow. The velocity distribution suggests that the flow behave like that in a bend junction. The inflow Q_1 on the right hand jets into the chamber with ambient water entrained from the north side (Figure 5.2) and approaches the other side of the chamber with fairly small deflection and part of entrained water being returned back to the circulation region. As the MicroADV probe was not able to reach the inlet sufficiently close, Figure 5.13(a) does not show how the inflow Q_2 enters the chamber. The inflow was visualized by injecting dye in the pipe some distance upstream from the junction chamber. The dye trace showed that a main

portion of the inflow Q_2 was squeezed into the circulation region at the north side of the chamber through the path sketched in Figure 5.13(a), while the rest just diffused along the wall right at the entrance.

When the two inflows are equal (Q_2/Q_3 = 0.5), as shown in Figure 5.13(b), the velocity filed is symmetrical. The two incoming streams meet at the center of the chamber (along the axis of the outlet pipe). They spread along the center respectively with the primary part running towards the outlet, as if the streams impinged on a vertical free-slip plane at the chamber center. One circulation region is formed at the north side for each stream. For both flows (especially for the flow of Q_2/Q_3 = 0.5), vertical velocities are relatively small (close to zero) and fairly uniform in the central plane.

5.8.2 Simulated Regime III Flow in the 45° Junction

Figure 5.14 shows velocity (U^*—V^*) vector fields (normalized using the average velocity in the outlet pipe) at the central plane (z/D = 0.5) for Q_2/Q_3 = 0.1, 0.5 and 0.9. The contours are for vertical velocity W^* and the red solid lines represent stream lines. Coordinates are defined in Figure 5.2 as that x is measured from the southwest corner of the chamber positively in the direction of the outgoing flow; y is the transverse axis; and z is measured from the pipe inverts positively pointing upwards. In Figure 5.14(a), Q_2/Q_3 = 0.1 and the straight incoming flow is dominant. The straight stream goes through the junction chamber with negligible influence of the lateral flow. Apparently, only a very small portion of Q_2 can squeeze into the outlet pipe at the central plane. Most of the other is diffused and lifted up. When the two incoming flows are equal as shown in Figure 5.14(b), they merge smoothly without noticeable deflection. While the lateral flow becomes prevailing in Figure 5.14(c), it directly jets into the outlet pipe and most of the

straight incoming flow appears to be diffused. For all three flow combinations, the vertical velocities in the central plane are relatively small and their distributions are very uniform.

Figure 5.15 presents velocity distributions at different planes for the flow of $Q_2/Q_3 = 0.5$. Figure 5.15 (a) shows the distribution in the plane $D/4$ lower than the central plane ($z/D = 0.25$) and Figure 5.15(b) is for the plane of $D/4$ higher ($z/D = 0.75$). The distributions of U^*—V^* vectors have similar patterns with that in the central plane (Figure 5.14b). At $z/D = 0.25$, the vertical velocity is downward (negative) when the two streams meet and upward (positive) when the flow is approaching the exit; at $z/D = 0.75$, it is reversed. In Figure 5.15(c) at the plane of $z/D = 1.1$ (slightly above the pipe crown), water is dragged toward the end wall by the two incoming jets underneath. Water rises up at the location where the two inflows meet and is sucked down at the outlet. Relatively high positive vertical velocities are also observed at the southeast corner of the chamber where water is dragged by the lateral inflow and hits on the end wall of the chamber. The plane of $z/D = 2.15$ in Figure 5.15(d) is very close to the water surface (about $0.1D$ below). The flow there is apparently reflected by the chamber end wall. The distribution of W^* is fairly uniform and upward.

5.9 Conclusions

Three flow regimes can exist at combining sewer junctions: free-surface flow through the junction (Regime I); partly surcharged flow with free-surface flow in the outlet pipe (Regime II); and fully surcharged flow (Regime III). These types of flow are discussed for three-way combining sewer junctions. Results of laboratory experiments and numerical simulations were generalized and presented based on theoretical analysis.

Criteria for regime transitions were developed and may be used in analyzing sewer junctions comparable with those studied. Once a surcharged flow regime is determined, the flow may be analyzed using the derived 1-D theoretical model. Regime III flow could also be analyzed using energy concepts with energy coefficients presented. Energy loss in junction flow could be reduced by decreasing junction angles; but the reduction may not be considerable in further degreasing the angle from 45°. When inflows are comparable, benching has insignificant effects on reducing energy loss in surcharged flow. However, benching could help to stabilize flow and have noticeable impacts on regime transitions. Detailed flow structures of Regime III flow in a T-shaped colliding junction and a 45° junction were presented.

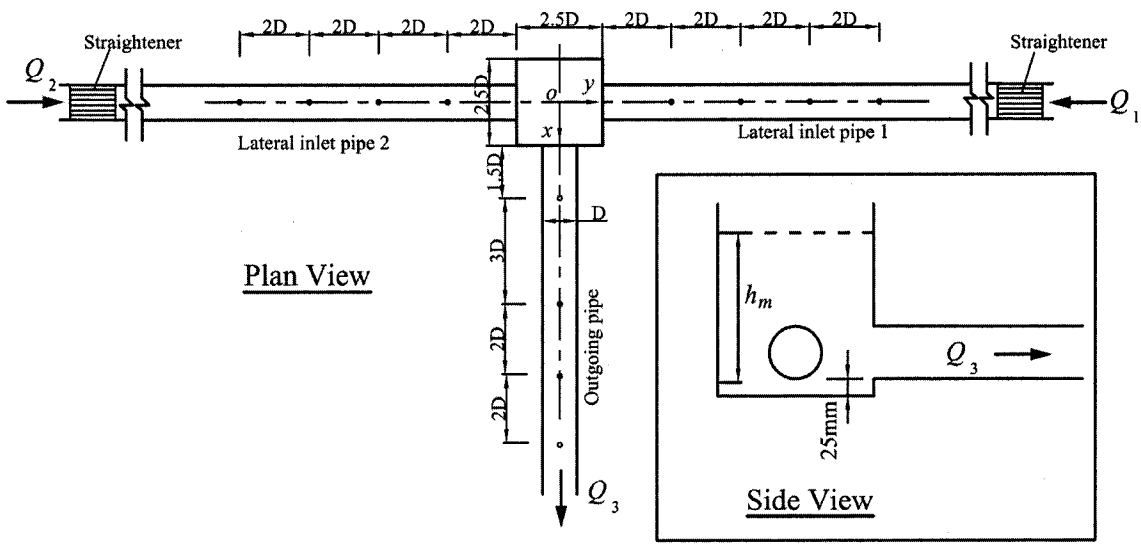

Figure 5.1 Experiment setup of a T-shaped colliding junction (○: piezometric taps)

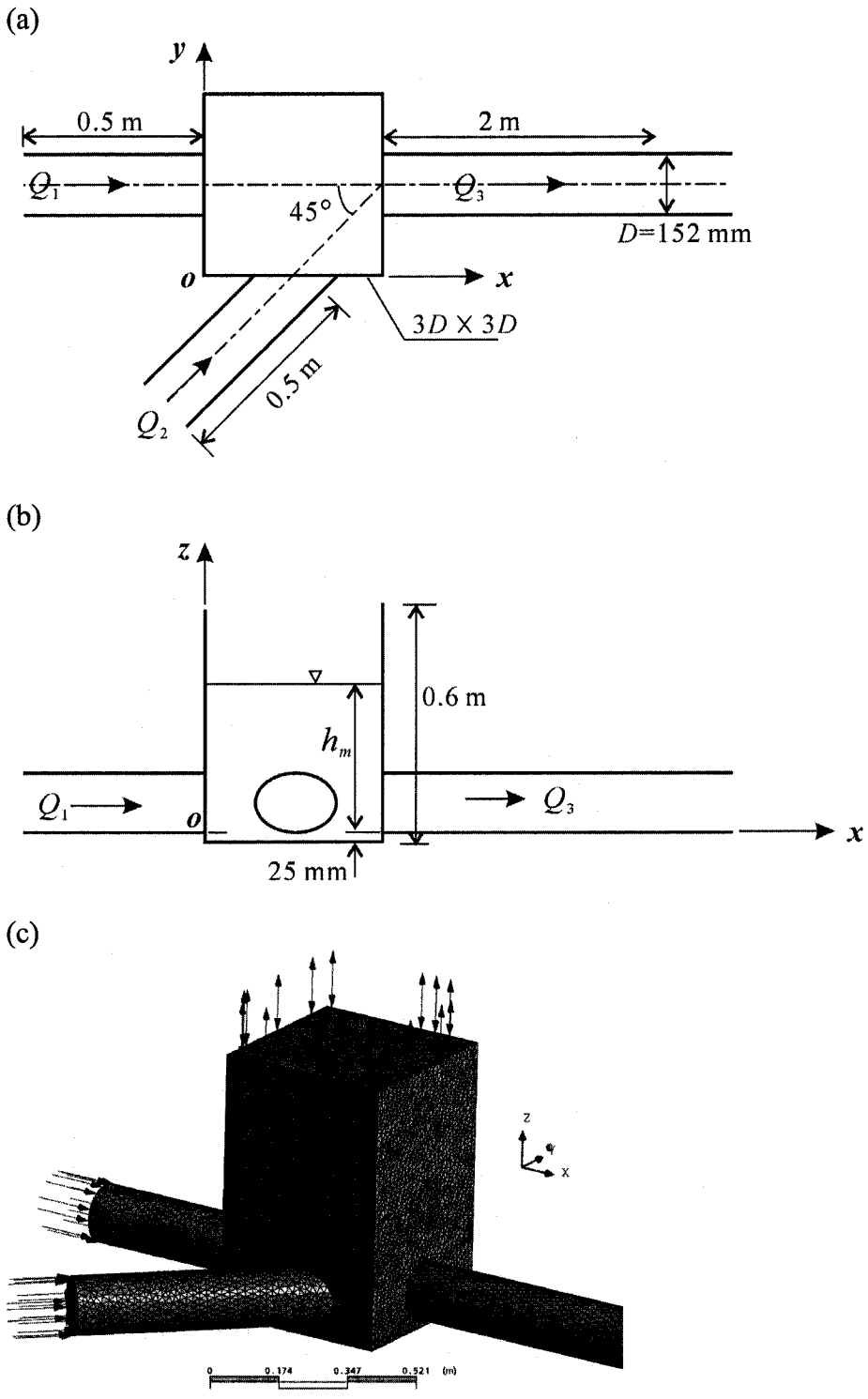

Figure 5.2 Simulated 45° combining sewer junction: (a) plan view; (b) side view; and (c) mesh used in the numerical model

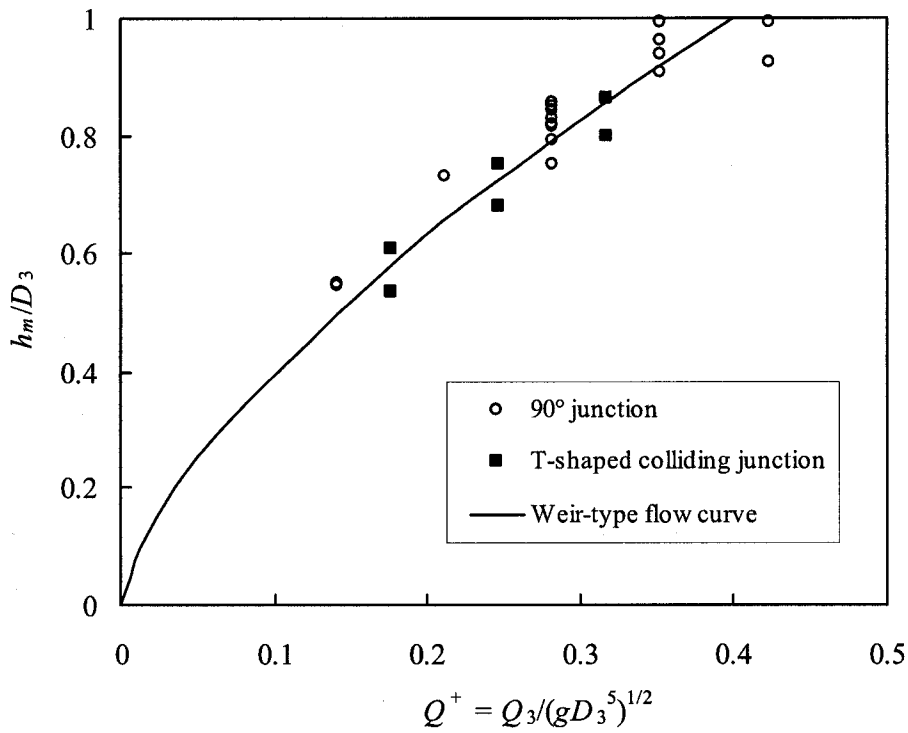

Figure 5.3 A depth-discharge relation for Regime I flow (subcritical) in junctions without benching

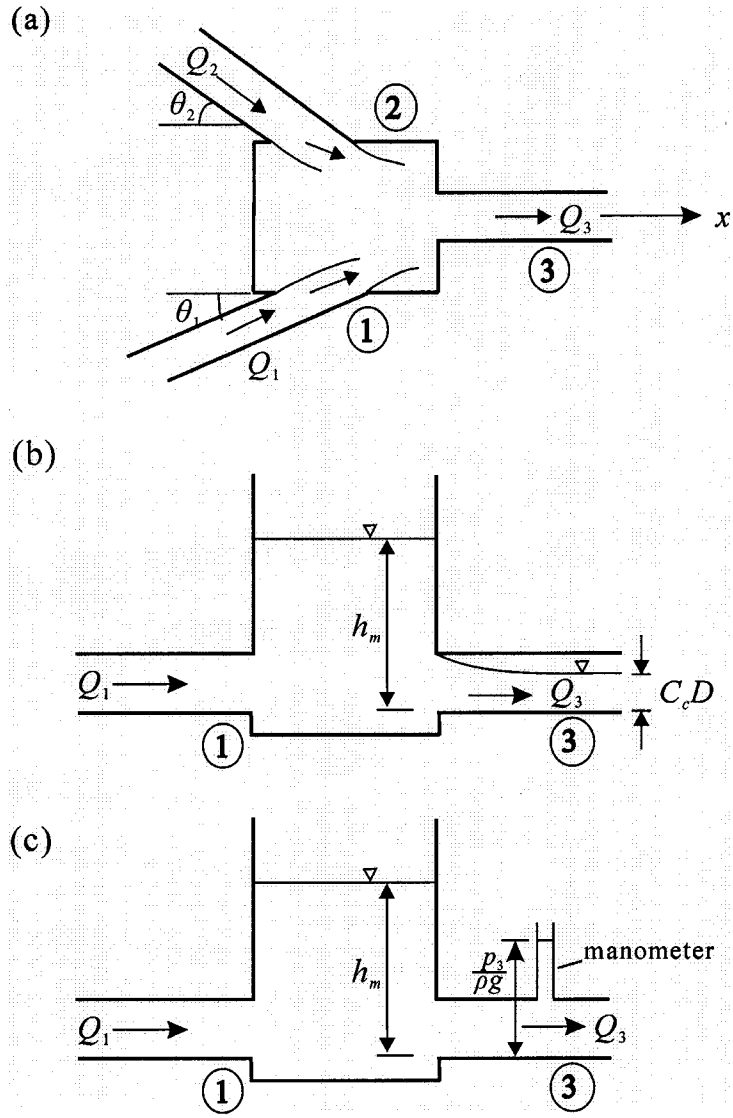

Figure 5.4 Schematic diagram of sewer flows in a three-way combining junction: (a) plan view; (b) side view of Regime II flow; and (c) side view of Regime III flow

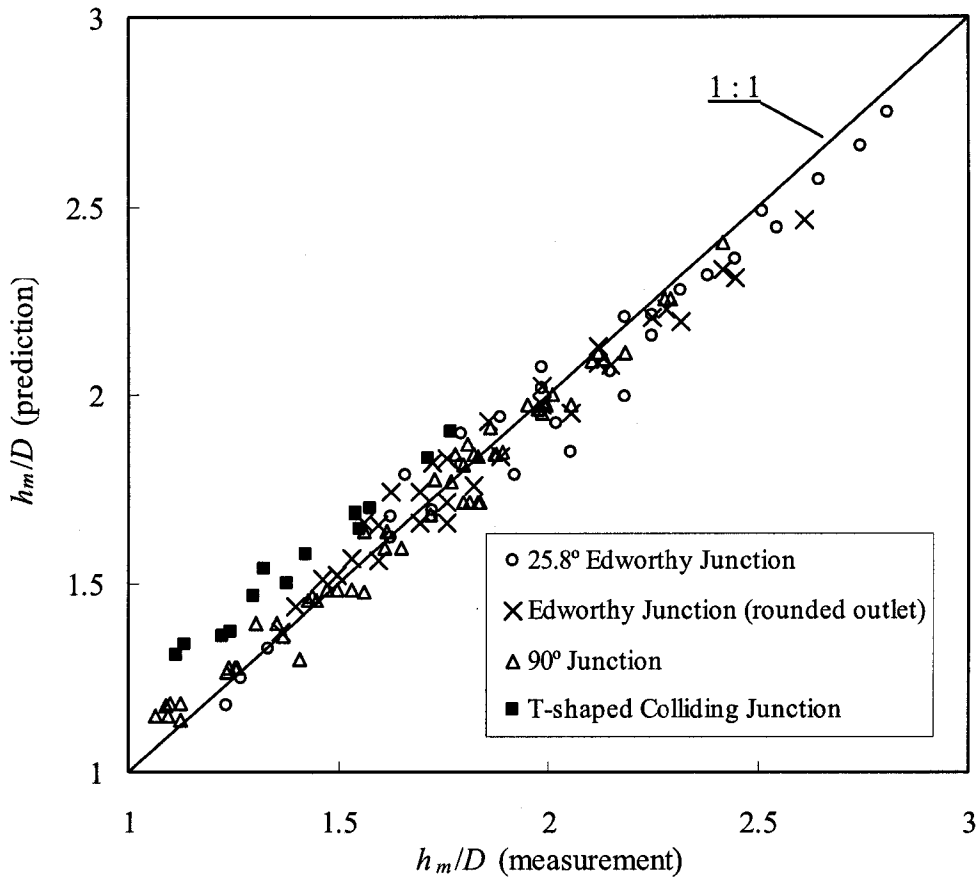

Figure 5.5 Comparisons of Eq.(5.2) with experimental measurements of water depths in junction chambers with Regime II flow

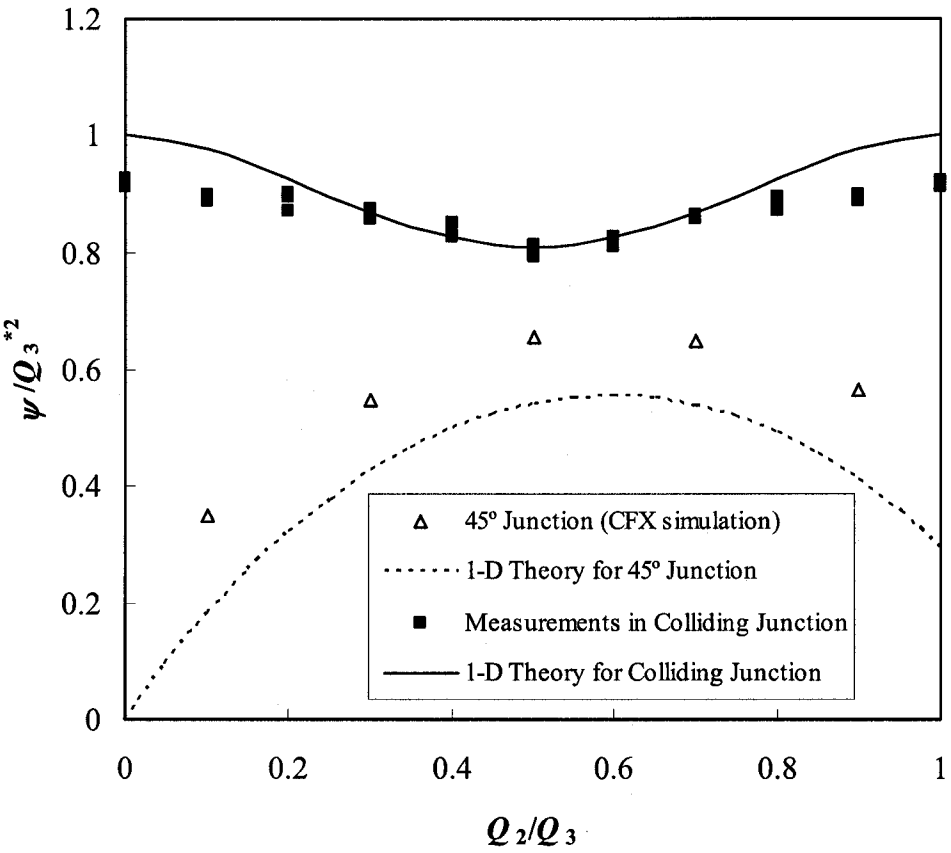

Figure 5.6 Comparison of the 1-D theory (Eq.5.6) with measured submergence factors in Regime III flows

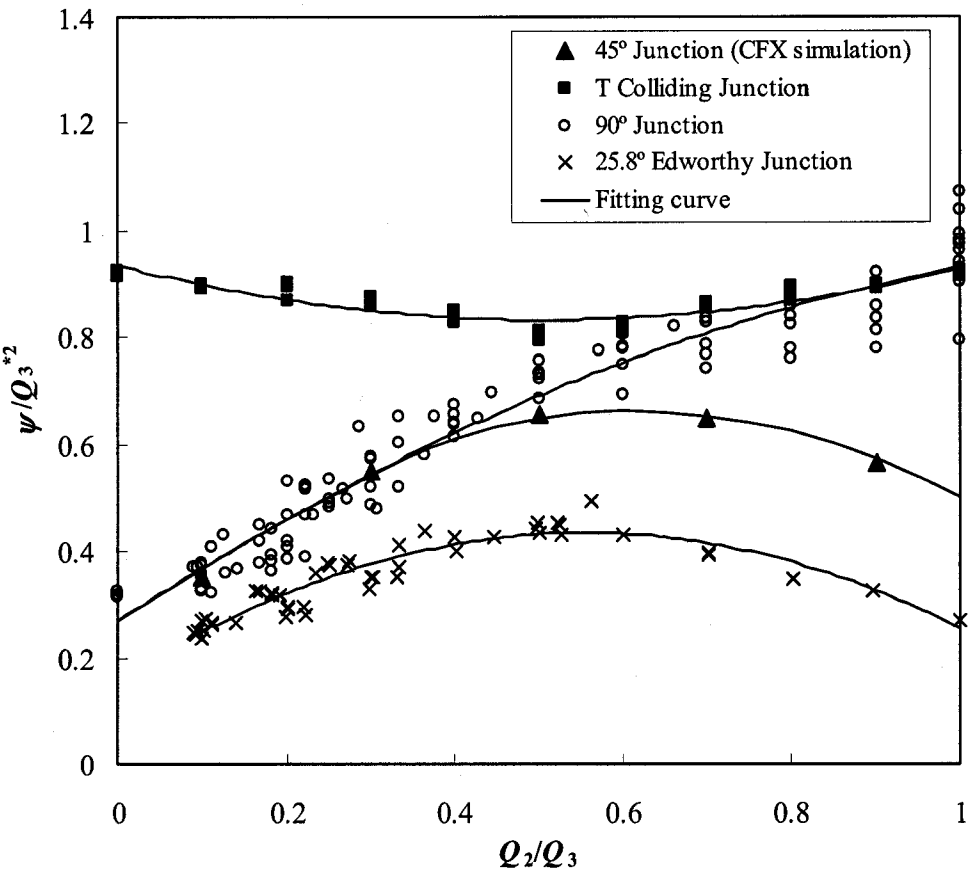

Figure 5.7 Submergence factor in Regime III flow

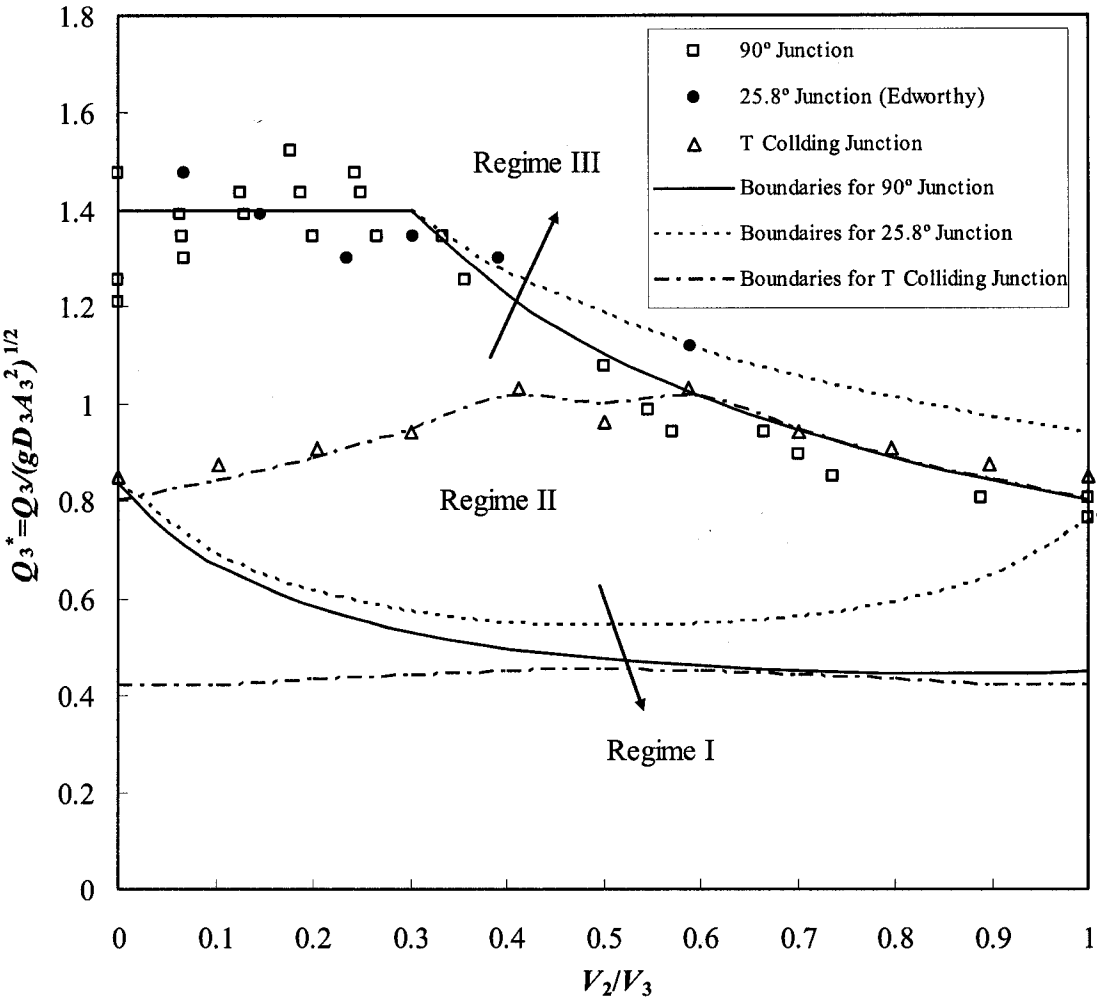

Figure 5.8 Onset of flow regimes in sewer junctions

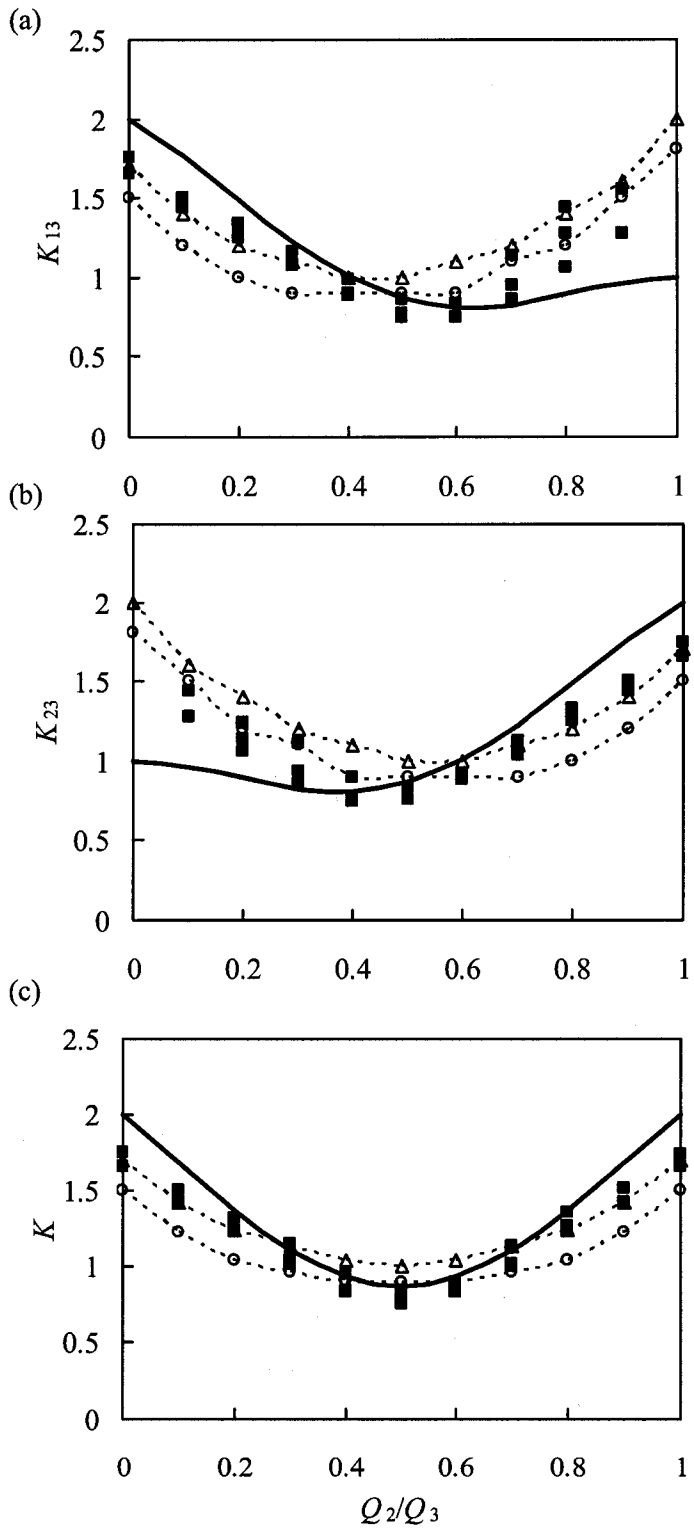

Figure 5.9 Energy coefficients for T-shaped colliding junctions: (a) K_{13}; (b) K_{23}; and (c) K. Present measurements (■); Marsalek (1985) for chamber size of 2.3D (---Δ---) and 4.6D (---o---); and predictions by Eq.(5.9) (———)

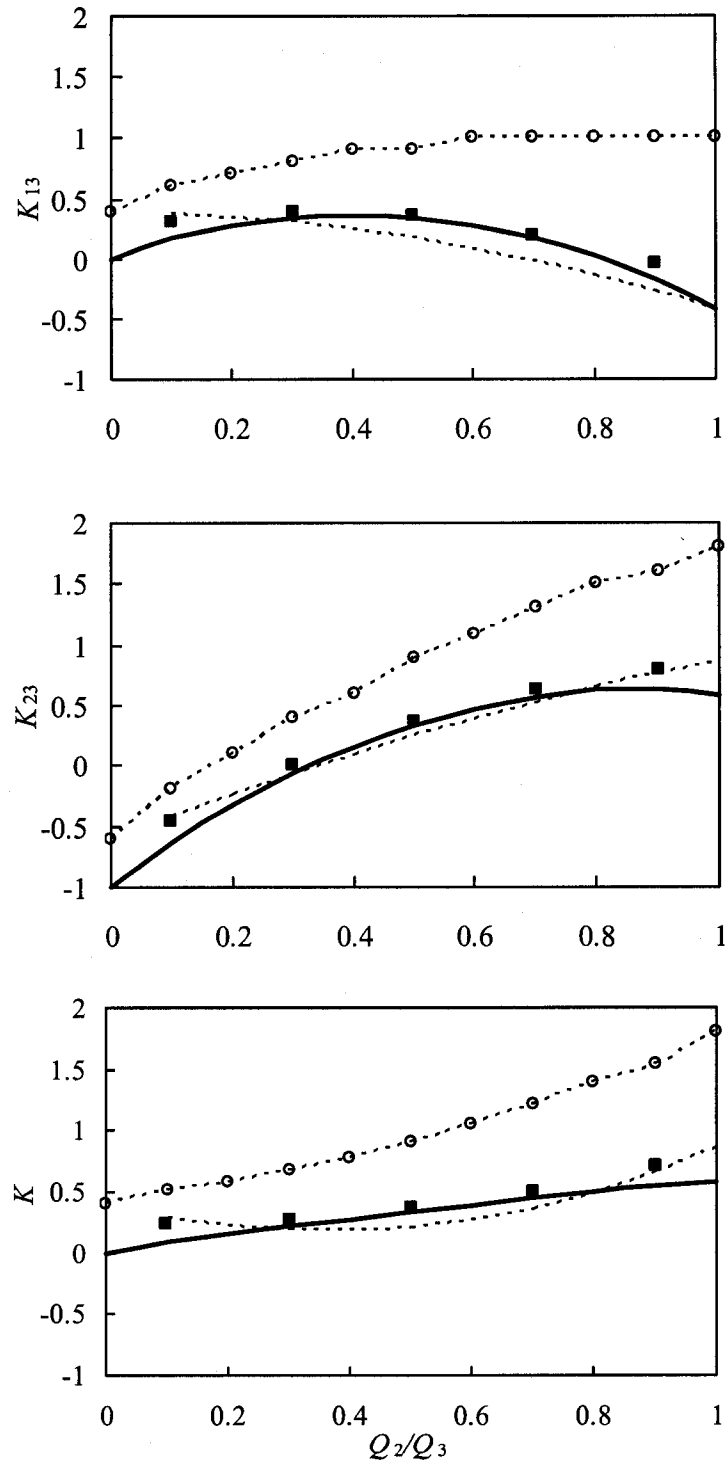

Figure 5.10 Energy coefficients for Regime III flow in combining sewer junctions: numerical simulation for a 45° junction (■); prediction of 1-D theory for the 45° junction (———); experimental results of Zhao et al. (2004) for the 25.8° Edworthy junction (----------) and Marsalek (1985) for a 90° junction (----○----)

(a)

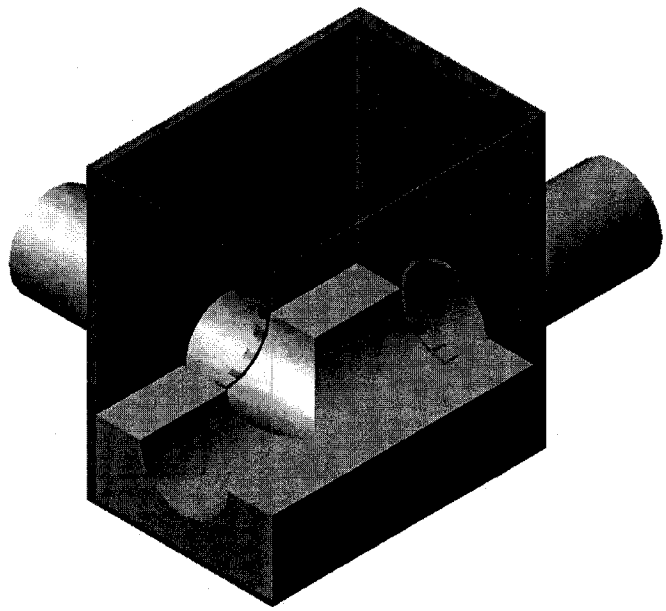

(b)

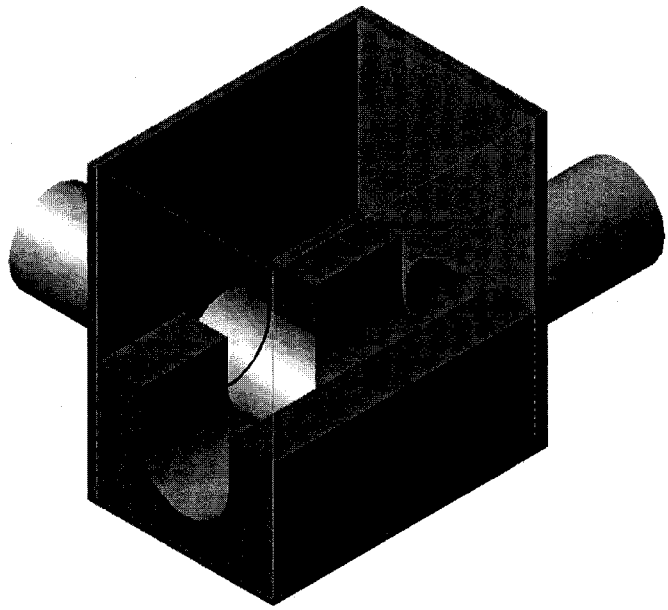

Figure 5.11 Schematic diagram of benching designs for sewer junctions: (a) half benching; and (b) full benching

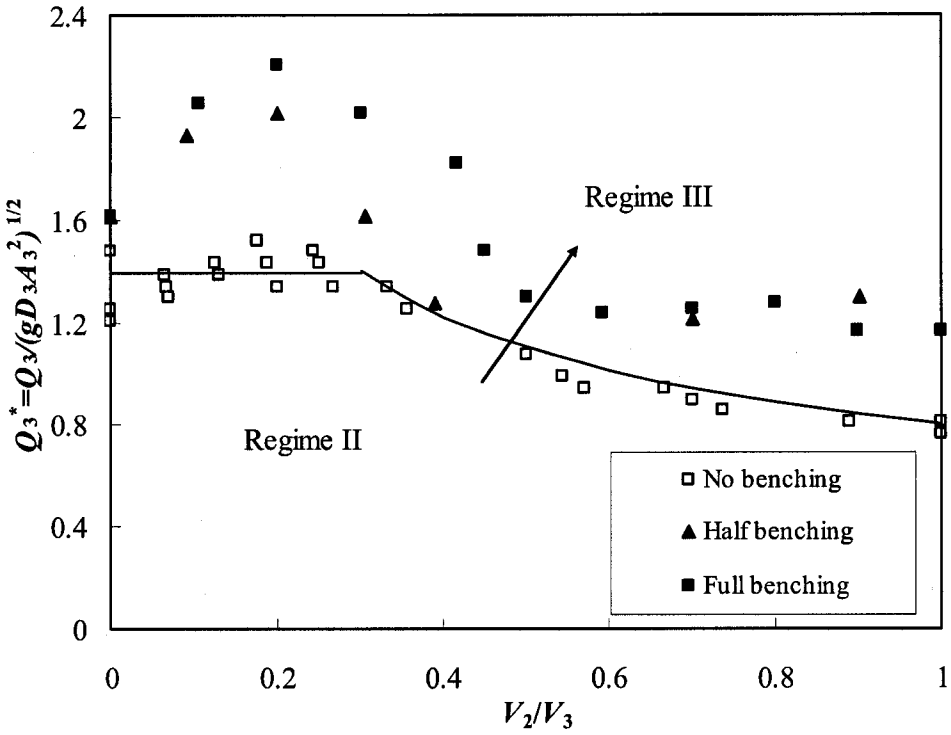

Figure 5.12 Effects of benching on the transition from Regime II to Regime III at a 90° junction

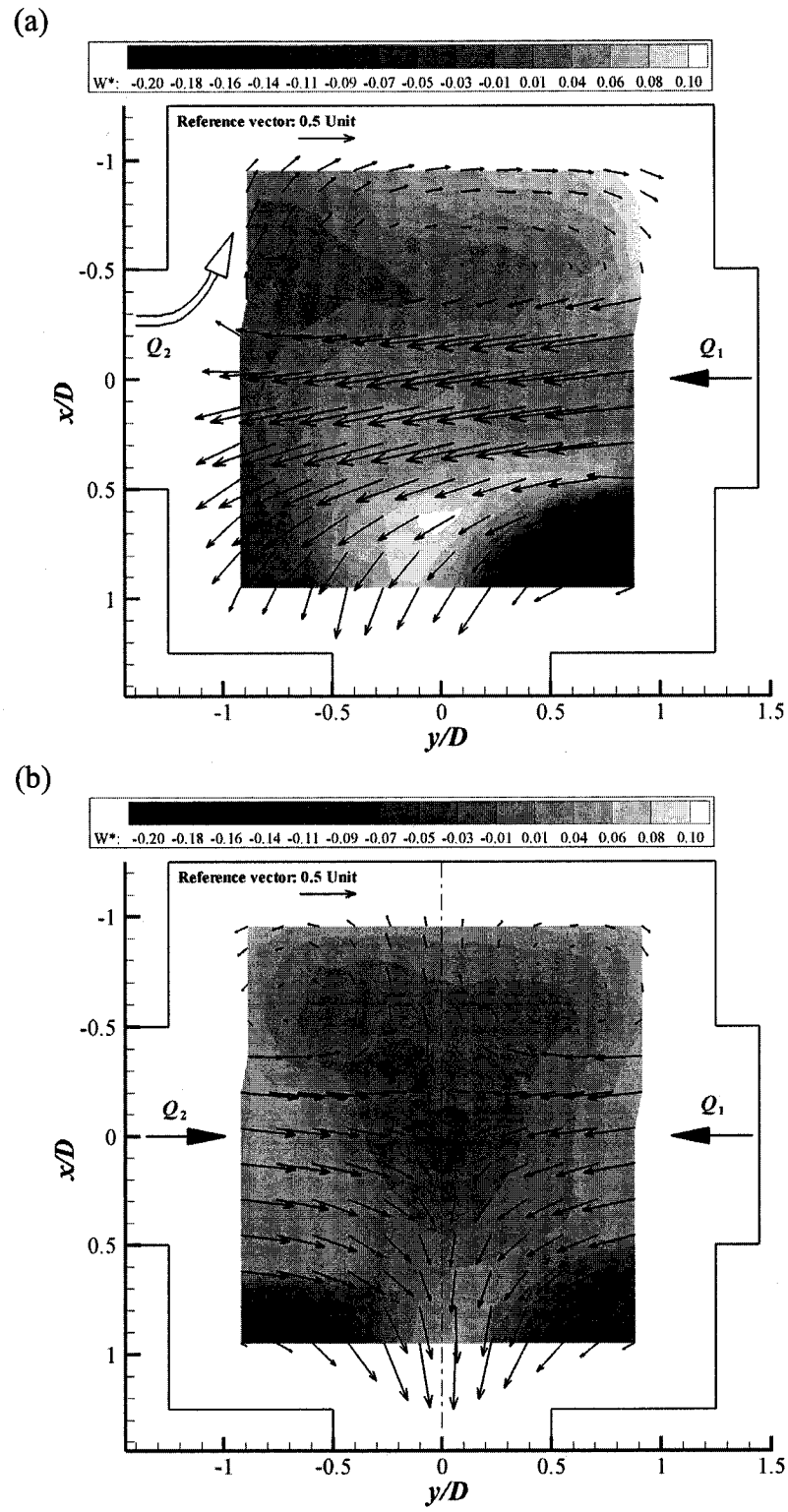

Figure 5.13 Normalized velocity distributions in the central plane of a T-shaped colliding junction for $Q_3 = 0.03$ m^3/s: (a) $Q_2/Q_3 = 0.2$ and (b) $Q_2/Q_3 = 0.5$

(a)

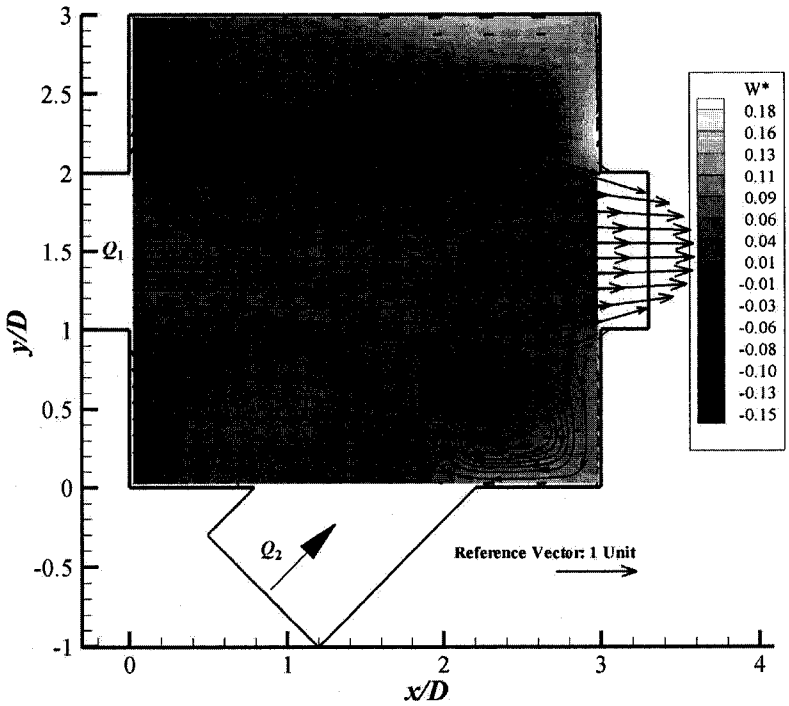

(b)

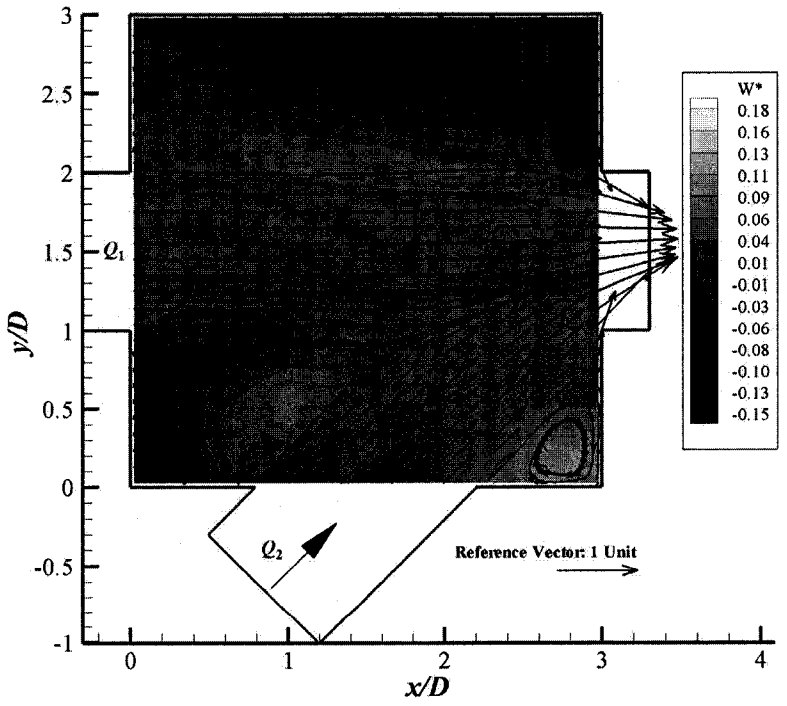

Figure 5.14 (a-c) Normalized velocity distribution at the central plane simulated in a 45° junction for $Q_3 = 0.035$ m^3/s: (a) $Q_2/Q_3 = 0.1$; (b) $Q_2/Q_3 = 0.5$; and (c) $Q_2/Q_3 = 0.9$

(c)

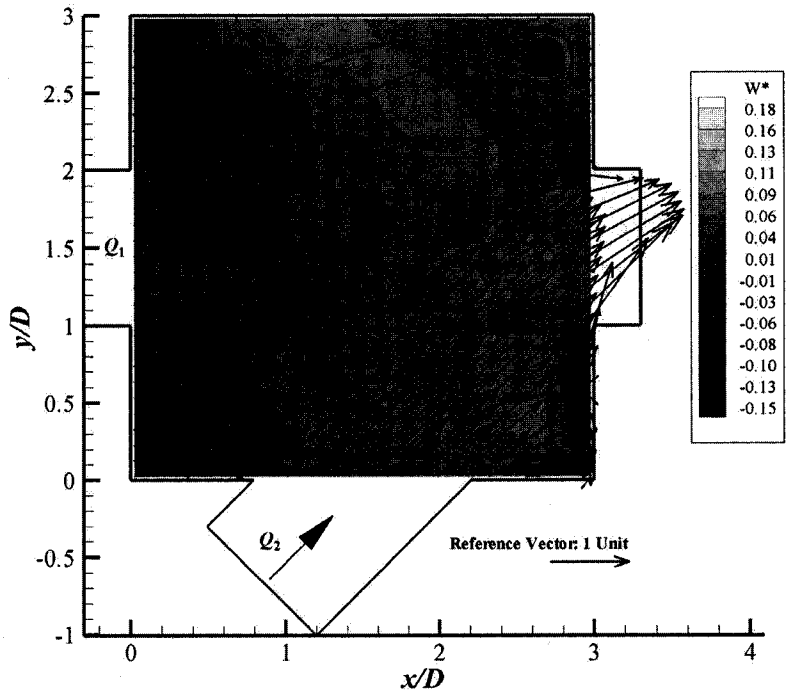

Figure 5.14 (a-c) Normalized velocity distribution at the central plane simulated in a 45° junction for $Q_3 = 0.035$ m^3/s: (a) $Q_2/Q_3 = 0.1$; (b) $Q_2/Q_3 = 0.5$; and (c) $Q_2/Q_3 = 0.9$

(a)

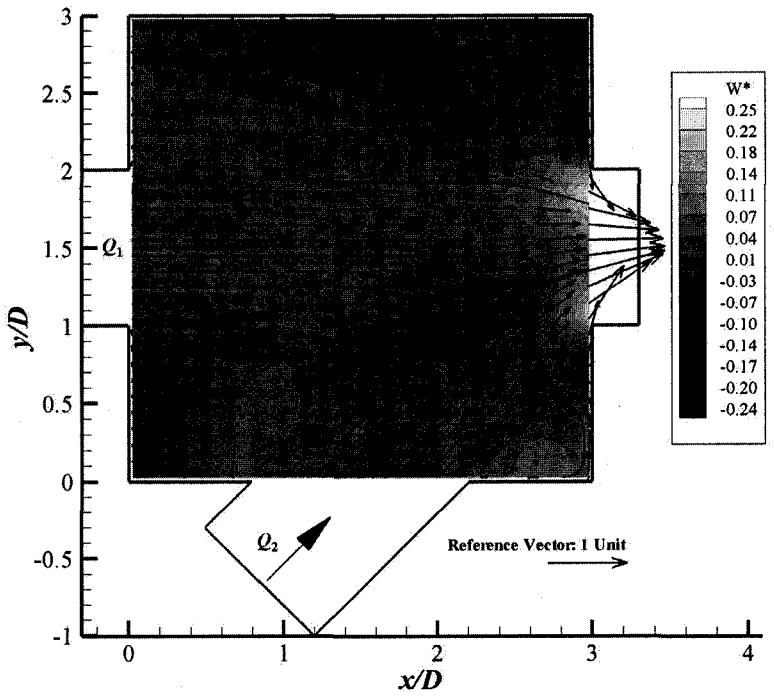

(b)

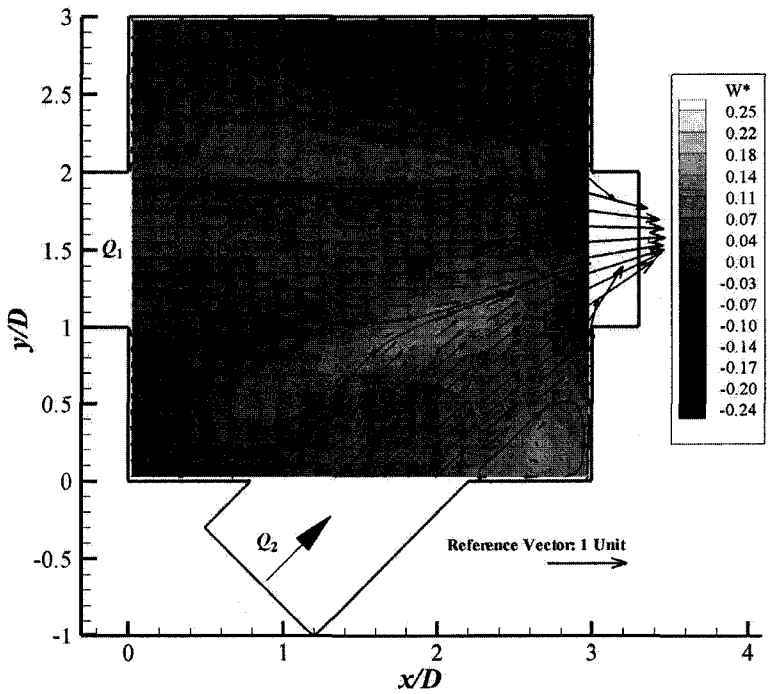

Figure 5.15 (a-d) Normalized velocity distribution for the 45° junction flow of Q_2/Q_3 = 0.5 at planes of (a) z/D = 0.25; (b) z/D = 0.75; (c) z/D = 1.1; and (d) z/D = 2.15.

(c)

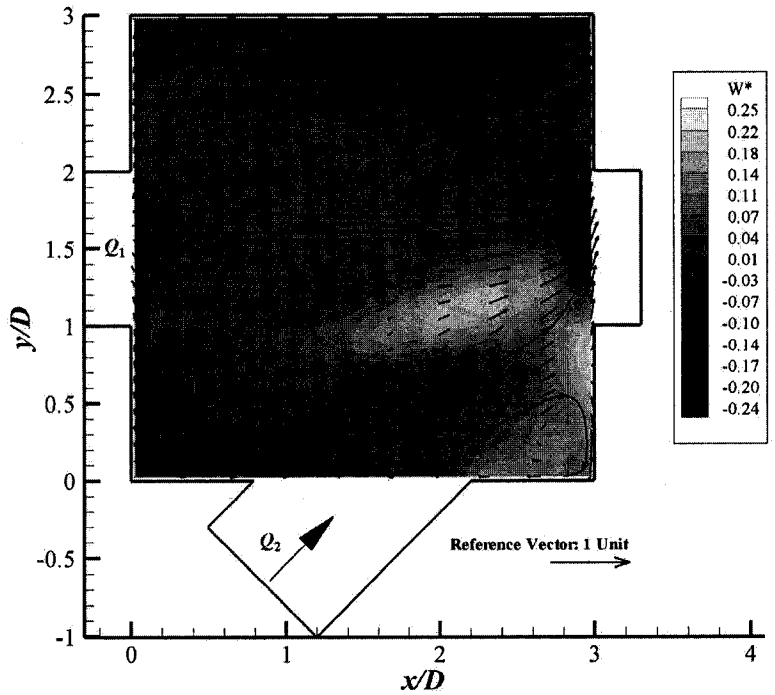

(d)

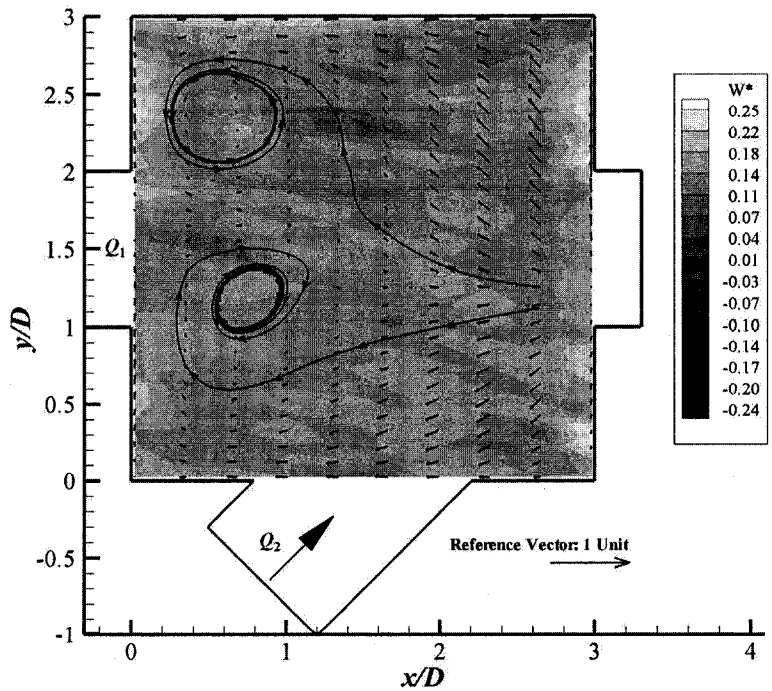

Figure 5.15 (a-d) Normalized velocity distribution for the 45° junction flow of Q_2/Q_3 = 0.5 at planes of (a) z/D = 0.25; (b) z/D = 0.75; (c) z/D = 1.1; and (d) z/D = 2.15

References

Del Giudice, G. and Hager, W. H. (2001). "Supercritical flow in 45 degree junction manhole." *Journal of Irrigation and Drainage Engineering*, ASCE, 127(2): 100-108.

Gisonni, C. and Hager, W. H. (2002). "Supercritical flow in the 90° junction." *Urban Water*, 4(4): 363-372. *Journal of Irrigation and Drainage Engineering*, ASCE, 126(1): 48-56.

Hsu, C.-C., Lee, W.-J. and Chang, C.-H. (1998). "Subcritical open-channel junction flow." *Journal of hydraulic Engineering*, ASCE, 124(8): 847-855.

Weber, L. J., Schumate, E. D., and Mawer, N. (2001). "Experiments on flow at a 90° open-channel junction." *Journal of Hydraulic Engineering*, ASCE, 127(5): 340-350.

Marsalek, J. (1985). *Head Losses at Selected Sewer Manholes*. National Water Research Institute, Canada Centre for Inland Waters, Burlington, Ontario.

Ramamurthy, A. S., Carballada, L. B., and Tran, D. M. (1988). "Combining open channel flow at right angled junctions." *Journal of hydraulic Engineering*, ASCE, 114(12): 1449-1460.

Sakakibari, T., Tanaka, S. and Imaida, T. (1997). "Energy loss at surcharged manholes – model experiment." Water Science and Technology, 36(8-9): 65-70.

Chapter 6

Conclusions

This thesis presents an investigation of hydraulic performance of three-way combining sewer junctions, both by an experimental and a computational approach. Sewer junctions are one of the most important components in drainage systems; however, few research is currently available on this topic. In this study, the 25.8° Edworthy junction, junctions of 45° and 90°, and a T-shaped colliding junction were investigated. The study includes both fundamental hydraulics of sewer junctions and practical considerations of sewer design and operation. It provides a basis of generalizing hydraulic descriptions for sewer junctions and helps to improve current municipal servicing guidelines of sewer design and construction.

The research started with a case study of the Edworthy storm trunk junction in the City of Calgary, Alberta. The junction had a merging angle of 25.8°. It was designed to retrofit a problematic junction. In the laboratory experiments, three flow regimes were identified: Regime I is featured by free-surface flow through the junction; Regime II is characterized with surcharged flow in the chamber and orifice flow to the outlet pipe, referred to as partly surcharged flow; and Regime III is fully surcharged flow which occurs accompanied with priming and pipe-full flow in the outlet pipe. Considerable changes of water depth in the junction were observed during the transition between Regime II and Regime III. Regime II flow has not received sufficient attention of engineers and previous researchers. It was omitted in previous studies in fact. However, it

can be a critical flow condition in sewer junction design such as the case of the Edworthy junction where the maximum submergence was observed in Regime II flow.

With further experiments of other junctions, the flow was analyzed in the respective regimes. A one-dimensional (1-D) theoretical model was derived for surcharged flows. The model produced reasonably good predictions of water depth in regime II flow, submergence factor and energy loss coefficients in regime III flow.

Transition from regime II to III was investigated in the 25.8° and 90° junctions and the T-shaped colliding junction. It was found that the transition is a complicated phenomenon and is possibly related to the inlet waves in the outlet pipe. When the flow in the outlet pipe reaches a certain rate, the inlet waves may cause the pipe choked and result in regime III flow. Criteria for regime transitions were presented based on experimental results and theoretical analysis. The criteria could be used to predict flow patterns for given conditions, which is crucial to carry out proper analysis in sewer junction design.

The slope of the outlet pipe is crucial to determine whether Regime II flow will present in surcharged sewer junctions. If the slope is sufficiently steep, Regime II flow can exist. However, once surcharged flow regimes are set up, the slope does not matter. It has no noticeable impacts on water depth variation in the junction chamber in Regime II flow; and, it will not affect submergence and energy loss in Regime III flow.

Effects of benching were evaluated in this study. In three-way combining junctions, benching appears to have limited impacts on surcharged flows. It helps to stabilize the flow, but influence on energy loss may be only noticeable when one inflow

is dominant. When the two inflows are comparable, their interactions are dominant and benching effects may be minor.

Energy loss in fully surcharged junction flow could also be affected by junction angles and chamber size. Smaller energy loss coefficients were found in junctions with smaller merging angles. However, the effect may not be considerable in further reducing the angle from 45°, as the difference in energy loss coefficients between a 45° junction and the 25.8° Edworthy junction were found to be relatively small. Energy loss in fully surcharged flow could increase with increasing the size of junction chambers, but the change may be negligible when the equivalent size of a junction chamber exceeds three times of pipe diameter.

Three-dimensional computational simulations were carried out for surcharged flow at the 90° combining sewer junction using a commercial computational fluid dynamics code, Ansys CFX 10.0. A homogeneous and an inhomogeneous two-phase free-surface flow models were employed with a k-ε turbulence model. The models were validated using experimental measurements. It was found that both the homogeneous and inhomogeneous models predicted well bulk variables of the flow, including the mean water depth in the junction chamber, the submergence factor, and the energy coefficients. The inhomogeneous model showed better performance in simulating flow details such as mean velocity distributions and shape of the water surface in the chamber. Air entrainment in the flow was discussed based on the simulation results. The path of air bubbles in the chamber and the variation of entrainment rate obtained from the homogeneous model are reasonable in comparison with experimental observation. It was found that the relative net air entrainment rate is related to the lateral flow ratio and water

depth in the chamber. It is expected that the air entrainment is insignificant and has negligible impacts on the flows studied.

This study adds to the present knowledge of the hydraulics at combining sewer junctions. A complete and detailed description of flow at sewer junctions was presented. From a practical viewpoint, the information explored provides assistance to sewer junction design and sewer flow analysis.

Due to the complexity of sewer junction flow, many aspects are still left to be studied, such as effects of junction geometry on free-surface (regime I) flow in junctions, pipe size, and vertical arrangement of connecting pipes. Three-dimensional numerical simulation using Ansys CFX could be a reliable approach to study fully-surcharged flow. It may also be able to simulate regime II flow and that will be useful to improve understanding of regime transition. Simulation of regime transition is still a challenge. When a numerical model can be set up and validated for all three types of flow, one may use it to study unsteady flow at combining sewer junctions. The 1-D theoretical model provided a basis for analyzing and predicting flow at sewer junctions. It may be improved to be a design tool for practical use when more data are available.